The Dissertation Committee for Jennifer L. Aschoff certifies that this is the approved version of the following dissertation:

CONTROLS ON THE DEVELOPMENT OF CLASTIC WEDGES AND GROWTH STRATA IN FORELAND BASINS: EXAMPLES FROM CRETACEOUS CORDILLERAN FORELAND BASIN STRATA, USA

Committee:

Ron Steel, Supervisor

Mark Cloos

Sean Gulick

Brian Horton

Kitty Milliken

CONTROLS ON THE DEVELOPMENT OF CLASTIC WEDGES AND GROWTH STRATA IN FORELAND BASINS: EXAMPLES FROM CRETACEOUS CORDILLERAN FORELAND BASIN STRATA, USA

by

Jennifer L. Aschoff, M.S.; B.S.

Dissertation

Presented to the Faculty of the Graduate School of

The University of Texas at Austin

in Partial Fulfillment

of the Requirements

for the Degree of

Doctor of Philosophy

The University of Texas at Austin

May, 2008

Acknowledgements

Above all, I thank my supervisor Dr. Ron Steel for his technical and professional guidance, endless encouragement, positive attitude, and financial support for "risky" aspects of this research that were not otherwise funded. I am indebted to Drs. Brian Horton and Mark Cloos, who provided many discussions and suggestions that helped me understand the influence of tectonics on sedimentary basin fill better. I thank Dr. Kitty Milliken for her numerous careful reviews, suggestions to improve my writing and invaluable guidance through the review process. Additionally, I thank Drs. Tim Lawton, Kate Giles and Jim Schmitt for their comments on various parts of my Ph.D. research, and continued mentorship. Dr. Sean Gullick also provided many comments that improved the quality of the research presented herein. Discussions with Cristian Carvajal and Shuji Yoshida are also appreciated. Field assistance was graciously provided by Sumiyyah Ahmed, Ben Herber, Ariana Osman, Jacob Proctor, Geoff Scotty and Blair Stanley. Undergraduate student research by Blair Avant Stanley concerning bay-head delta deposits in the Neslen Fm. contributed to my understanding of bay-head deltas. My close friends and family were very supportive during this entire process. I extend my sincerest thanks to Kyle Graff, Sarah Hamman, Patrick Moran, Rosalba Mendoza, Melissa Boysun, Kelly Titkemeiyer, Jessica Hersey, Melissa Brown, Alan Aschoff and Diane Aschoff for their invaluable support.

The research presented herein would not have been possible without the generous support by numerous donors. For funding, I thank ConocoPhillips Subsurface Technology, ConocoPhillips SPIRIT Program, University of Texas Continuing Fellowship, Rocky Mountain Association of Geologists (Norman Foster Scholarship), Colorado Scientific Society (S.S. Oriel Grant), Houston Geological Society (Calvert Scholarship), AAPG Grants in Aid (R.D. Woods Grant), Geological Society of America Student Grant, T.R. Banks Foundation Fellowship, Anderson Endowment Scholarship, Sedimentary Geology Division of GSA (Proposal Award), the Jackson School of Geosciences, and Dr. Ron Steel.

CONTROLS ON THE DEVELOPMENT OF CLASTIC WEDGES AND GROWTH STRATA IN FORELAND BASINS: EXAMPLES FROM CRETACEOUS CORDILLERAN FORELAND BASIN STRATA, USA

Publication No._____

Jennifer L. Aschoff, Ph.D.

The University of Texas at Austin, 2008

Supervisor: Ron Steel

Tectonic signatures such as growth strata, clastic progradation, detrital composition, thickness trends, paleoflow shifts, lithofacies distribution, and vertical stratigraphic stacking patterns provide the basis for a range of tectonic/structural interpretations. Complete understanding of the application and limitations of tectonic signatures is important to maintain consistency and reduce uncertainty of interpretations that use them. This study provides insight into the external controls on two frequently used tectonic signatures in foreland basins: (1) growth strata, and (2) clastic wedge progradation. *First*, two syntectonic unconformity types are recognized in non-marine, Cenomanian growth strata adjacent to the Sevier thrust-belt in southeastern Nevada, USA. Unconformities with larger angular discordance (>10°, "Traditional Type") developed when uplift outpaced sediment accumulation. More subtle unconformities with less discordance (2-10°, "Subtle Type") developed when sediment accumulation

nearly kept pace with uplift. Increasing sediment supply with positive net accommodation, allows syntectonic deposits to aggrade above a growing structure, with no change in uplift rate. Hence, sediment supply and regional accommodation impart an important control over growth strata geometries that are often interpreted on the basis of tectonics alone. Identification of unconformity types in growth strata can therefore document additional phases of uplift, particularly for intervals where sediments aggraded above an active structure due to higher sediment supply during regional subsidence, or sea level rise. *Second*, an anomalous, Campanian clastic wedge is identified in Cordilleran Foreland basin fill, Utah and Colorado. The complex internal architecture, tide-dominated facies and characteristic flat-to-falling shoreline stacking patterns of the wedge reflect rapid progradation of wide (60-80 km), embayed, tide-influenced shorelines; these characteristics distinguish the anomalous wedge from the underlying and overlying clastic wedges in the basin. A high-resolution regional correlation and isopach maps for the anomalous wedge provide evidence that extensive clastic progradation was coeval with both Sevier- and Laramide-style deformation. Stratigraphic relations suggest that development of the anomalous character of Wedge B was due to uplift of a Laramide structure within the foredeep, and possibly enhanced by reduced dynamic subsidence.

Table of Contents

List of Figures

List of Plates

Chapter 1: Introduction

PROBLEM AND SIGNIFICANCE

Previous studies of foreland basins have integrated conceptual, physical and numerical models to explain the development of foreland basins, and have addressed the relative importance of eustatic sea level fluctuation, local topographic development and changing subsidence (Flemings and Jordan, 1988; Heller et al., 1988; DeCelles et al., 1995; Burbank and Verges, 1994). These studies typically use either generalized regional stratigraphic datasets coupled with modeling approaches, or detailed local stratigraphic datasets to understand the links between tectonics and foreland basin fill. However, few studies integrate the kinematics of basin-margin structures with the basin fill. Recent investigations (e.g., Castle, 2001; Clevis et al., 2004; among others) have suggested that foreland basins models do not adequately reflect the complex interplay between uplift, denudation, subsidence, and eustasy; in particular, the three dimensional complexities are rarely considered in detail. Additionally, few studies integrate foreland basin systems, comprising four main depozones, with basin-margin structures; yet such studies provide the direct link between tectonics and foreland basin development.

Proximal deposits, especially well developed growth strata, provide information about the kinematics of adjoining structures (i.e., local tectonics) and are key to understanding structural development of orogens (Suppe, 1992; Verges et al., 2002). Because these deposits can yield high-resolution kinematics, emphasis has been placed on "proximal" foreland successions such as the wedge-top and proximal foredeep depozones. Equally important information is contained in *all* foreland basin depozones (DeCelles and Giles, 1996; Lawton et al., 2003). This additional information and regional stratigraphic information is necessary to interpret foreland basin evolution as a

complete system, including the forebulge and backbulge depozones (e.g., Bruhn and Steel, 2001). Our understanding of foreland basin evolution is presently biased because excessive emphasis has been placed on interpreting proximal zones (e.g., wedge-top and proximal foredeep depozones) of the foreland basin or, to a lesser degree, distal foreland basin deposits (e.g., foredeep), not a complete foreland basin system.

Signatures frequently used to interpret the tectonic control on sedimentary basins, include growth strata, clastic progradation, detrital composition, paleocurrent variations in space and time, depositional patterns, and unconformity development. This study focuses on the application of two of these tectonic signatures: growth strata (as an indicator of local structural development) and source-to-sink clastic progradation (an indicator of regional tectonic movements and subsidence in relation to sediment supply).

Growth Strata

Progressive unconformities, or growth strata, are produced synchronously with uplift caused by fold growth, faulting and diapirism. The geometry of the resultant growth strata depends on the structural style and kinematics of the structure. Fold-related, diapir-related, and contractional growth strata tend to form wedge-shaped stratigraphic packages that have a hinterland-directed, or uplift-directed, tapering wedge pattern. By contrast, extensional- and growth-fault-related growth strata tend to thicken toward the fault; the exception is during the initial phase of fault initiation where a fault-propagation fold causes fold-directed tapering of the growth strata.

In fold-related and contractional growth strata, growth of the structure is accompanied by phases of uplift, tilting and erosion of strata followed by onlapping. Phases of uplift produce thinning, up-section decrease in bedding dip and angular syntectonic unconformities; by contrast, phases of quiescence produce successions of onlapping and overlapping synorogenic strata that generally thicken away from the fault-

related relief (Riba, 1976). The cycles of uplift and quiescence alternate and form a wedge-shaped package of strata that contains a series of syntectonic unconformities and onlapping/offlapping successions, termed “progressive unconformity” after Riba (1976), or “growth strata” after Suppe et al. (1992) and Zapata and Allmendinger (1996).

Growth strata are recognized by a distinctive fanning of dips and multiple, wedge-shaped, unconformity-bound packages (termed “cumulative wedge sequences” by Riba, 1976). In outcrop, dip changes are generally more apparent, whereas unconformities and the overall wedge geometry are typically more obvious in seismic data. Such strata have been used in a number of tectonic settings from salt diapirs (Giles and Lawton, 1999) to fold and thrust belts (Horton et al., 2004). Recent work on growth strata suggests that the internal and lateral geometries of such strata delineate the style and geometry of fault-related folds (Suppe et al., 1992; Zapata and Allmendinger, 1996; Ford et al., 1997). Because progressive unconformities are synchronous with actively building structures they provide the only unequivocal link between the kinematic history of a structure and syntectonic sedimentation.

Unfortunately, many fold-related growth strata are only developed within a few kilometers of an active structure, and are subject to destruction with increased uplift. As a result, growth strata are preserved where growth strata are not subsequently uplifted and destroyed; typically, this includes the youngest structures or regions that have been subsequently subsided. However, when these unique tectonic signatures are preserved they provide a high-resolution reconstruction of local structural development.

Clastic Progradation: “Syntectonic” versus “Antitectonic” Models

Until the late 1980’s, clastic progradation was generally assumed to indicate uplift in the hinterland (e.g., Armstrong, 1960). Several studies provided direct evidence that clastic progradation occurs when relief is created (Burbank, 1996; Crabaugh, 2002;

Horton et al., 2004). By contrast, some contended that there is a significant lag-time (as much as a few million years) between clastic progradation and mountain building because of high initial basin subsidence or reorganization of depositional systems (Jordan, 1981; Heller et al. 1996; Blair and Bilodeau, 1998; Jones et al., 2004). In general terms, the "syntectonic" progradation model predicts that progradation is coeval with uplift; whereas, the "antitectonic" model predicts that progradation is coeval with quiescence and isostatic adjustment.

Controversies concerning the two models of progradation resulted, in part, from differences in the scales (time and space) of the studies that investigated progradation. Some workers focused on generalized basin-scale (> ½ basin width) studies of progradation, whereas others focus on more detailed local (< ½ basin width) studies of progradation. Some studies documented progradation of a single depositional system, such as a fluvial megafan at a smaller scale (< ½ basin width) (Burbank et al., 1988), while others documented progradation of an entire clastic wedge at a larger scale (> ½ basin width) (Heller et al., 1988). Additionally, few workers focus on the time-scale of progradation because age constraints are usually scant. As a result, the spatial and temporal scales of tectonic-induced progradation are unclear. Although each study contributes valuable data and insight into the problem of progradation, it is crucial to highlight the amount, type, and time-scales of progradation. Progradation of alluvial fans or fluvial megafans (i.e., a single depositional system) into a small (10-100 km), confined basin is distinctly different from clastic wedges (i.e., composed of several, connected depositional systems) that prograded great distances into a foreland basin (100's-1000's km).

Inconsistencies resulting from generalized approaches, or isolated local studies can be overcome by integrating detailed observations from both proximal (i.e., growth

strata) and distal foreland basin deposits. This allows basin-scale linkages between clastic wedge development, depositional systems comprising the wedges and tectonics to be delineated. Unfortunately, few such studies have been completed. The dearth of these studies is due to limitations in outcrop or subsurface data coverage and complicated regional (100's km's) correlations with numerous facies changes and erosion surfaces, coupled with the physical challenge of accessing extensive outcrop exposures. However, superb outcrop exposures, dating and improved non-marine to marine sequence stratigraphic techniques can overcome these challenges.

Project Objectives

The primary goals of this study are to evaluate two frequently used indicators of tectonics (e.g., growth strata and clastic wedge progradation), and improve understanding of the basin-fill response to basin-margin kinematics in foreland basins. These goals are met by: (1) reviewing a wide array of frequently used "tectonic signatures", or stratigraphic characteristics used to interpret tectonics; (2) examining growth-strata development in detail, and exploring non-tectonic factors that may mask the kinematic record within growth strata (the most widely accepted indicator tectonics); (3) determining connections, or disconnections, between growth strata and the anomalously extensive clastic wedge emanating from the former thrust-belt front (the most controversial indicator of tectonics) and (4) describing geometric and facies variability within different clastic wedges, and postulating how this may reflect tectonics, sediment supply and climate. Multiple field-sites were necessary to complete the research goals. These field sites include an oblique, 3-D exposure of Upper Cretaceous growth strata in the southeast Nevada segment of the Cordilleran foreland basin, and a regionally contiguous outcrop belt that extends from the eastern edge of the Wasatch Plateau, Utah to Redstone, Colorado- 400 km.

Methods

To determine how growth stratal packages exposed in the Wasatch Plateau relate to distally extending marine sandstone tongues exposed in Central Colorado, and to identify the phase of foreland basin development in which progradation occurred I integrated new outcrop data (46 new profiles) with subsurface data and published stratigraphic data (69 additional datapoints) to construct a biostratigraphically constrained sequence-stratigraphic correlation to relate basin-margin structural development with the basin-fill.

Growth Strata Analysis

Analysis of growth strata involves an examination of both the external and the internal morphologies and their mutual relationships. Recognizing the flattening-upward character of bedding, identifying dip discordances between beds and locating syntectonic unconformities within the succession are key components of these analyses (Verges, 2002). Unconformity-bound packages within the growth strata are thought to reflect distinct phases of uplift and quiescence (Riba, 1976). Syntectonic unconformities form when the net uplift exceeds the net rate of sedimentation, whereas overlapping strata reflect periods when sedimentation exceeds the net uplift.

In the southeast Nevada study site, growth strata analysis was the key focus of the investigation. Here, I documented bedding attitude changes every 3 meters in 3 vertical profiles. I used the location of dip discordances to guide reconnaissance of syntectonic unconformities. Three stratigraphic profiles were measured and correlated through the growth strata ~3 km away from the growth strata assemblage, the other was measured through the entire growth strata assemblage where the most unconformities were present. Using high-resolution air photos and satellite images each unconformity was mapped along strike. Each syntectonic unconformity was carefully described, and key

sedimentologic features that help identify the unconformity were documented with photomosaics.

Stratigraphic Correlation and Measured Stratigraphic Sections

Existing less detailed, sequence stratigraphic and biostratigraphic correlations (Hettinger and Kirschbaum, 2002; Horton et al., 2004) were extended further up-dip to the Western edge of the Wasatch Plateau (Utah), and down-dip to South Park and Denver Basins (Colorado). Stratigraphic sections were measured within a laterally continuous, third-order clastic wedge. Stratigraphic units comprising the third-order wedge (ca. 2 My) are:

upper part of the lower Castlegate Sandstone,
middle Castlegate Sandstone,
Buck Tongue,
Sego Sandstone,
Neslen Formation,
Corcoran Member of the Iles Formation
Cozzette Member of the Iles Formation
Price River Formation, and
Bluecastle Tongue.

Stratigraphic profiles were measured at a 25 cm scale detail, and located 5-16 km apart. The spacing of stratigraphic sections was dependent on the quality and accessibility of exposures. A total of 46 sections were measured between the Wasatch Plateau, Utah, where growth strata are exposed, and Crested Butte, Colorado, where distal marine sandstone tongues are exposed. At each measured section, special attention was given to documenting:

unconformities;
bedding attitude changes;
lithofacies;
onlapping and offlapping surfaces;
paleosol development;
stratal architecture and thickness;
grain-size;
paleoflow current indicators;
detrital composition changes (field-estimated detrital composition)

Published stratigraphic data from multiple sources were compared with data I collected, and integrated into the final regional correlation and/or isopach maps. The resultant correlation is the first high-resolution correlation from structurally deformed non-marine conglomerates (wedge-top depozone) to distal marine sandstone tongues (distal backbulge depozone). Because of the copious new outcrop data, and integration with abundant published stratigraphic research this correlation may be the most complete, high-resolution stratigraphic cross section through a clastic wedge in the North American Cordilleran foreland basin.

Seismic and Well Log Data

Subsurface data are essential to fill the small outcrop gap between the eastern edge of the Wasatch Plateau and Price Canyon area connecting growth strata assemblages with foredeep deposits. Recently published seismic data (e.g., Horton et al., 2004) was used to guide correlation from the growth-strata assemblage to the adjacent foreland basin fill. An additional 69 published, or publicly available, well logs and stratigraphic sections (from Utah and Colorado State Geological Surveys, and US Geological Survey) were used to fill gaps in outcrop exposure and to construct regional isopach maps of the Uinta and Piceance basins where the strata are in the subsurface. Well logs located near the outcrop belt were used to calibrate outcrop facies and correlations with well log signatures. This helped guide correlations of facies and sequence-stratigraphic correlation, and aided connecting the biostratigraphic correlation with the sequence-stratigraphic correlation because ammonites tend to be found near marine flooding surfaces that show up well in well-logs.

Regional Photomosaics and On-ground Validation

Photomosaics of the entire outcrop belt from the eastern margin of the Wasatch Plateau to Grand Junction were assembled for the entire Book Cliffs from Grand Junction, Colorado to Spring Canyon, Utah using oblique aerial photographs taken from a fixed-wing airplane. Airplane-shot photomosaics were used to trace key sequence-stratigraphic surfaces in the field.

Summary of Chapters

Chapter 2: Tectonic Signatures in Clastic Stratigraphy: What are they, and how do we best apply them?

Tectonic signatures are stratigraphic characteristics that suggest deposition was synchronous with tectonic development. This chapter provides a brief history of tectonics and sedimentation, and an overview of previously used tectonic signatures. In addition, I provide an array of examples where these signatures have been used, and a discussion of the pragmatic application (and limitations) of these signatures. To do this, I use an extensive literature review. This chapter also highlights the non-tectonic factors such as climate (and sediment supply) and eustasy that may influence the development of these widely used "tectonic signatures" in stratigraphy.

Chapter 3: Enhancing Growth Strata Analysis by Distinguishing Syntectonic Unconformity Types: An Example from Southeastern Nevada

Growth strata assemblages are the most widely accepted signature of tectonics in stratigraphy. Such assemblages are identified by the presence of a wedge-shaped, hinterland-tapering body of strata containing progressively rotated, flattening-upward beds. The progressive rotation of strata directly reflects the uplift of the adjacent structure. As a result, growth strata are commonly used to reconstruct the kinematics of an individual structure. Multiple growth structures located throughout an ancient orogen

can provide the relative timing of mountain building. In this chapter I describe and interpret depositional facies and syntectonic unconformities in Upper Cretaceous growth strata exposed in southeastern Nevada. Using this dataset, I define two types of syntectonic unconformities and propose sedimentologic criteria to distinguish them in the field. The new classification acknowledges tectonic signals in syntectonic strata when they contain small, but cumulative angular discordances, and is especially important when high sediment supply masks signatures of uplift in growth strata. This chapter is important because it highlights the close association between uplift and sedimentation, and postulates that syntectonic unconformities can be masked during high-supply conditions imposed by climate, drainage basin size/relief and source lithology.

Chapter 4: Anomalous Clastic Progradation in the Cordilleran Foreland Basin: Implications for the Sevier-Laramide Transition, Utah and Colorado, USA

Enigmatic alluvial-to-marine clastic wedges transit 300-500 km eastward across the Cordilleran foreland basin from the front of the Sevier fold-thrust belt. In some cases, the shorelines that comprise the clastic wedges prograded hundreds of kilometers in less than 50,000 years- remarkably fast. In this chapter the relationship of extensive progradation to tectonics and foreland basin development are explored. To determine how clastic wedges relate to the development of the Sevier orogenic belt a detailed, proximal-to-distal correlation from the front of the Sevier orogenic belt to central Colorado was constructed. This detailed correlation integrates sequence stratigraphy, biostratigraphy, published work on detrital composition, key marker horizons, and field-based validation. The correlation indicates that two growth-strata packages correlate with the extensive clasitic wedge. Younger and older growth-strata packages correlate to less extensive, high-volume classic wedges. Biostratigraphically constrained isopach maps show thinning and truncation of the anomalously extensive wedge across the crest of a

basement cored, Laramide-style structure (San Rafael Swell). Thinning trends and stratigraphic truncation across the San Rafael Swell indicate motion of the structure as early as ca. 77 ma, roughly 2-3 million years earlier than previously thought. The regional correlation and isopach maps indicate that the middle clastic wedge developed during both Laramide- and Sevier-style deformation. The overlap, or transition, of deformation styles reduced subsidence in the foredeep and catalyzed extensive, rapid progradation.

Chapter 5: Anatomy of an Extensive, Low-accommodation Clastic Wedge: Insights from Isopach Maps and Regional Correlation in the Uinta-Piceance Basins

Several previous studies demonstrate that clastic wedge progradation is coincident with structural development (Burbank et al., 1988; Horton et al., 2004 among others), whereas others show that progradation lags behind (Heller et al., 1988; Jones et al., 2004). Delineating architectural and geometric variation within clastic wedges can help resolve these discrepancies because different wedges may record tectonics differently. In this dissertation chapter, I describe the internal morphology and facies assemblages within a low-accommodation clastic wedge in the Cordilleran foreland basin. In addition, to gain a 3-dimensional perspective of the wedge and architectural components, I show regional isopach maps of the Uinta-Piceance basins. These isopach maps were constructed using a database of 69 datapoints compiled from new and published data. The data presented in this chapter illustrate the high level of detail within a regional stratigraphic transect, coupled with the 3D perspective of basin-fill. Whereas many studies use generalized regional transects, or shorter but detailed transects, this study contributes a detailed stratigraphic study from a "foreland basin *system*" perspective.

Chapter 2: Tectonic Signatures in Stratigraphy: What are they and how are they best applied?

ABSTRACT

Tectonic signatures are characteristics within the stratigraphic record that can be used to infer the nature and relative timing of tectonics. These signatures are the fundamental building blocks for a wide array of geologic interpretations including basin evolution, and plate tectonic and paleogeographic reconstructions. Previously used tectonic signatures include growth strata, clastic progradation, detrital composition, thickness trends, paleoflow shifts, lithofacies distribution, and vertical stratigraphic stacking patterns. Additionally, more subtle tectonic signatures include unique lithofacies such as seismites and better paleosol development or paleosol clustering. Understanding the context in which tectonic signatures are best applied, as well as their limitations, is important to maintain consistency and reduce uncertainty in geologic interpretations. However, the practical utility and limitations of commonly used tectonic signatures has not been fully assessed despite their widespread application. Unraveling the role of tectonics is best approached using a complete suite of criteria. Some stand-alone stratigraphic signatures of structural development and tectonics are growth strata, changes in detrital composition, paleocurrent shifts and thickness trends. Clear limitations of the best tectonic signatures are 1) local development, 2) low preservation potential, 3) poor or cryptic development of some signatures distal to the structure, and 4) potential time-lag between structural uplift and the stratigraphic response. Clastic progradation, lithofacies distribution, stratigraphic stacking patterns, seismites, paleosols development and preferential cementation are more subjective because they are sensitive

to non-tectonic controls. The later are more subjective and are most useful when integrated with other signatures.

INTRODUCTION

"Tectonic signatures", or indicators, are criteria that are routinely used to deduce the role of tectonics in sedimentary basin fill and kinematic development of structures (Frostick and Steel, 1993). Such signatures refer to characteristics within synorogenic sedimentary successions that suggest deposition synchronous with tectonism, and supply the best record of uplift and subsidence (Frostick and Steel, 1993). Previously recognized signatures of tectonics and accompanying base-level change include: progressive unconformities, or growth strata (e.g., Riba, 1976; Suppe, 1992), lithofacies (e.g., Pivnik, 1990; Cant, 1991), stratal architecture (e.g., Ravnas and Steel, 1998; Miall and Arush, 2001; Martinsen et al., 1999), grain-size (e.g., Robinson and Slingerland, 1999), sandstone composition (e.g., Dickinson, 1974; Dickinson and Suczek, 1979; Dickinson et al., 1986; Lawton, 1986; Damanti, 1993), conglomerate composition (e.g., Haley, 1985; Graham et al., 1986; DeCelles, 1988; Schmitt and Steidtmann, 1990; Lawton et al., 1994), changes in paleoflow and drainage patterns (e.g., Burbank et al., 1996) and paleosol/cement development (e.g., Miall and Arush, 2001; Ketzer et al., 2003).

Interpretations of sedimentary basin evolution, tectonic processes and paleogeography are often based on tectonic signatures recognized in stratigraphy. However, non-tectonic processes, such as climate and eustasy are also recorded in stratigraphy, are intertwined with many frequently used "tectonic signatures". Numerous studies have relied on tectonic signatures, yet their limitations and spatial variability within a sedimentary basin are unclear. Critical evaluation of these signatures improves the wide application of tectonic signatures.

Review of the historical evolution of tectonic signatures highlights their initial intent and assumptions that have become clouded through years of application. The purpose of this paper is to review routinely used stratigraphic signatures of tectonics and clarify their application and limitations. Certain signatures are more clearly related to tectonics, whereas others reflect a more coupled interplay between tectonic, eustatic and climatic control. In cases where tectonic indicators are subjective because of the overprint by non-tectonic processes, it is essential to use multiple criteria.

This paper highlights traditional, inexpensive methods for determining the relative importance of tectonics on sedimentation. The goals are to 1) provide a historical perspective on tectonics and sedimentation, 2) describe a suite of common methods used to determine tectonic influence, 3) discuss examples of how the method was applied, and 4) assess the applicability and limitations associated with each of these common methods.

A BRIEF HISTORY OF TECTONICS AND SEDIMENTATION

Sedimentation and tectonics is traced back to the late 1800's with the proposed link between deep-sea trenches (sites of sediment accumulation) and volcanic arcs by E. Suess, and the link between anticlinoria and the adjacent troughs that collect sediment (geosynclines) by J.D. Dana (Grabeau, 1913; Dott, 1978). These early studies explained the thick stratigraphic successions with downwarping of the crust by tectonics and incremental infilling by sediment. Nascent "tectonics" and uplift was initially explained by thermal expansion/cooling of the earth, and later by isostasy. Although their concept of "tectonics" was quite different from modern "plate tectonics", early workers recognized the close relationship between mountain belts ("anticlinoria") and sites of sediment accumulation ("troughs").

Geosynclines explained the origin of mountains using a coupling of downwarping, depositional loading and upheaval of rock adjacent to depositional

troughs. Initially, geosynclines were classified by the composition of rocks present, and included the mountain belt and associated sediments (Stille 1941). Later, geosynclines were classified using multiple criteria, including their orientation with respect to mountain belts, character of sediments (i.e., shallow or deep-water) and composition. Geosynclines were exhaustively described and classified by Stille (1936), Knopf (1948) and Kay (1951; 1974). Most notable are “miogeosynclines”, which contained shallow water successions, and “eugeosynclines”, which contained deeper-water successions. The early geosynclinal paradigm contrasts sharply with the current “plate tectonic” paradigm, in that the former suggests sedimentation precedes uplift whereas the latter suggests that uplift is first required for sedimentation. Isostasy eventually became the favorite mechanism to explain the geosynclines and their relationship to mountain belts, and was deeply embedded in this paradigm. Geosynclinal thought prevailed into the 1960’s.

Using different approaches, petrographers and stratigraphers independently developed the link between modern tectonic concepts and sedimentation in parallel (Figure 2.1). Petrographers focused on trends in detrital composition to illustrate the link between *nascent* tectonics and sedimentary basin fill (Krynine, 1948; Folk 1974)). Krynine linked detrital composition of sandstones with tectonic setting and proposed a series of petrographic-tectonic sandstone clans.

Stratigraphers developed regional correlations, reconstructed paleogeography and investigated synchronic, stratigraphic cycles in stratigraphy to understand the link between nascent tectonics and sedimentation. Sloss et al. (1949) and Krumbein and Sloss (1963) introduced sedimentary facies analysis to improve regional correlation methods

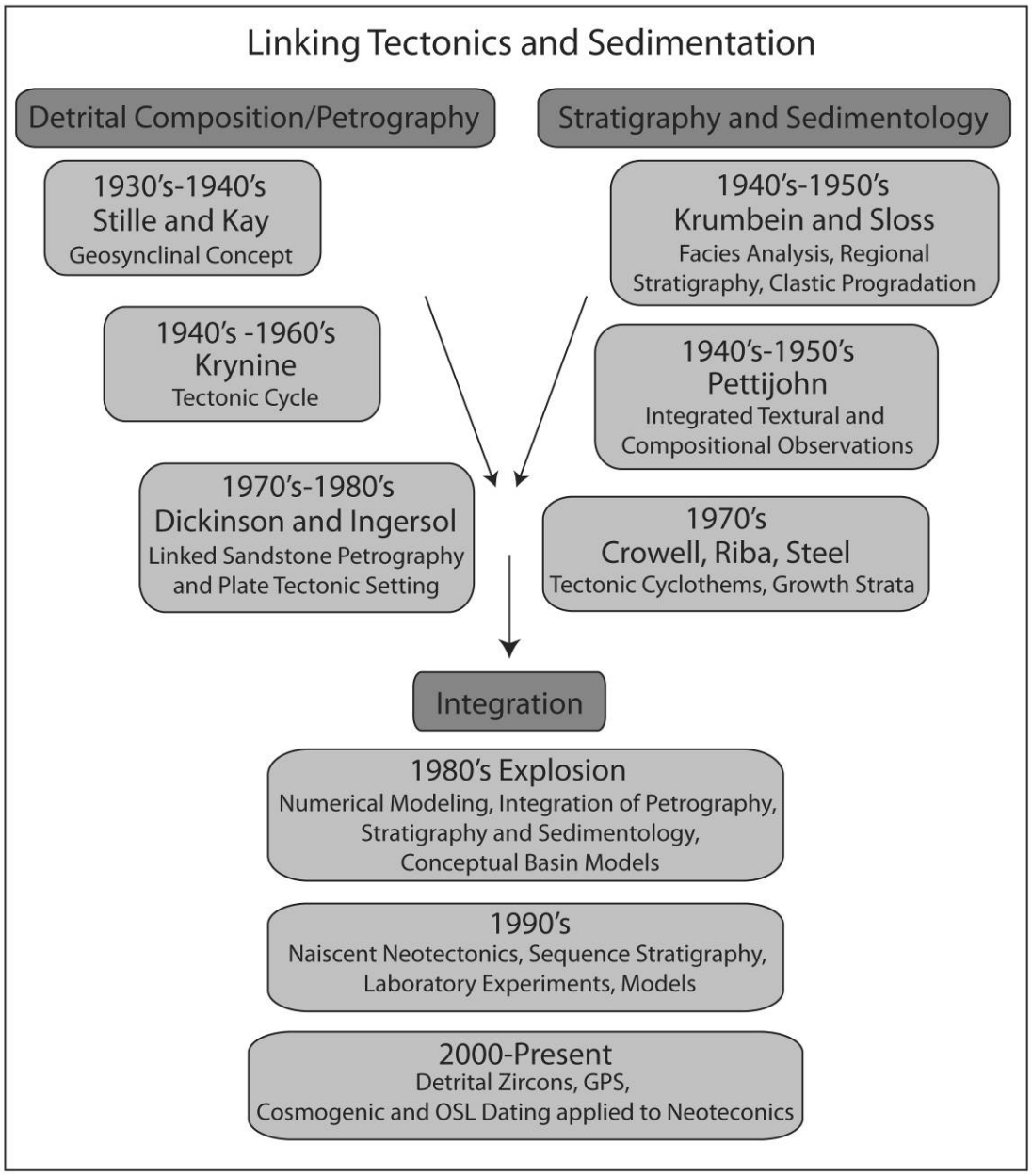

Figure 2.1 A general overview of the evolution of tectonics and sedimentation as a discipline. Note that this is intended to be a *gross summary*, not a comprehensive list of all those who contributed significantly to the development of tectonics and sedimentation.

and paleogeographic reconstruction. Pettijohn (1964) placed emphasis on sedimentary structures and paleocurrent analysis, and later integrated paleocurrent and petrographic analysis to reconstruct paleogeography and sediment source areas. Sloss (1972, 1979) recognized discrete stratigraphic sequences of Phanerozoic sedimentary rock that corresponded to specific tectonic events, and postulated that stratigraphic patterns were related to eustasy and tectonics; concepts that are still debated.

The emergence of plate tectonic concepts in the 1960-1970's provided much-needed insight into the relationship between tectonics, mountain belts and the accumulation of sediment. One of the first true links between modern plate tectonic concepts and sedimentary basins used detrital sandstone composition to define progressive changes in the plate tectonic setting (Dickinson and Rich, 1972; Dickinson and Suczek, 1979; Ingersoll, 1983). At about the same time, stratigraphers developed better regional correlations, facies analysis and paleocurrent analysis for better paleogeographic reconstructions and began investigating external controls on stratigraphic cycles (Figure 2.1). In the 1970's R. Dietz reevaluated geosyncline classification in the context of plate tectonics, and proposed "miogeocline" and "eugeocline" instead of the classical mio- and eugeo*syncline*s.

John Crowell (1974) was at the forefront of linking stratigraphy and tectonics. He recognized patterns in conglomerate composition that helped reconstruct motion along the San Andreas fault (i.e., "conveyer-belt model"). Crowell's pivotal work on the San Andreas fault indicated that strike-slip fault systems were much more complex, and can have much larger displacements than previously thought.

Riba (1976) proposed a direct link between structural development and successions of progressively rotated, flattening-upward strata that contain internal discordances. Steel et al. (1977) described similar tectonic cyclothems (ca. 50 Ky

duration), in alluvial strata within the Hornelen Basin that record the vertical component of fault motion and subsidence of the basin (Figure 2.2). Furthermore, Steel (1988) recognized the lateral component of fault motion using the "skewness" (e.g., strike-directed offset) in alluvial fan bodies that follow the lateral fault motion. Later, Anderson and Cross (2001) recognized growth strata corroborated the strong tectonic influence on Hornelen basin cyclothems. Recognition of tectonically controlled stratigraphic stacking patterns inspired numerous subsequent studies, and provided a key tool in basin analysis. Most notable, S. Prosser (1993) linked depositional systems and systems tracts with specific stages of extensional basin formation.

Numerous advances in tectonics and sedimentation were made in the 1980's and 1990's, including models of intra-basin subsidence (e.g., Beaumont, 1981; Jordan, 1981; Flemings and Jordan, 1989), integration of seismic stratigraphy (e.g., Vail, 1976) and neotectonic studies. Advances in understanding the long-term controls on basin-fill architecture using quantitative models and flume experiments provided insight into the roles of tectonic and non-tectonic processes on stratal architecture (Paola, 2000). Furthermore, integrative studies of tectonics and sedimentation became more common, typically using detrital composition, facies analysis and detailed startigraphic analysis (e.g., Haley, 1985; Graham et al., 1986; Schmitt and Steidtmann, 1990; DeCelles et al., 1995). More recently, dating and fission track analysis of detrital minerals, geochemical and paleobotanical methods for paleoaltimetry determination, cosmogenic nuclide dating, GPS measurements and advanced numerical modeling have furthered our understanding of tectonics and sedimentation in modern and ancient settings.

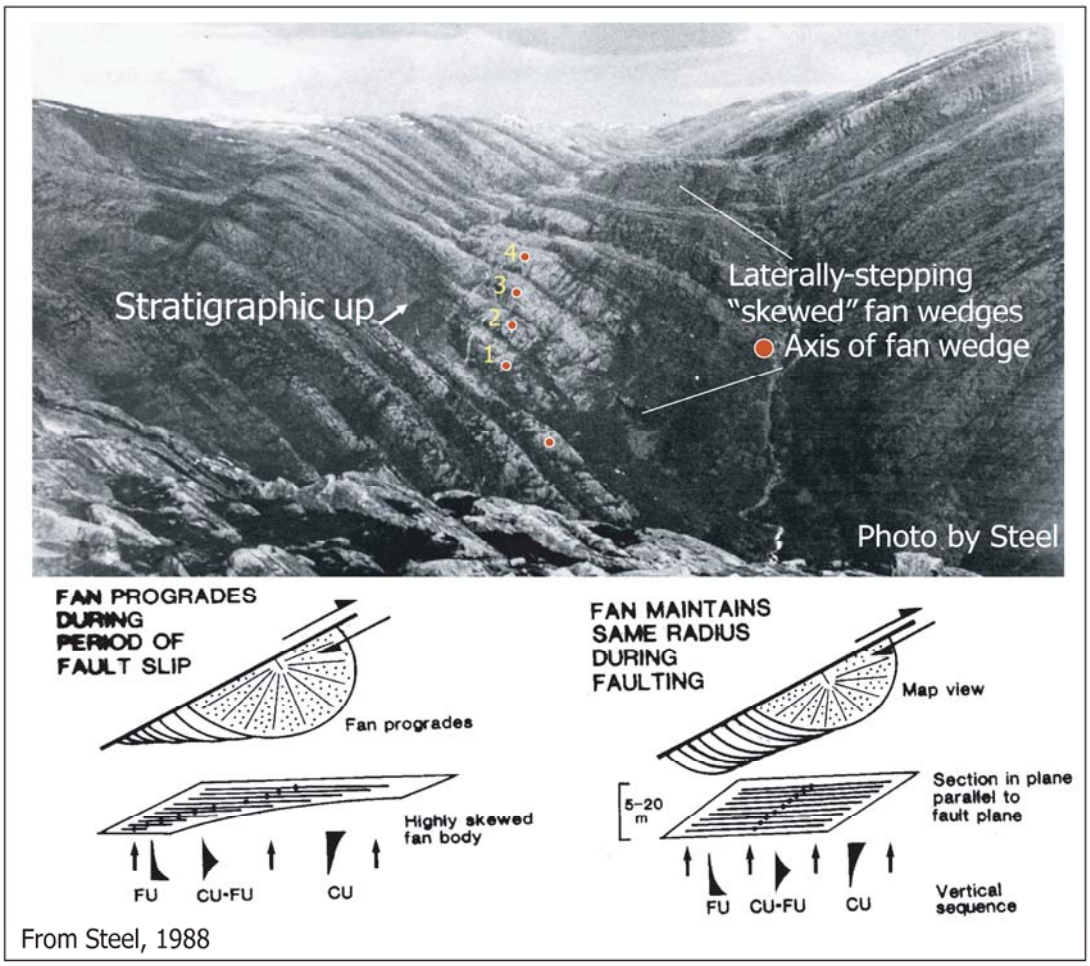

Figure 2.2 Summary of tectonic cyclothems, and "fan skewness" recognized in the Hornelen Basin, Norway. Vertically stacked cyclothems record the vertical component of fault motion. Laterally translated, or "skewed", fan bodies record the lateral component of fault motion. Notation: Fining-upward succession (FU); Coarsening-upward succession (CU). Numbers indicate individual "fan-bodies" and outline their lateral-stepping nature. (From Steel, 1988).

CLASSIC STRATIGRAPHIC SIGNATURES OF TECTONICS

Growth Strata and Thinning Trends

Progressive unconformities, or growth strata, can be produced synchronously with incremental structural development (Figure 2.2). "Growth strata" can develop adjacent to all types of faults, folds and diapirs (McClay, 1992; Ford et al., 1997; Giles and Lawton, 2002; Verges, 2002; Ford, 2004 among others). Phases when structural uplift is greater than sedimentation limbs are progressively rotated and involved into the structure; these strata are later onlapped and overlapped by when sedimentation exceeds uplift. Repetition of this process results in a distinctive fanning of dips and progressive angular unconformity development. The resultant strata with syntectonic unconformities are termed a "progressive unconformity" after Riba (1973) or "growth strata" after McClay (1992) and Suppe et al. (1992) and Zapata and Allmendinger (1996).

Growth strata have been utilized in a number of tectonic settings including salt diapir-influenced settings (Giles and Lawton, 2002), fold and thrust belts (Burbank and Verges, 1994; Ford et al., 1997; Fernàndez et al., 2004; Horton et al., 2004 among many others) and extensional settings (Gawthorpe and Hardy, 2002). The location, geometries, and scale of the resultant growth structure supplies information about the types and kinematic histories of structures (e.g., Bernal et al., 2004). Contractional and salt-uplift growth strata are recognized by a wedge-shaped (generally thinning toward the structure) succession with distinctive fanning of dips (or, incrementally rotated beds) and localized unconformity-bound packages. In outcrop, dip changes are most apparent and take attention away from more subtle unconformities that can develop when uplift rates are slower or sedimentation is higher (Aschoff and Schmitt, 2008). In seismic data small changes in dip are difficult to detect and Subtle-type syntectonic unconformities cannot be distinguished from autogenic unconformities. Extensional growth strata are wedge-

shaped successions (generally thickening toward the structure) distinctive fanning of dips (or, incrementally rotated beds) and localized unconformity-bound packages. Growth-faulted strata are a specific type of growth strata that develop adjacent to syndepositional, listric normal faults in high-supply depositional settings. Growth-faulted strata are most similar to extensional growth strata in that they tend to thicken toward the uplifted footwall and thin toward the rotated hanging wall (Lopez, 1990).

Numerous studies have relied on growth strata to delineate the structural histories of mountain belts and understand kinematics of a wide array of geologic structures. Some of the most widely known examples are from Spanish outcrop studies (Figure 2.3). Crowell (1974), Riba (1976), Steel et al. (1977) and Anadon et al. (1986) were among the first to fully understand the importance of growth strata, even though few studies used the terminology. Growth strata provide unequivocal evidence of syndepositional deformation because the strata are progressively integrated with the growing structure. Furthermore, these successions are easily recognized in outcrop and subsurface datasets. However, there are some practical limitations to consider.

Four main attributes of growth strata limit their application as tectonic signatures: (1) low preservation potential in contractional settings, (2) local development, (3) small scale, sometimes below seismic resolution, and (4) along-strike variation in growth strata (Figure 2.4) First, because growth strata develop adjacent to active structures, their preservation potential can be low; this is the case in contractional settings and in the early phases of rift development. As such, in orogenic belts most growth strata are found at the front of fold-thrust belts adjacent to the younger structures.

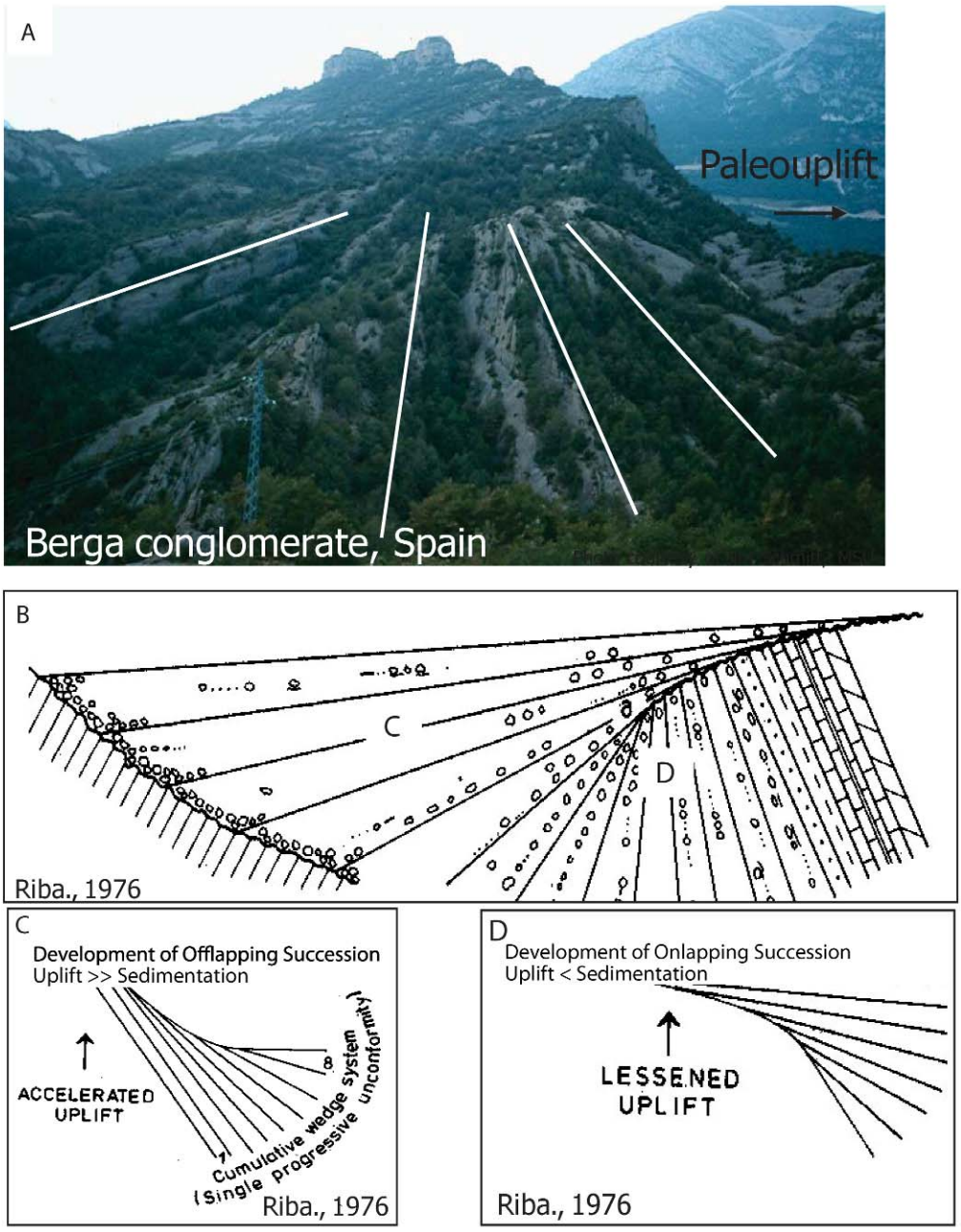

Figure 2.3 A. The classic outcrop of the Berga conglomerate, Spain where Riba (1976) defined progressive unconformities. B. Sketch of key surfaces in growth strata (Riba, 1976). C. Schematic illustration showing the development of an“offlapping cumulative wedge system” during accelerated uplift. D. Schematic diagram showing the development of an “onlapping cumulative wedge system” during reduced uplift.

However, locally, growth strata are found in the interior of mountain belts (Horton et al., 2001). Second, growth strata generally develop within a few kilometers of the structure. Such local development makes the structures easy to overlook in a large area, and only allows interpretation of a single structure, unless multiple locales are integrated. The small scale of growth strata (generally less than15 km) can also make them difficult to recognize in subsurface datasets. This is especially true when growth strata develop adjacent to short-lived structures that may have influenced a relatively thin stratigraphic interval that is below seismic resolution. been only recently addressed by Bernal et al. (2004).

Numerical modeling (Patton, 2005) suggests that angularities within growth strata are somewhat diminished if regional subsidence or sea-level rise creates accommodation space above a growing structure. When high regional accommodation is coupled with high sedimentation, thinning may be the only signature of structural development, despite no change in uplift rate. Thinning trends are routinely used to infer the timing and relative influence of structural development. For example, Lawton (1983) used stratal thinning patterns to interpret the timing of a Laramide structure in the Cordilleran foreland basin. Also, Aschoff and Giles (2005) used thinning trends to interpret the relative uplift of salt diapirs in La Popa basin, Mexico (Figure 2.5).

Detrital Composition

McBride (1963) proposed that all sedimentary rocks have three primary attributes including: composition, texture and structure. Since the 1970's, the importance of sandstone and conglomerate composition has been emphasized as a powerful indicator of paleogeography and paleotectonics (among them: Dickinson and Rich, 1972; Dickinson and Suczek, 1979; Ingersoll, 1983). Dickinson et al. (1986) suggested that application of

a petrofacies method can be used to 1) separate detrital contributions from mixed source areas, 2) detect successive stages in basin evolution and 3) identify significant tectonic transitions.

Recent studies by Lawton et al. (2003) provide a reminder that sandstone petrography and dispersal data are important for fluvial sequence analysis because these data record the source-area evolution and resultant sediment dispersal. Without such data, architecturally similar, compositionally distinct fluvial successions can be wrongly interpreted as a contiguous, time-equivalent fluvial system, thereby yielding misinterpretations of the tectonics.

Lawton et al. (2003) documented deposition of amalgamated fluvial channel successions coeval with movement along thrust-belt structures based on the temporal relationships of thrust-belt structures and fluvial deposits. Furthermore, the authors noted the importance of compositional and dispersal direction congruence in overlying and underlying strata. Lawton et al. (2003) proposed that tectonically driven basinward-shifts in amalgamated fluvial sandstone packages could be differentiated from climatic- and eustatically driven shifts based on integrating changes in sediment type, sediment dispersal and architecture. Although climatic and eustatic controls can cause changes in fluvial architecture, these processes are less capable of changing sediment composition and dispersal. Lawton et al. (2003) defined “Incongruent Shifts” that signify a surface that marks a change in dispersal direction, composition and architecture; these shifts were interpreted to indicate a change in tectonics/basin subsidence based on the change in composition and dispersal. Interpretation of tectonics based solely on stratal architecture, composition or sediment transport direction is subjective. However, Lawton et al. (2003) showed that stratal architecture and sediment transport direction coupled with vertical changes in sandstone composition provides a more reliable signature of tectonics.

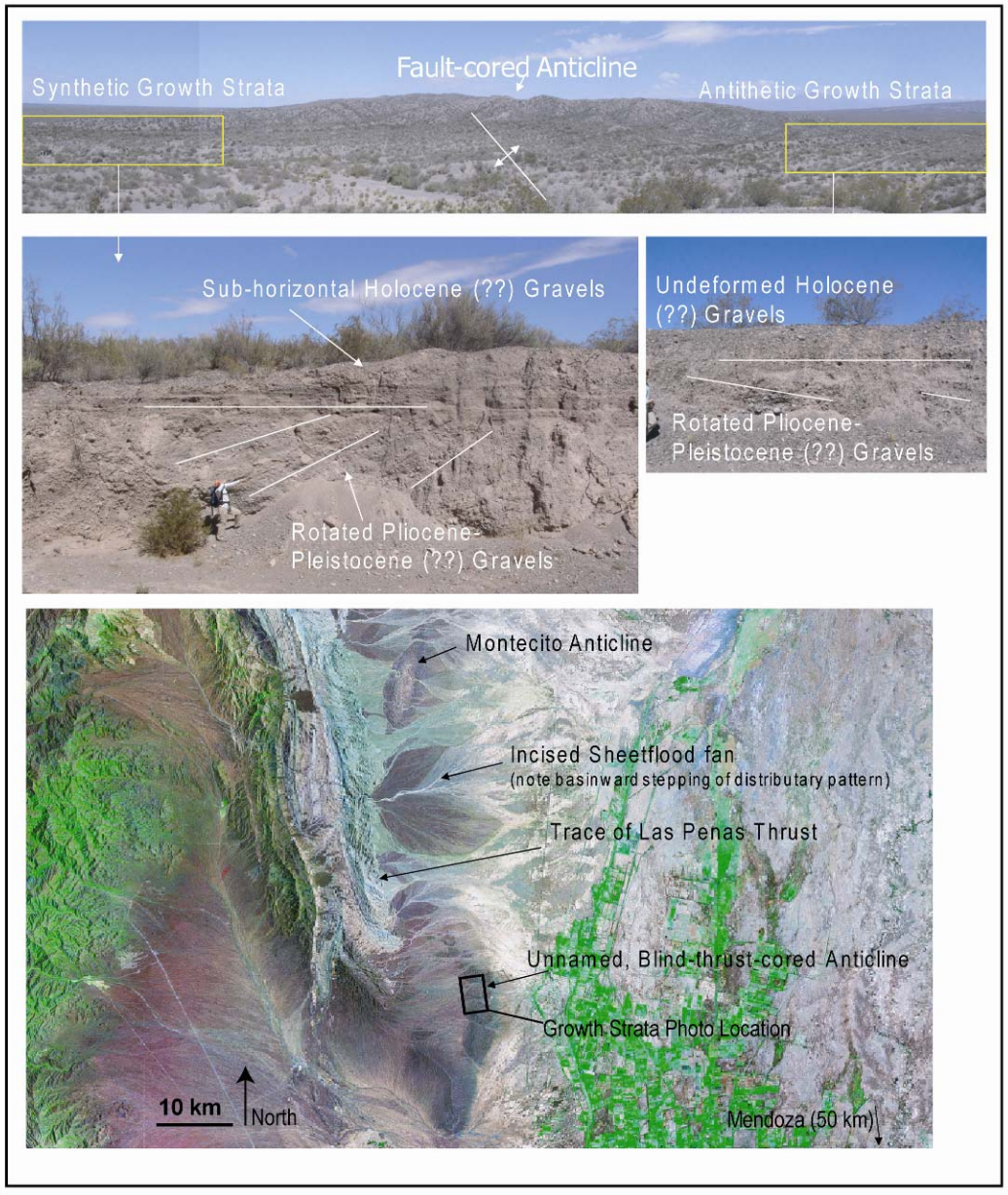

Figure 2.4 Examples of growth strata adjacent to an active thrust-cored anticline at the front of the Precordillera, Argentina. Note that the anticline has been breached by younger drainages and growth strata are being destroyed. Satellite image from NASA.

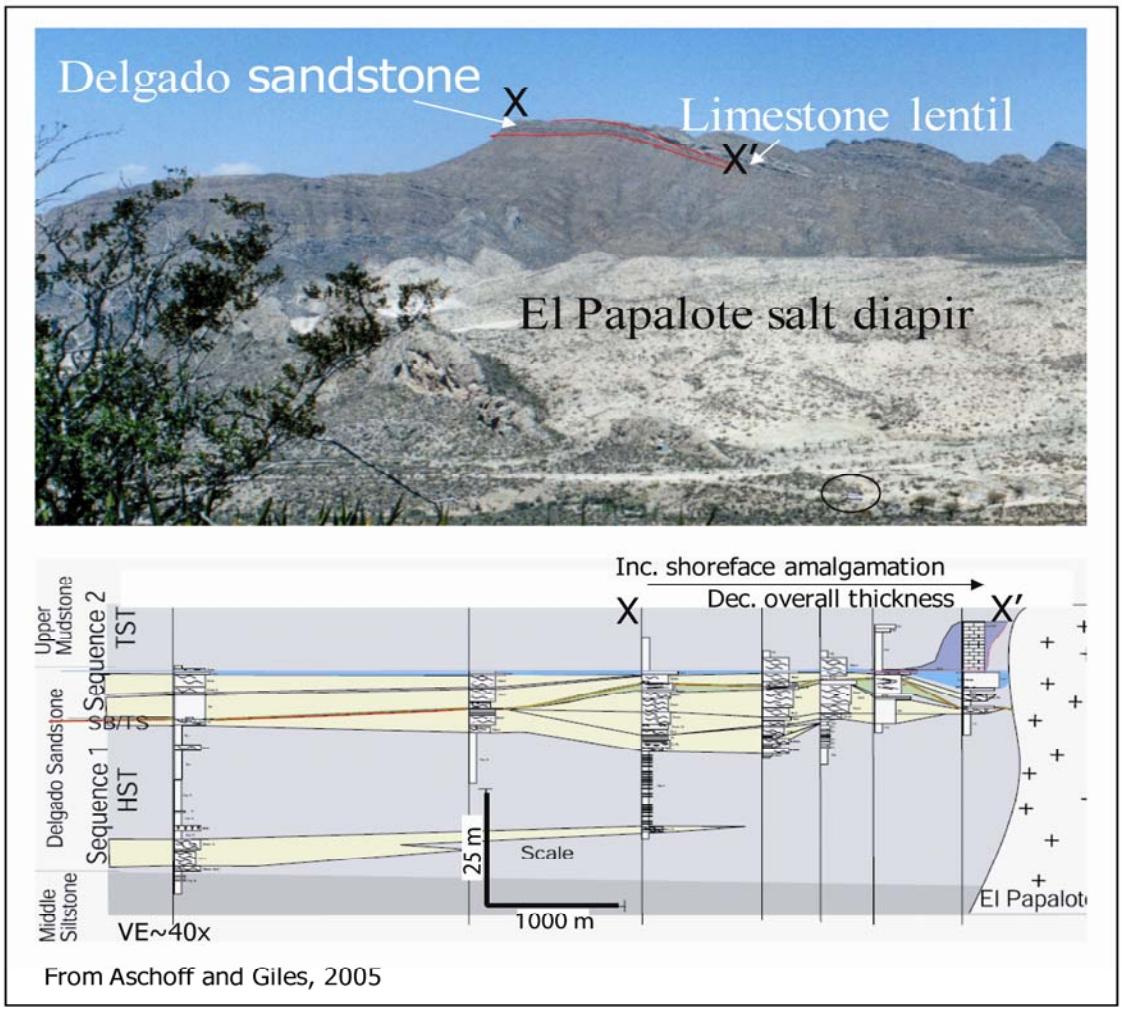

Figure 2.5 Cretaceous-Tertiary stratal thickness trends adjacent to a salt diapir, La Popa basin, Mexico. The upper diagram shows thinning trends in outcrop. The lower diagram shows a stratigraphic cross section X-X' of the same strata approaching a salt diapir that formed sea-floor relief during deposition

Conglomerate composition is another important record of tectonics because clast lithologies record the rock types exposed the sediment source area. Graham et al. (1986) and DeCelles (1988) proposed methods of provenance modeling, each designed to accommodate datasets with varying degrees of completeness. The common theme in provenance modeling is that progressive unroofing of the hinterland is recorded by the vertical succession of clast types. By comparing the synorogenic clast-type stratigraphy with several unroofing models identifies the most plausible unroofing rate and mechanisms. Although rarely preserved due to the complex and cannibalistic nature of fold and thrust belts, unroofing sequences (sensu Royse et al., 1975), also provide information about specific stratigraphic successions exposed within uplifts. The introduction of recycled clasts (e.g., clasts of synorogenic conglomerate) indicates uplift and reworking of synorogenic sediments. When coupled with facies, growth strata and paleocurrent analysis, conglomerate composition is a useful tool to interpret tectonics.

Sediment Dispersal and Paleocurrents

Depositional systems reorganize themselves in accordance with spatial and temporal patterns in accommodation. The location, character and orientation of depositional systems act as a tracer of spatial accommodation trends. In extensional basins, Leeder and Gawthorpre (1987) and Ravnås et al (1997) proposed that depositional facies belts and the character/extent of depositional systems are primarily controlled by the activity and geometry of basin-margin faults. Their models predict that subsidence is greater adjacent to the footwall of an active normal fault, and causes fluvial systems to follow the trend of the fault and aggrade adjacent to the footwall. In the Ridge Basin (pull-apart basin type), Crowell and Link (1982) showed a thickness (>5,000 m) of alluvial fan and lacustrine facies along the San Gabriel Fault, where alluvial fan facies were most proximal to the fault and lacustrine facies were more distal.

Paleodrainage patterns have been used to interpret the relative control of regional flexure and local structural development. Several studies have suggested that local structures cause deflection of fluvial systems around an active structure (Figure 2.6) (Burbank et al., 1996; DeCelles, 1986). Additionally, Holbrook and Schumm (1999) noted that rivers change their longitudinal profile, channel pattern, cross-sectional geometry, and can have preferential aggradation on the up-dip side, and degradation on the down-dip side of uplifts. Clustering of fluvial channels and aggradation of fluvial deposits were recognized adjacent to faults and lineaments (DeCelles, 1986; Meyers et al., 1992; Kvale and Vondra, 1993), and are predicted in rapidly subsiding parts of basin models (Paola, 1988; Jervey, 1991; Heller et al., 1993).

Paleoflow analysis has been applied in numerous areas, including the Ebro Basin, Spain and the Cordilleran foreland basin, USA (Lawton, 1983; Burbank et al., 1988; Steidtmann and Schmitt, 1988; Lawton et al., 1999). Furthermore, stratigraphic changes in paleoflow are also used to infer the stratigraphic position of tectonically generated sequence boundaries (Lawton et al., 2003). Dalrymple (2002) suggested that incised valleys often follow important structural trends. Structural control on paleo-valley orientation was supported by data from the Western Canada Cordilleran foreland basin (Plint and Wadsworth, 2006). This was one of the first to distinguish signals of local structural influence from those produced by regional flexure. Plint and Wadsworth (2006) found that paleo-valley orientations are influenced by forebulge uplift when flexural subsidence is generally high, but less influenced when flexural subsidence is low. Additionally, paleo-valley patterns mimicked the patterns of rectilinear faults only during times of low flexural subsidence.

Spatial Lithofacies Patterns

Some of the first studies to consider the influence of structure on adjacent stratigraphy relied on the spatial distribution of lithofacies, in a general sense, to interpret the location of highlands. Generally, coarse-grained facies were thought to develop near uplifts, and were used to infer the relative location of uplifts. Heller et al. (1988) suggested that the orientation of depositional systems change in response to tectonics due to spatial variation in accommodation. Specifically, their model applied to foreland basins predicts that during times of tectonic uplift, accommodation is greatest directly adjacent to the culminating structure causing fluvial systems to hug the edge of the fold belt adopting a longitudinal trend. By contrast, during times of tectonic quiescence erosional unroofing of the orogen induces isostatic rebound reduces the amount of space available for sediment deposition and preservation in the proximal zone, thereby causing transverse depositional systems to develop. However, this model is contested by numerous studies and does not consider the down-dip stratigraphic response to the reorganization of up-dip systems.

Recent work by Clevis et al. (2004a, b) suggested that, in the Tremp-Ainsa Basin, up-dip depositional systems are structurally translated atop basin-propagating thrust sheets. Phases of basinward translation cause progradation of deltas and can change the orientation of the delta systems, depending on the structural geometry. Additionally, these authors noted that during times of tectonic quiescence, flexural subsidence becomes more important because it creates accommodation and causes deltas to retreat, thereby starving the distal basin.

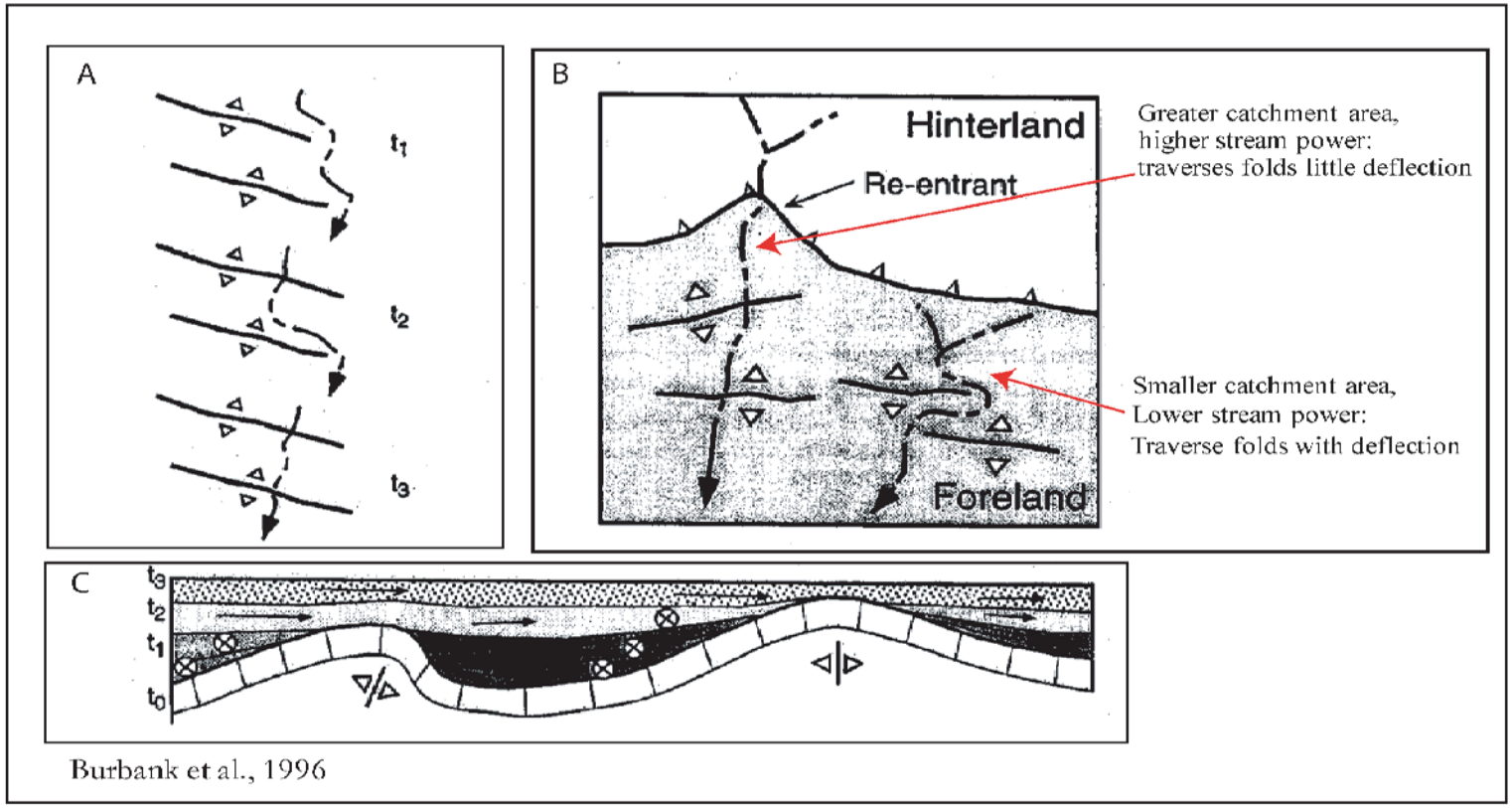

Figure 2.6 A. Decreasing deflection of fluvial systems around uplifting anticlines with increasing stream power. B. Comparison of high-power (left) and low-power (right) fluvial deflection across uplifting anticlines. C. Schematic of fluvial deflection and paleocurrent through time. (From Burbank et al., 1996).

Clastic Progradation

In the context of foreland basin models, progradation of clastic material into a sedimentary basin was generally assumed to be coeval with uplift at the basin-margin until the 1980's. Heller et al. (1988) challenged the traditional "syntectonic" paradigm, and suggested an "antitectonic" model where isostatic rebound of the basin was responsible for clastic progradation, not hinterland uplift. However, the antitectonic model was challenged by others who documented clastic progradation synchronous with tectonics (Burbank et al., 1988; Horton et al., 2004). Two opposing viewpoints eventually developed: (1) that sedimentation and clastic-wedge progradation is synchronous with hinterland uplift (Burbank et al., 1988; Marzo and Steel, 2000), and (2) that clastic progradation lags behind hinterland uplift due to initially high foredeep subsidence associated with orogenic wedge thickening (Heller et al., 1988; Blair and Bilodeau, 1988; Flemings and Jordan, 1990).

The "syntectonic" model predicts that coarse sediment is produced and distributed in the adjacent basin during times of uplift new material is available for erosion (Figure 2.7). The model predicts that strongly progradational stacking patterns in the basin fill correspond with times of active uplift or tectonism, and the preferential yield of sediment. Alternatively, the "antitectonic" model proposes two general phases of foreland basin evolution (Figure 2.8). In this model, the first phase produces uplift-derived, coarse-grained sediment, but this is deposited adjacent to the thrust front where subsidence is greatest during thickening of the orogenic wedge. When rates of tectonic movement slow, foredeep subsidence decreases and highlands are eroded. Regional isostatic rebound of the basin reduces accommodation and allows clastic material to prograded out of the foredeep. Hence, in the latter model the major progradation of coarse-grained sediment occurs during quiescence in the thrust-belt. The main assumptions in both

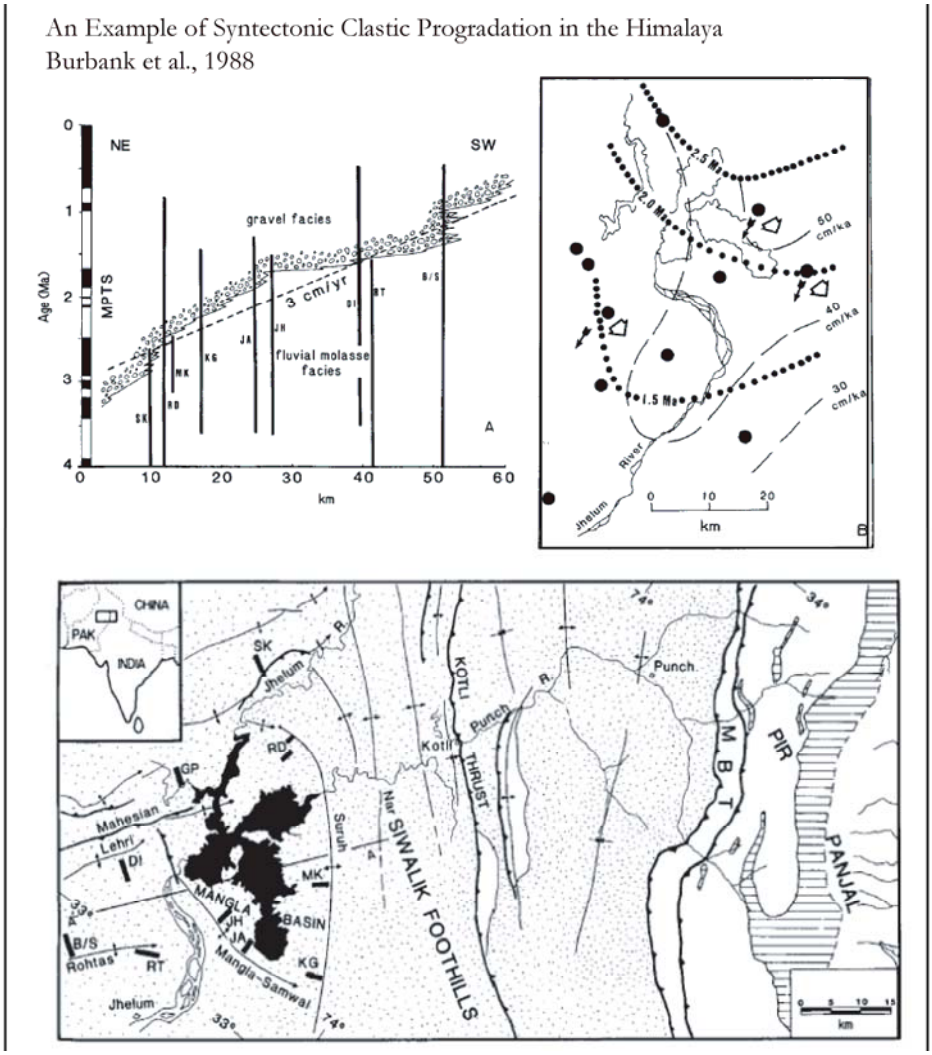

Figure 2.7 Summary of the “syntectonic” model for clastic progradation (From Burbank et al., 1988).

models are that that the source rock is erodible, and that the sediment can be transported.

Syn- and anti-tectonic models of progradation only focus on the tectonic controls, not all of the possible external controls on basin-fill. This is a critical point because Flemings and Jordan (1989) provide numerical models that suggest progradation can be caused by 4 main drivers: (1) increased erosion rate, (2) increased transport efficiency, (3) lower thrust velocities and (4) larger flexural rigidities. Marzo and Steel (2000) provided outcrop evidence supporting the Flemings and Jordan models; their study indicated that extensive clastic progradation can occur during intervals of highest subsidence rates when sedimentation rates are very high. The response of clastic progradation to tectonics remains unclear, yet numerous studies still use the presence of clastic wedges to infer tectonics.

Stacking Patterns, Vertical Stratigraphic Amalgamation and A/S Ratio

Stratigraphic stacking patterns and internal architecture are sensitive indicators of accommodation, or the space made available for sediment accumulation (Jervey, 1988; Paola, 1988). In many basins, accommodation can be created by raising sea-level or by tectonic subsidence. The resultant stratal architecture can be explained with the A/S ratio (accommodation/sediment supply ratio), relating accommodation to the amount of sediment available to fill the space. Shanley and McCabe (1994) summarize the relationship between accommodation and sediment supply as follows: (1) when accommodation space is a positive value, architecture is governed by the relative rates of accommodation increase and sediment supply; (2) when accommodation space is zero, sediment bypass results; (3) when accommodation space is a negative value, erosion and incision are probable. Following this relationship, when accommodation space is limited, alluvial systems laterally and vertically amalgamate forming sheet-like or “nested” sandstone body architectures, depending on the specific type of depositional system;

when accommodation space is high alluvial systems are more stable, thus preserving thicker muddy successions within which isolated sandstone bodies occur (Miall, 1996). Martinson et al. (1999) used cyclic variations in fluvial architecture of the Upper Cretaceous Ericson Sandstone and A/S ratios to infer base-level change related to the repeated uplift of the Wind River Range. Furthermore, these authors linked the low preservation of point bars, channel and floodplain to periods with low A/S ratios; conversely, better preserved bars, channels, floodplains coupled with more channels, and thicker successions are attributed to periods with high A/S ratios.

Stacking patterns, fluvial architecture and paleosol development are also the basis for sequence stratigraphic interpretations of nonmarine strata because such patterns are sometimes more easily recognized than regional unconformities (Shanley and McCabe, 1994). These characteristics are interpreted as a direct reflection of the A/S ratio and provide a means to investigate accommodation.

SUBTLE SIGNATURES OF TECTONICS

Evidence of Sediment Bypass (low sedimentation rates with longer residence time): Application of Paleosol Development and Preferential Cementation

Over the past 10 years, the value of paleosols in constructing sequence stratigraphic frameworks of nonmarine strata has been recognized. Blum and Tournqvist (2000) note that tectonics is the fundamental control on the organization of landmasses, development of sediment source areas and transport systems, thereby playing a key role in the accumulation of alluvial deposits. In addition to correlation purposes, paleosols are useful indicators of local and regional landscape evolution (McCarthy and Plint, 2003). Two aspects of paleosols are equally important, namely the “soil-forming stratigraphic interval” and detailed paleosol profiles.

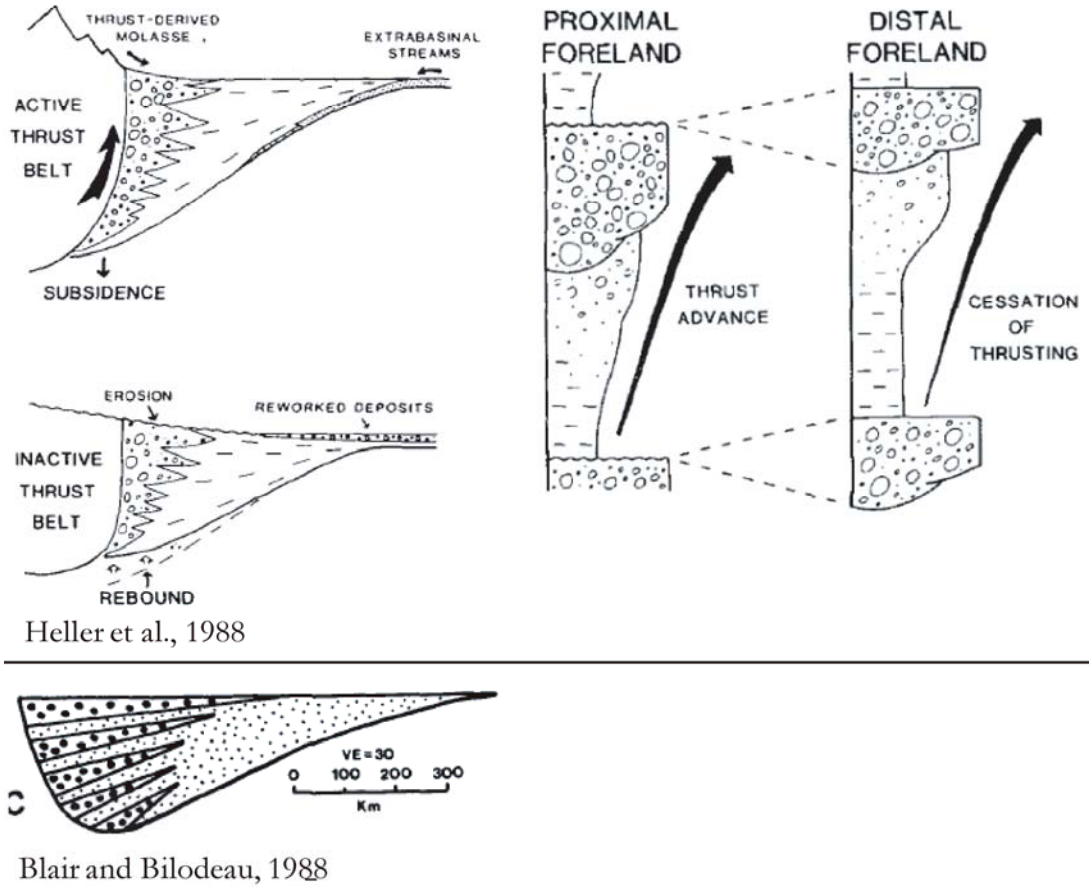

Figure 2.8 Summary of the "antitectonic" model for clastic progradation (From Heller et al., 1988; Blair and Bilodeau, 1988)

Paleosol-rich intervals are important markers for correlation and record stable interfluve surfaces that are characterized by low sedimentation and erosion rates (sequence boundaries). Investigations of detailed paleosol profile and chemistry provide information about river channel avulsion rates, climate, parent material and subsidence rates (Kraus, 2002). As such, locations and internal details of horizons with preferential paleosol development provide an important record of landscape evolution (McCarthy and Plint, 2003).

The presence, composition and morphology of early cements coupled with other early and preferential cementation features provide clues about sedimentation and base-level change. Taylor et al. (2000) showed a systematic relationship between sedimentation (related to relative sea-level fluctuation) and early and preferential cementation within the sequence stratigraphic framework of Book Cliffs strata, Utah. This study highlighted that laterally extensive carbonate-cemented horizons systematically occupy marine flooding surfaces. The authors attribute the carbonate-cemented horizon to pauses in sediment accumulation during marine flooding events. Ketzer et al. (2003) summarizes the distribution of several important cement types within a sequence stratigraphic framework and notes that long residence times, location of coal deposits and relative position of the meteoric water zone are important controls on the distribution of early and preferential cementation. For example, early carbonate cements are concentrated on flooding surfaces due to the low sedimentation rates and prolonged residence time required to thoroughly diffuse calcium ions. Kaolinite cements are closely related to meteoric water infiltration that can be tied to subaerial exposure and basinward shifting of the meteoric water zone (Ketzer et al., 2003).

In contrast to the recent studies that place cementation in a predictable sequence-stratigraphic context, McBride et al. (1995) have pointed out that the distribution of

calcite at the outcrop scale is chaotic and unpredictable in some sandstones. Although the significance of early and preferential cementation is controversial, the systematic distribution and interpretation of early and preferential cementation documented by some authors has potential as a subtle signature of base-level change when it is combined with other more reliable signatures such as growth strata, detrital composition and paleocurrents.

DISCUSSION

Two key aspects are commonly ignored in the debate about clastic progradation: 1) sediment supply and 2) scale of progradation. First, the volume of sediment yield relative to the space available may easily vary through time with climate, sediment transport efficiency and erodablility of source units. Sharp increases in sediment supply can overwhelm high subsidence rates causing extensive clastic progradation. For example, Marzo and Steel (2000) documented considerable (>100 km) clastic progradation during the period of highest subsidence due to very high sediment supply.

Second, spatial and temporal scales are important to consider when interpreting the influence of tectonics on the stratigraphic record. "Progradation" of clastic material can occur at the parasequence time-scale (<10,000 years), or at the sequence set scale (1-100 million years). Additionally, "progradation" may occur proximal to active structures (< ½ basin width; generally <100 km), or at a basin scale (> ½ basin width; generally >100 km). Progradation of a single alluvial fan (1-10 km) or fluvial megafan (10's-100's km) into a basin differs considerably from progradation of a complete clastic wedge (many constituent depositional systems) into a basin. In foreland basins, proximal (<100 km) uplift and basinward-propagation of thrust structures will cause proximal progradation. Yet, proximal crustal thickening will cause subsidence in the adjacent basin in a pattern that is determined by the flexural wavelength of the crust.

Controversy about the cause of clastic progradation has, in part, resulted from studies that argue for a syntectonic model or antitectonic model but present vastly different scales of progradation. Studies that suggest that progradation of clastic material lags behind structural development typically present basin-scale models (>200 km) and datasets on long time-scales (10's millions of years) (Heller et al., 1988; Flemings and Jordan, 1990; Jordan and Flemings, 1991). Conversely, Burbank et al. (1988) advocate a syntectonic progradation model, but present stratigraphic data relatively proximal to the hinterland (<100 km) on shorter time-scales (millions of years).

Additionally, subsidence mechanisms differ between basin types (Busby and Ingersoll, 1995). Differences in basin-margin and regional tectonic styles influence the spatial and temporal pattern of subsidence. In turn, this influences the distribution of depositional facies and vertical stratigraphic patterns. For this reason it is unreasonable to assume that tectonic signatures will be the same in all sedimentary basin types.

CONCLUSIONS

Tectonic signatures are characteristics within stratigraphic successions that indicate deposition coeval with tectonics. A wide array of tectonic signatures has been used to interpret the timing and style of structural development, including growth strata, detrital composition, lithofacies patterns, paleodrainage patterns, stratigraphic stacking patterns and clastic progradation. Although "tectonic signatures" indicate deposition coeval with uplift, they form by the interplay between tectonic *and* non-tectonic processes. The overprint of non-tectonic processes such as climate, sediment supply and eustasy can be profound on some "tectonic" signatures. For this reason, disentangling the role of tectonics is best approached using a complete suite of criteria, and understanding the limitations of each tectonic signature.

Growth strata are the best stratigraphic indicators of tectonics, and provide high-resolution kinematics of a wide array of geologic structures. The wedge-shaped, flattening-up successions are easily identified in outcrop and seismic datasets, and form by progressive uplift/tilting and subsequent onlap/truncation of depositional surfaces. However, this tectonic signature is only locally developed (< 10 km of the adjacent structure) and can be susceptible to destruction, and/or cannibalization, with continued uplift. As a result, nonmarine growth strata are usually only preserved adjacent to the youngest structures, and are only found within a few kilometers of the structure. Moreover, growth strata are modulated by regional accommodation patterns and sediment supply. Angularities within growth strata may be muted during times of high regional accommodation and sediment supply because sediment accumulation above the structure keeps pace with uplift; in this case, only a thinning pattern may result despite no change in the uplift rate. Hence, growth strata are useful indicators of local structural development, and provide a direct link to basin dynamics only when correlated with adjacent basin-fill.

Detrital composition is a traditional signature of tectonics, dating back to the geosyncline paradigm that first linked mountain belts with sedimentary basins. Provenance analysis of sandstones and conglomerates provides a direct correlation to tectonic setting, and the location and geology of the sediment source-area. However, detrital modes can be altered by physical and chemical destruction of labile grains. Grain destruction is especially important with increasing distance from the sediment source area and under humid climatic conditions when labile grains are preferentially removed, thereby biasing the stratigraphic record. Additionally, local input of sediment, particularly pedogenic carbonate grains, can overprint and/or alter the results of provenance analysis. Detrital composition is thus useful for interpreting the exhumation

of structures and tectonic setting; in this sense, detrital composition records structures that had relief and provided sediment.

In conclusion, determining the role of tectonics is best approached using a complete suite of criteria. However, stand-alone signatures of structural development and tectonics are growth strata, changes in detrital composition, paleocurrent shifts and thickness trends. Each of these signatures may be used alone to interpret deposition coeval with tectonics, with minimal limitation. Some important limitations of these tectonic signatures are 1) local development, 2) low preservation potential, 3) poor, or cryptic development distal to the structure, and 4) potential time-lag between structural uplift and the stratigraphic response.

Other tectonic signatures such as lithofacies patterns, paleodrainage patterns, stratigraphic stacking patterns and clastic-wedge progradation are also useful, but are likely to be overprinted by other modulating processes such as climate and eustasy. Integration of numerous tectonic signatures is the best practice for interpreting tectonics from the stratigraphic record. Additionally, integration of observations from proximal and distal zones of sedimentary basins, and multiple tectonic signatures provides the most complete interpretation.

Chapter 3: Distinguishing Syntectonic Unconformity Types to Enhance Growth Strata Analysis: An Example from the Cretaceous, Southeastern Nevada, USA

ABSTRACT

Two types of syntectonic unconformities are recognized in non-marine, Upper Cretaceous growth strata adjacent to the Willow Tank thrust in southeastern Nevada, USA. Unconformities with larger angular discordance (>10°, "Traditional Type") developed when uplift outpaced sediment accumulation. More subtle unconformities with less discordance (2-10°, "Subtle Type") developed when sediment accumulation nearly kept pace with uplift. Traditional Type unconformities are the focus of most growth strata studies because the discordances are obvious in the field. By contrast, Subtle Type unconformities are more difficult to identify. Subtle Type unconformities are mappable surfaces of erosion or non-deposition located within progressive, flattening-up stratigraphic successions, and are associated with clustering of large-scale (>1 m) soft sediment deformation features (possible seismites), better-developed or clustered paleosols, greater reworking and/or grain-size increase. Increasing sedimentation supply, in the presence of positive net accommodation, allows syntectonic deposits to aggrade above a growing structure despite no change in uplift rate. Aggradation across a structure is punctuated when uplift is slightly higher than sedimentation, producing subtle discordances (Subtle Type) with evidence of slope destabilization, seismicity, or longer residence time, instead of the Traditional Type angular unconformities. Identification of unconformity types in growth strata can document additional phases of uplift, particularly for intervals where sediments aggraded above an active structure due to higher sediment supply, and regional subsidence or sea level rise. Although these syntectonic

unconformity types are identified in non-marine, contractional growth strata, they are likely present in many other depositional and structural settings.

INTRODUCTION

Growth strata are proximal syntectonic successions that develop in response to the uplift, surface tilting, and erosional denudation of a wide array of geologic structures (Riba, 1976; Anadón et al., 1986; Burbank et al., 1996; Ford et al., 1997; Giles and Lawton, 2002; Hoy and Ridgway, 2002). Analysis of growth strata can determine phases, rates, and styles of uplift of a structure (Anadón et al., 1986; Holl and Anastasio, 1993; Burbank and Vergés, 1994; Vergés et al., 1996; Vergés et al., 2002; Fernàndez et al., 2004). Although there is some disagreement concerning the roles of fold-limb lengthening (kink-band migration) and fold-limb rotation mechanisms in fold-related growth strata generation (e.g., Erslev, 1991; Suppe et al., 1992; Hardy and Poblet, 1994; Ford et al., 1997), the value of information provided by growth strata analysis is undisputed.

Analysis of growth strata began with the recognition of syntectonic discordances, or unconformities (Riba, 1976). Riba (1976) classified these discordances as (1) "progressive" syntectonic unconformities, a succession of strata that flatten up-section but have no apparent dip discordance between beds, and (2) "angular" unconformities, surfaces that separate successions of strata with obviously different bedding dips. As originally defined by Riba (1976), a progressive unconformity is not a single unconformity, but a succession of strata. Few details were provided about the character of surfaces comprising the monotonous flattening-up successions (i.e., "progressive" unconformities). Angular discordances were not previously identified within the flattening-up successions described by Riba (1976), and subsequent studies (Suppe et al., 1997; Ford et al., 1997). However, recent numerical models predict differences in

syntectonic unconformities and growth strata geometries under different local and regional accommodation conditions (Patton, 2004).

Syntectonic unconformities with erosional, angular discordances ("Traditional Type" unconformity of this study) are the basis for many growth strata studies because the discordances are more obvious, and mark an increase in uplift relative to sedimentation. Holl and Anastasio (1993) pointed out that syntectonic unconformities were typically thought to be erosional, but that they could also form by continuous aggradation across a structure during deformation. In the latter case, a progressive unconformity results from progressive tilting of depositional surfaces with continued sedimentation, and may contain numerous, smaller dip discordances that are easily overlooked ("Subtle Type" unconformity of this study). Conceptually, progressive tilting of a depositional surface would be associated with seismicity, destabilization or steepening of depositional surfaces during tilting, and eventual shift of deposition away from high relief areas, thereby increasing residence time of sediments deposited in higher-relief areas. All of these processes are recorded in the details of the stratigraphy. Several studies link detailed sedimentologic analysis with growth strata development in contractional settings (DeCelles et al., 1991; Burbank and Vergés, 1994; Williams et al., 1998; Lawton et al., 1999). However, no sedimentologic criteria have yet been provided to guide field-based recognition of subtle surfaces that may be found within the seemingly continuous, flattening-upward successions.

This paper provides (1) a two-fold classification that includes traditional, "angular" syntectonic unconformities (Traditional Type) and subtle syntectonic unconformities (Subtle Type) within progressively flattening growth strata intervals, (2) objective sedimentologic criteria to distinguish both types of unconformities in non-

marine strata and (3) qualitative observations suggesting that sediment supply influences the type of syntectonic unconformity that develops.

GEOLOGIC CONTEXT

The southern Nevada segment of the Sevier thrust belt is a NE-SW trending belt of east-vergent thrusts and folds involving Paleozoic and Proterozoic sedimentary rocks (Bohannon, 1983; Axen et al., 1990; Taylor et al., 1993). The evolution of this segment of the Sevier thrust belt is difficult to unravel because it is overprinted by Neogene extensional deformation that created three distinct structural blocks including the Muddy-North Muddy Mountains, Las Vegas-Sheep Ranges, and Spring Mountains blocks (Bohannon 1983; Taylor et al. 1993). Upper Cretaceous foreland basin fill and growth strata are exposed primarily in the North Muddy Mountains structural block (Figures. 3.1a, 1b) near the eastern edge of the Sevier thrust belt and western edge of the Cordilleran foreland basin (DeCelles, 2004).

Structural features that likely influenced sedimentation in the study area include the Muddy Mountain thrust and its frontal splay, the Willow Tank thrust (Figures 3.2a, 2b). The Muddy Mountain thrust places a thick hanging-wall succession of Paleozoic carbonate rocks upon Jurassic sandstone (Figure 3.3). The Muddy Mountain thrust is thought to be laterally equivalent to the Glendale thrust to the north, and possibly the Keystone thrust to the south (Bohannon, 1983). The Willow Tank thrust is a frontal splay of this structure and is found approximately 12 kilometers northeast of the Muddy Mountain thrust trace in the North Muddy Mountains (Figure 3.2b). The Willow Tank thrust places the Jurassic Aztec Sandstone upon strata of the Lower Cretaceous (Albian) Willow Tank Sandstone that record earliest deposition in the Sevier foreland basin (Reese 1989).

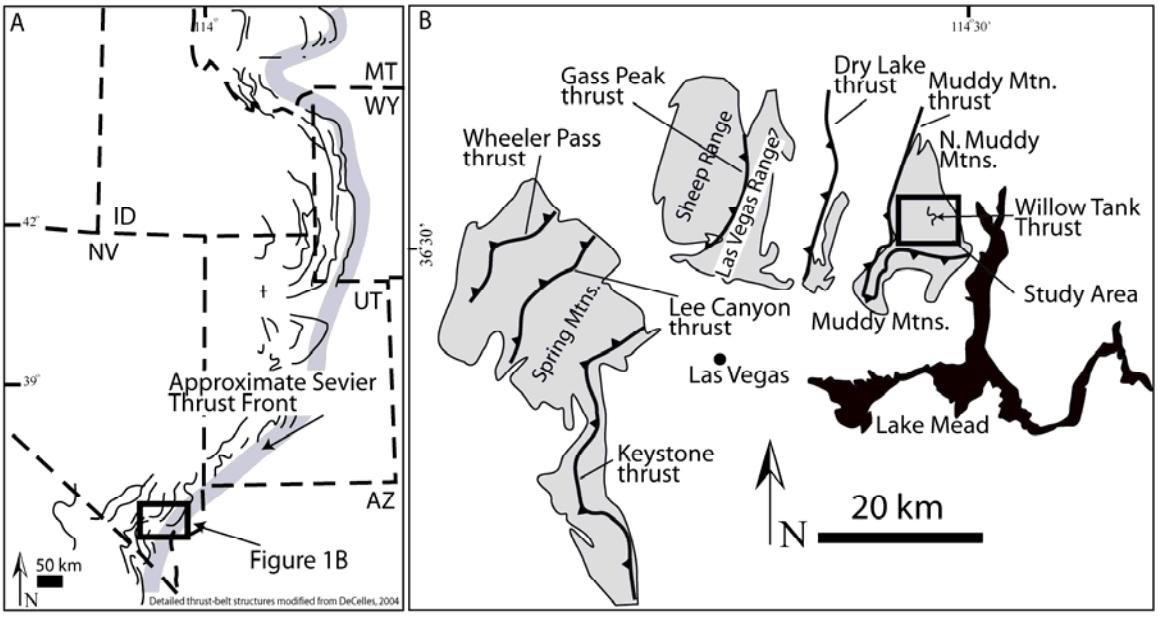

Figure 3.1 Location and geologic setting of study area. A. General location of the study area at the southern part of the North American Cordilleran Foreland basin. B. Detailed map showing key Sevier Fold-thrust structures with respect to the North Muddy Mountains study area (noted by dark box).

Growth strata are developed in the lower part of the White Member of the Baseline Sandstone and are present in the oblique-lateral footwall of the Willow Tank thrust. Locally, this thrust was later reactivated as a small displacement tear fault (Figure 3.4a). Stratal thinning toward the trace of the Willow Tank thrust and growth strata development suggest positive relief and vertical motion associated with the Willow Tank thrust allochthon. Presently, the Willow Tank thrust fault is near-horizontal (5-10˚), however the attitude of the fault plane is unclear due to lack of exposure.

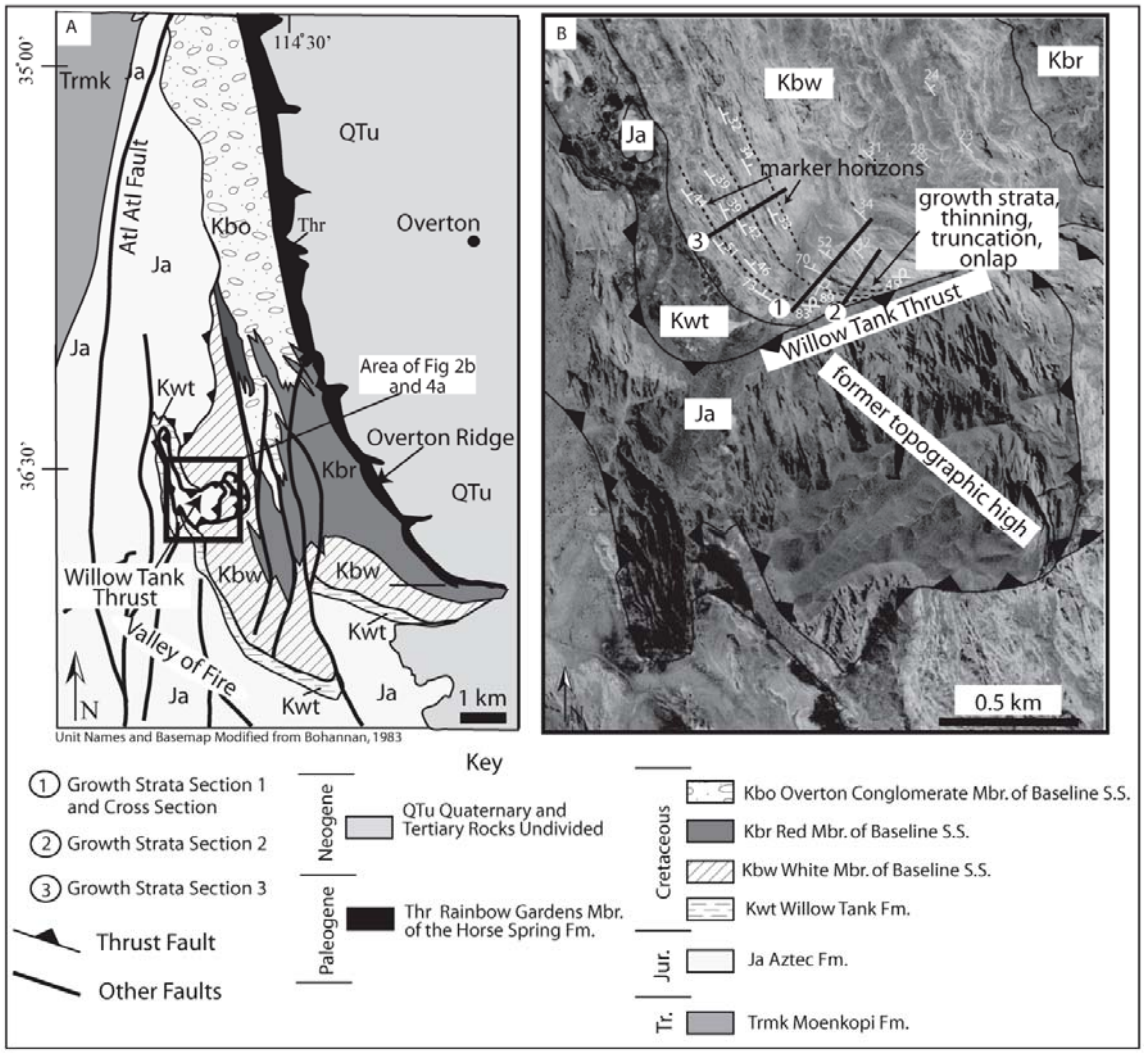

Figure 3.2 Detailed geologic map (A) and air photo (B) of the study area. The geologic map (A) shows the location and context of the Willow Tank Thrust (oblique-lateral ramp) responsible for growth strata development. Growth strata are located in the White Mbr. Of the Baseline S.S. (Kbw) on the northern flank of the Willow Tank Thrust. The ariphoto (B) shows the relationship between Aztec Sandstone, uplifted in the hangingwall of the Willow Tank Thrust, and the Baseline S.S.. Note the thinning, truncation and up-section decrease in bedding dip at locations 1-3 (measured sections in growth strata).

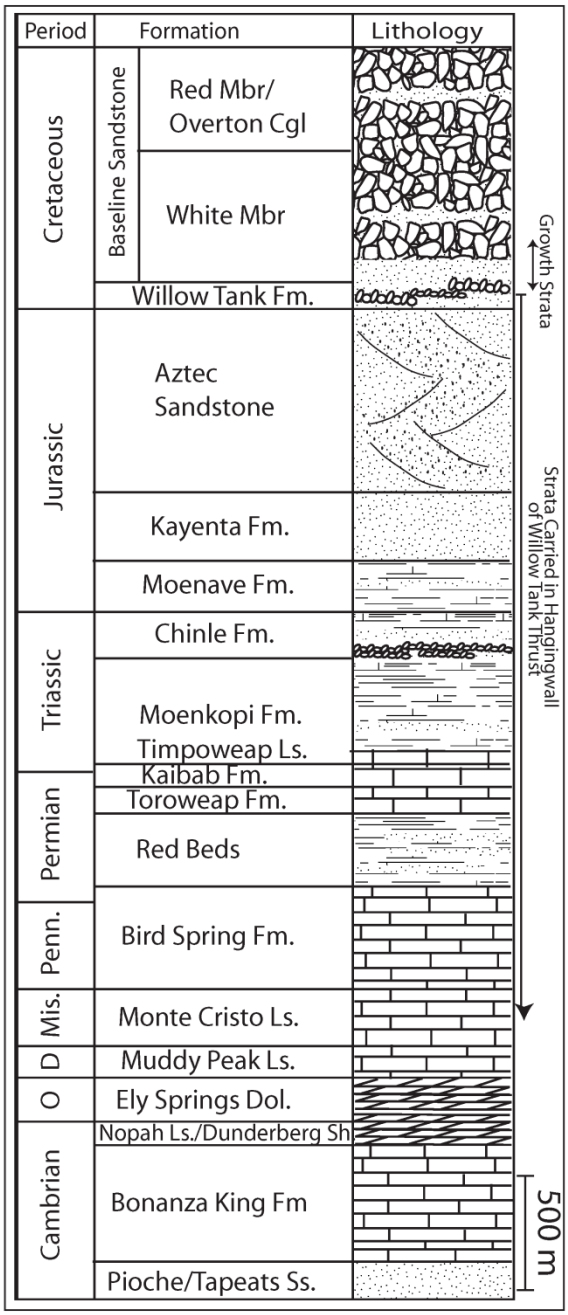

Figure 3.3 Generalized stratigraphic column for the North Muddy Mountains area, Nevada. Note that growth strata are developed in the lower part of the White Member of the Baseline Sandstone. Thrust faults uplift Jurassic- through Cambrian-aged strata; these units would have been the sediment source for the Baseline Sandstone.

Additionally, it is unclear if the Willow Tank thrust was reactivated during a younger phase of extension, as is suggested for other thrusts (Taylor et al., 1993). Carpenter (1989) bracketed motion along the Willow Tank thrust between 95.8 and 93.1 Ma based on radiometric dates of ashes found within the youngest and oldest deformed rocks but did not recognize the growth strata.

GROWTH STRATA

The growth strata described in this study are identified based on the presence of a northeast-tapering wedge of strata characterized by a progressive, decreasing upward trend in bedding dip (from 7˚ OT to 24˚). Figures 3.4a-c show the geometry of these growth strata in map-view and cross-sectional view, respectively. The flattening-upward pattern within the lower part of the White Member of the Baseline Sandstone is shown on geologic maps compiled by Bohannon (1983) and Carpenter (1989) (Figures. 3.2a and 2b) and in a detailed measured section (Figure 3.5). The air photo (Figure 3.4a) highlights syntectonic unconformity-bound strata that onlap and thin toward the trace of the Willow Tank thrust in the southeast.

The Cretaceous stratigraphic section in the Willow Tank thrust autochthon was subdivided into pre-, syn-, and post-growth strata (sensu Burbank et al., 1996). This subdivision allows comparison of depositional character in relation to the timing of uplift of the Willow Tank thrust allochthon. Pre-growth strata (Willow Tank Formation) were deposited before local deformation by the Willow Tank thrust Pre-growth strata, are locally involved in deformation and do not show progressive thinning or changes in attitude. Syn-growth strata (White Member of the Baseline Sandstone), referred to more simply as “growth strata”, were deposited coeval with uplift of the hanging-wall anticline in the Willow Tank thrust allochthon.

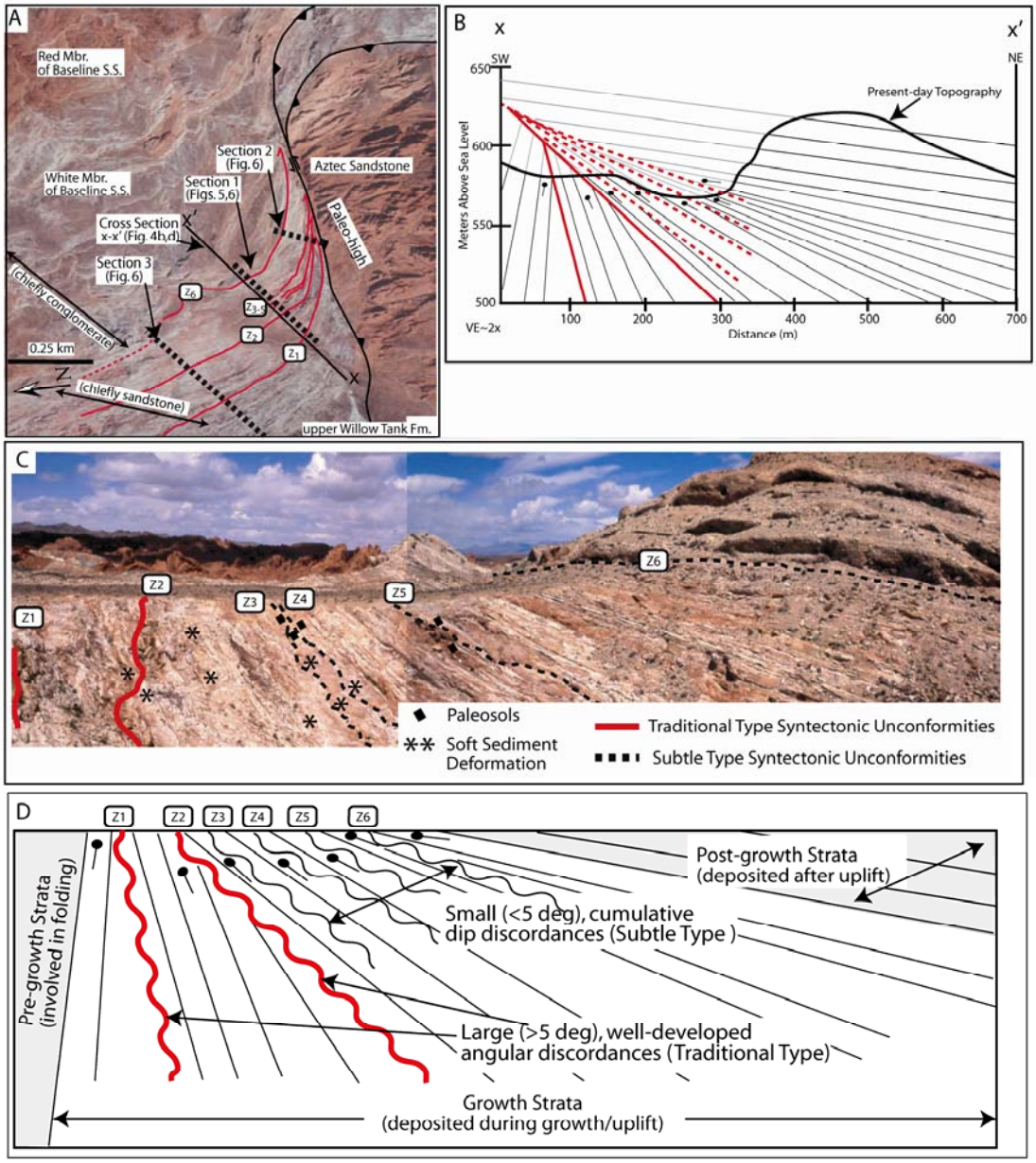

Figure 3.4 Map- and cross-sectional-views of growth strata in the Baseline Sandstone. A. Note that the lower two syntectonic unconformities are more extensive than the others. B. Cross section through the growth strata. C. Growth strata outcrop with overturned beds located on the left (southwest) near the base of the succession, and near-horizontal beds near the top of the succession to the right of the photo (northeast). D. Schematic cross section showing the internal distribution of Traditional Type and Subtle Type syntectonic unconformities.

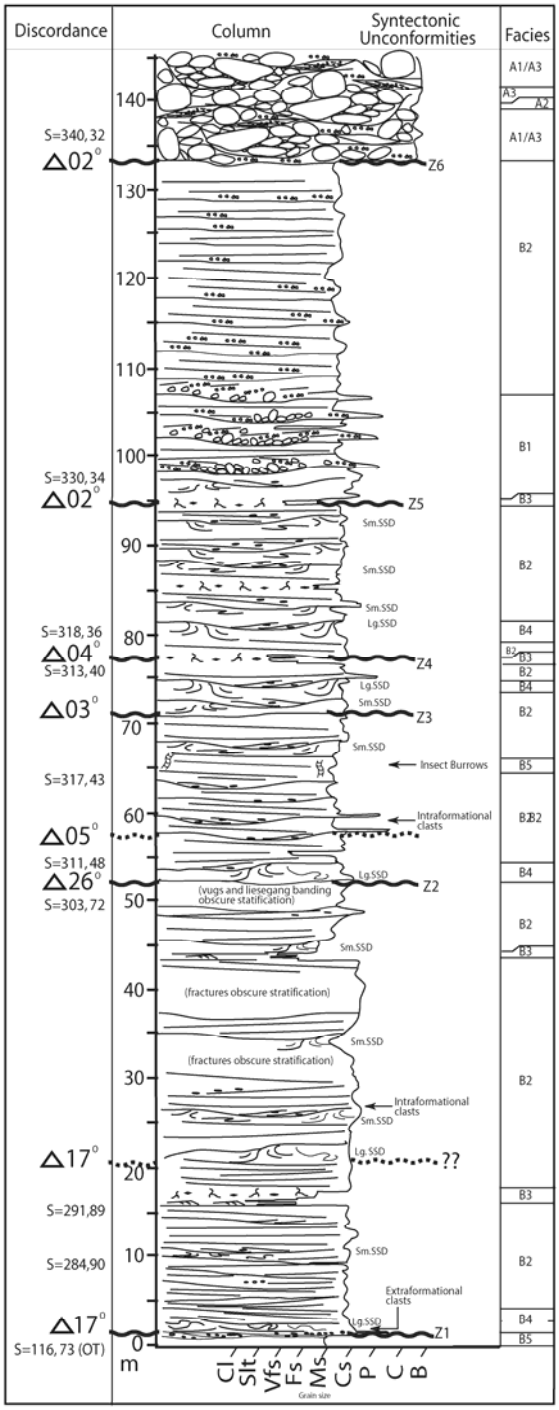

Figure 3.5 Detailed stratigraphic column through the growth strata succession highlighting syntectonic angular unconformities, sedimentary structures and facies stacking pattern.

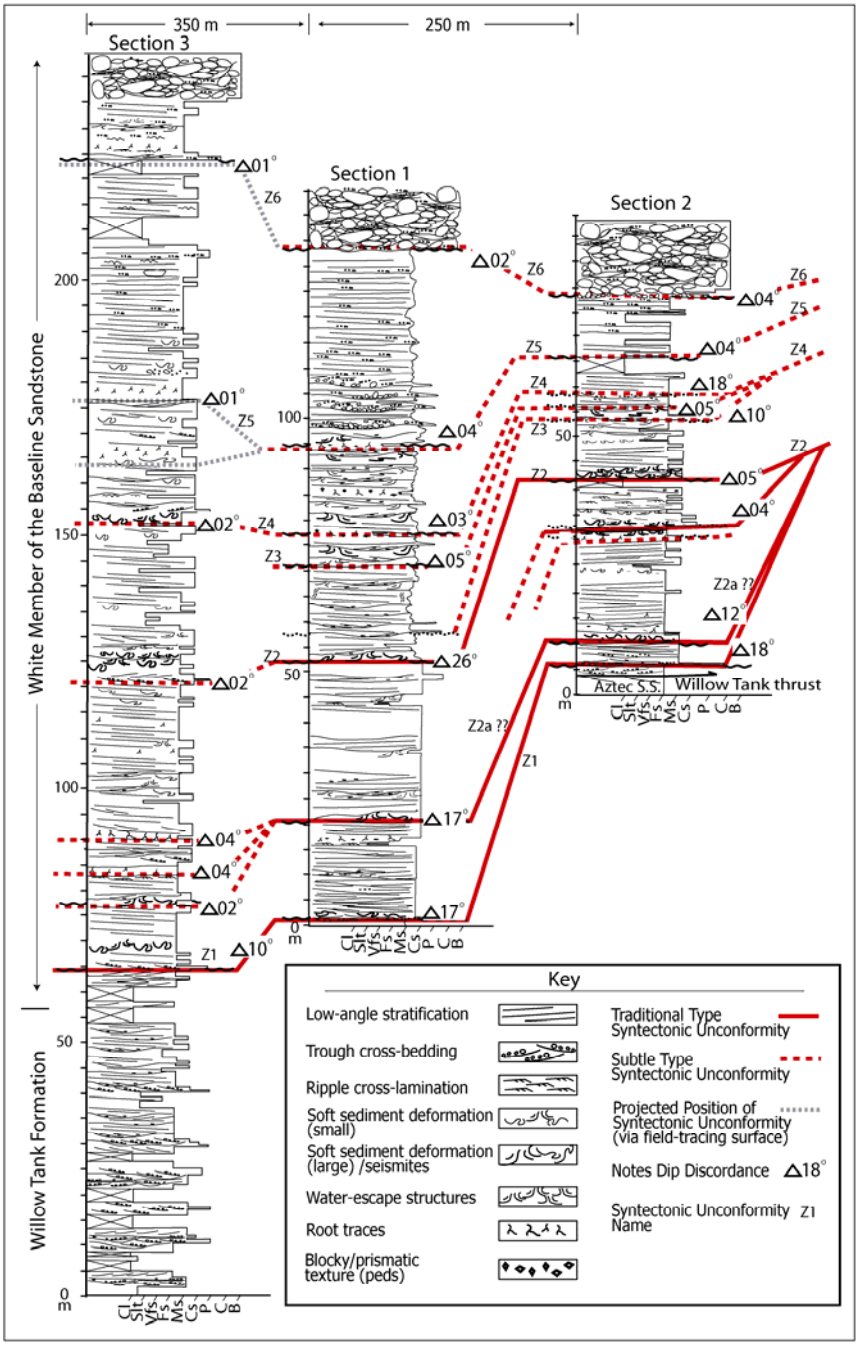

Figure 3.6 Stratigraphic correlation through growth strata showing oblique, down-dip (away from structure) changes in syntectonic unconformity development and persistence of key criteria that help distinguish syntectonic unconformity types- Suble and Traditional Type.

Growth strata show thinning, truncation and changes in attitude toward the Willow Tank thrust. Post-growth strata (Red Member of the Baseline Sandstone and laterally equivalent Overton Conglomerate) onlap and overlap the entire succession and were deposited after cessation of local uplift related to the Willow Tank thrust. The post-growth strata are not involved in deformation and do not show thinning or attitude changes.

METHODS

The strategy that I used to distinguish syntectonic unconformity types involved three steps. First, I identified growth strata packages, high-angle dip discordances and less obvious, low-angle dip discordances within flattening-up successions. Second, depositional facies that comprise the growth strata were described and interpreted to establish the depositional context. Finally, surfaces with slight changes in dip were described and mapped in detail, with special attention given to characteristics of the surface itself and the adjacent depositional facies.

Detailed stratigraphic columns, numerous bedding attitudes and a map of syntectonic unconformities comprise the dataset for this study. I present three stratigraphic columns measured proximal to the structure (~0.25 km) where growth strata are best developed (Section 1; Figures 3.4a and 3.5), slightly off the structure (~0.75 km) (Section 2; Figure 3.6), and distal to the structure (~3 km) (Section 3; Figure 3.6). Bedding attitudes were measured every 2-5 meters in the stratigraphic columns, and at several locations along strike. Each recorded measurement represents an average of between 3-10 attitude measurements. Syntectonic unconformities were documented in stratigraphic columns then correlated and mapped onto air photos.

Assemblage A

Facies	Description	Example	Interpretation
1	Very thick-bedded (1-3 m), lenticular beds of poorly sorted, clast-supported, massive, ungraded to inversely-graded, cobble to boulder conglomerate with a preponderance of angular to subangular clasts, and disorganized internal fabric. Matrix consists of poorly sorted sand, granules and pebbles with a dearth of mud-sized material. Typically fill large (2-4 m wide) gully-like features.		Clast-rich, Debris-flow Deposits "Plug"
2	Very thick-bedded (1-2 m), lenticular beds of poorly-sorted, matrix-supported, massive, ungraded to normally-graded, cobble conglomerate chiefly composed of subangular clasts. Matrix consists of poorly sorted sand, granules and pebbles with a dearth of mud-sized material. Typically fill large (2-4 m wide) gully-like features.	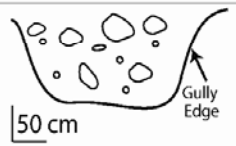	Clast-poor, Debris-flow Deposits "Tail"
3	Medium-bedded (10- 25 cm), discontinuous, lenticular beds of low-angle-stratified pebble conglomerate and pebbly sandstone. These deposits are typically adjacent to, and interfinger with facies 1 and 2.		"Winnowed" Debris Flow Deposits

Figure 3.7 Summary of depositional facies comprising facies Assemblage A- debris flow alluvial fan deposits.

GROWTH STRATA FACIES

Growth strata consist of sheet-like to broadly lenticular sandstones overlain by massive, poorly stratified, boulder to cobble conglomerates. Two facies assemblages were defined within this succession. Each assemblage consists of 3-5 individual facies. Facies Assemblage A is conglomeratic, and is present in the upper 20-30 meters of the growth-strata succession. Facies Assemblage B is sandstone-rich, and comprises the basal 130 meters of the section (Figure 3.5).

Facies Assemblage A: Debris-flow-dominated Alluvial Fan Deposits

Description

Facies Assemblage A comprises the coarsest-grained deposits within the White Member of the Baseline Sandstone. It contains three distinctive facies (Figure 3.7). Facies A1 is a poorly sorted, clast-supported, unstratified, ungraded to inversely graded, cobble to boulder conglomerate with a preponderance of angular to subangular clasts and disorganized internal fabric. Facies A2 is a poorly sorted, matrix-supported, ungraded to normally graded cobble conglomerate chiefly composed of subangular clasts. Facies A3 is a low-angle stratified, pebble to cobble conglomerate. Clast lithology within all three facies is overwhelmingly well-sorted, medium-grained, stratified sandstone. Some boulder-sized clasts of sandstone contain annealed, conjugate fractures with many different orientations.

Facies A1 and A2 typically occur as 2 to 4 m wide lenses up to 2 m thick with sharp basal contacts and steep margins. These facies alternate and form stacked successions of poorly organized, poorly sorted, irregular-shaped conglomerate lenses. Basal contacts outline 2-4 m wide, gully like features and have less than a few 10's of centimeters of incision into underlying material (Figure 3.8a).

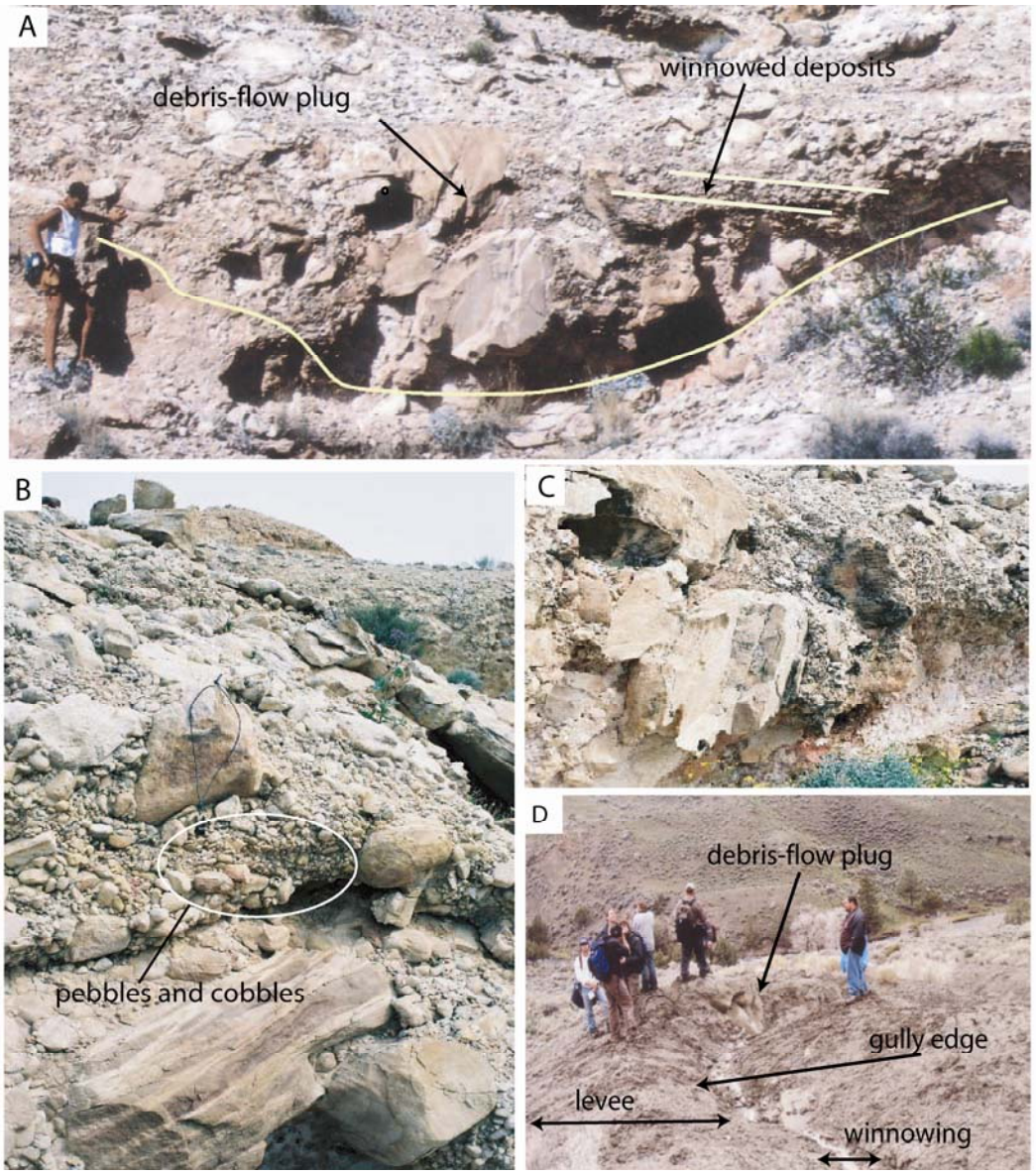

Figure 3.8 A. Boulder debris-flow deposits in the White Member of the Upper Cretaceous Baseline Sandstone. The lower line marks the base of the gully filled by the debris flow; the two upper lines outline faint, low-angle stratification in the levee deposits. B. Finer-grained cobble- to pebble-dominated debris-flow deposits illustrating the preponderance of Aztec Sandstone clasts, and angular character of clasts. C. An example of fractured, angular boulders of Aztec Sandstone in debris-flow deposits. D. A modern example of a debris-flow dominated alluvial fan from Mt. Everts, near Gardner, Montana.

In Facies A1 and A2, boulders are concentrated near the center of conglomerate lenses, whereas cobble-dominated material is concentrated on the margins (Figures. 3.8b and 8c). Facies A2 is similar to Facies A1 in lenticular bedding style, grain-size and disorganized fabric. However, Facies A2 tends to be clast-poor; locally, angular sandstone clasts are completely suspended within a poorly sorted matrix consisting of pebbles, granules and sand. There is a dearth of mud-sized material throughout Facies A1 and A2.

Facies A3 interfingers with Facies A1 and A2, and forms discontinuous, 25- 50 cm wide, 10-25 cm thick lenses of pebble conglomerate and pebbly sandstone with low-angle bedding (Figure 3.8b). Internally, beds consist of a basal, poorly sorted granule-pebble conglomerate overlain by moderately sorted granule-rich sandstone in a fining-upward succession.

Facies Assemblage A contains chiefly angular to subangular clasts of friable, well-sorted, quartz arenite with frosted sand grains (Figures. 3.8a and 8b). Locally, rounded chert and quartzite pebbles are found at the base of lenses, or interspersed with the more friable sandstone clasts within Facies A2.

Interpretation

In general, Facies Assemblage A is interpreted as debris-flow dominated alluvial fan deposits (Figure 3.7). In Facies A1, the poor sorting and disorganized fabric are consistent with deposition as a single mass of sediment, or flow. The presence of numerous, large, intact, angular clasts of friable sandstone suggests minimal grain-to-grain interaction and deposition by laminar flow. The clast-rich, matrix-poor character and dearth of mud-sized sediment is consistent with deposition by non-cohesive debris flows (Postma, 1986). Collectively, the disorganized fabric, angularity of clasts, local inverse grading and thick, lenticular geometry of Facies A1 suggests deposition by non-

cohesive debris flows (Gloppen and Steel, 1981; Blair and McPherson, 1994; Blair and McPherson, 1998; Sohn et al., 2000).

For comparison, Figure 3.8d shows a modern debris flow with a boulder-rich, inversely graded central plug flanked by cobble- and pebble-rich levees. This debris flow is only a few days old. Note that it is raining in this picture, and surface water runoff is funneled in the gully created by relief of underlying debris flow deposits. Focused runoff winnows-, and sorts debris-flow material. However, unlike the modern deposits shown in Figure 3.8c, the lack of mud-sized material within Facies A1 suggests that the debris flows were mud-poor, non-cohesive, clast-rich flows (Blair, 2000).

Facies A2 also has many of the key characteristics of non-cohesive debris flow deposits including the disorganized fabric, angular clasts, massive bedding and poorly sorted, pebble-granule-sand matrix (Figures 3.7 and 3.8). The higher relative proportion of matrix in Facies A2 suggests it was a product of clast-poor debris-flows. The lenticular geometry of both Facies A1 and A2 deposits is interpreted to be a product of debris flows filling negative relief created by the funneling of surface runoff (winnowing) between older debris-flow lobes and levees on the fan surface (Figure 3.8c).

The pebble-granule conglomerates of Facies A3 are interpreted as the waning-flow phase of debris flows (i.e., debris-flow tail and finer-grained levees) and winnowed deposits (Figures 3.7 and 3.8). Waning-flow levee deposits, such as the modern examples in Figure 3.8c, accumulate on the edges of debris flow tracks where friction between the flow and fan surface reduce the downslope momentum of the flow. Sediment is therefore deposited on the edges of the debris-flow track, where the flow lost momentum, forming ridges parallel to the path of the debris flow (Blair and McPherson, 1994).

I infer a proximal sediment source for Facies Asssemblage A. Non-cohesive debris flows are generally thought to travel only a few kilometers from the fan apex (Postma, 1986). Blair (2003) refined this view using an example from the anomalously large Cucomungo Canyon alluvial fan, where he pointed out that clast-rich debris flows can travel as far as 17 km from the fan apex, but that their deposits are much more abundant within 6 km. Non-cohesive debris flow deposits in Facies Assemblage A are consistent with a proximal sediment source area (2 -6 km).

The composition of conglomerate clasts further suggests a proximal source for Facies Assemblage A. The clast population includes fine-grained, well-sorted, quartz arenite clasts with frosted sand grains and is identical to the eolian Jurassic Aztec Sandstone exposed in the hangingwall of the Willow Tank thrust. Such friable clasts would likely not survive a long transport in turbulent flow conditions. In addition, clasts with annealed conjugate fractures are found with many different orientations suggesting that these fractures were inherited from the fractured Aztec Sandstone. Inheritance from the thick, eolian sandstone source unit would also explain the anomalously sandy, better-sorted debris flow matrix.

Facies Assemblage B: Sheetflood-dominated Alluvial Fan Deposits

Description

Facies Assemblage B contains five sand-rich lithologies (Figure 3.9) Facies B1 is a low-angle and trough cross-stratified, medium- to coarse-grained sandstone (Figure 3.10a) with lenses of clast-supported, poorly to moderately sorted, monomict, sandstone-clast pebble to cobble conglomerate 0.25 to 0.5 m thick. Facies B2 consists of flat-bedded, low-angle cross-stratified to planar-laminated, fine-to medium-grained sandstone with non-erosive, undulatory bases. Beds of Facies B2 contain subordinate pebble

stringers and common small-scale (<0.5 m thick) soft-sediment deformation is common (Figures 3.10a, b). Facies B3 is a chalky, white, massive mudstone to claystone that locally exhibits a blocky texture (Figure 3.10a). These fine-grained deposits are interbedded with horizontally laminated and ripple cross-laminated, very fine-grained sandstone. Facies B4 consists of flat-bedded, fine- to medium-grained sandstone with relict, oversteepened cross-lamination, and small- and large-scale (0.5 to 2 m thick) soft-sediment deformation structures (Figure 3.10c, d). Facies B5 is a medium-grained sandstone with relict low-angle stratification and small-scale trough cross-bedding in 10-20 cm deep scours (Figure 3.10a; far left). Red-purple and white coloration is pervasive, as is Liesegang banding.

Facies B1, B2, B4 and B5 of Facies Assemblage B have sharp, undulatory basal contacts and, in some cases, fill small depressions. Although some incision (< 0.5 m) is locally present at the base, sandstones commonly fill negative relief in or deform underlying sandstone (Figure 3.10d). Facies B1, B2, B4 and B5 typically form thick (up to 80 m), stacked successions of broadly lenticular units. Sharp basal contacts define broadly lenticular sandstone bodies. Individual lenticular sandstone units are 10's of meters wide and 1-2 m thick (Figure 3.10b). Internally, the sandstone bodies contain abundant low-angle cross-stratification with local pebble stringers, outsized clasts and thin (<0.25 m) intervals of low-angle cross-stratified pebble conglomerate. Sandstone facies adjacent to angular unconformities exhibit preferential carbonate, iron oxide and/or clay cementation within 1-2 meters of the unconformity.

Facies B3 is quite distinct from the other facies in this assemblage because it is fine- to very fine-grained, and horizontally bedded or massive. It also has a blocky or mottled texture with subordinate root traces (Figure 3.10a).

Assemblage B

Facies	Description	Example	Interpretation
1	Thickly-bedded, low-angle and trough cross-stratified medium- to coarse-grained sandstone with thick (0.25 -0.5 m) lenses of clast-supported, poorly- to moderately-sorted, monomictic pebble to cobble conglomerate. Conglomerate lenses are poorly-sorted and unstratified near the base of low-relief scours but become stratified upward.	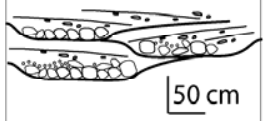	Interbedded Sheetflood and Gully-fill/ Lag Deposits
2	Thick to very thick (0.5-1 m), flat-bedded, low-angle- stratified, fine-to medium-grained sandstone with non-erosive, undulatory bases and subordinate pebble stringers. Beds have a broad, lenticular geometry . Oversteepened foresets, water-escape structures (dish and pillar) and small-scale (<0.5 m) soft-sediment deformation is common.	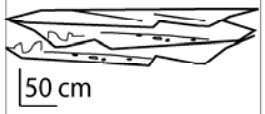	Sheetflood Deposits
3	Thin- to medium-bedded, chalky, white, massive mudstone/claystone with subordinate blocky peds, interbedded with horizontally-laminted, and ripple cross-laminated very fine-grained sandstone. Locally, this unit is pervasively bleached, oxidized giving a red, purple or orange color that cuts across bedding.	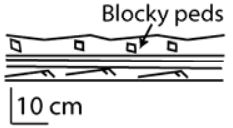	Pedogenically-modified Winnowed Sheetflood Deposits
4	Thick to very thick (0.5-1 m), flat-bedded, internally-deformed, fine- to medium-grained sandstone with relict, oversteepened laminations. Sandstone units have sharp, slightly erosive, undulatory bases. Basal contacts locally contain 5-10 cm thick zones that are preferentially cemented with clay (?); rip-up clasts of the white, preferentially-cemented basal contact are found in overlying sandstone units. Large-scale (0.5-2 m) soft-sediment deformation features including convolute lamination, dish and pillar structures (water-escape) are common.	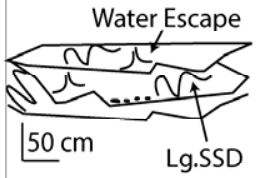	Deformed Sheetflood Deposits
5	Thick-bedded, locally intensely-burrowed (insect burrows?), medium-grained sandstone with relict low-angle stratification and cross-bedding in scours. Pervasive, red-purple oxidation, Liesegang banding and bleaching is common.	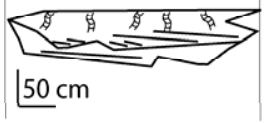	Bioturbated and Diagenetically-altered Sheetflood Deposits

Figure 3.9 Summary of depositional facies comprising facies Assemblage B- sheetflood alluvial fan deposits.

Locally, relict ripple cross-laminations are present. Facies B3 is laterally continuous except locally, where it has been cut by overlying sandstone bodies. Although Facies B3 occurs at multiple levels in the growth strata, it is more abundant near syntectonic unconformities that have smaller discordances (Figure 3.5).

Small-scale (<0.5 m thick) oversteepened, overturned, and truncated cross-laminations with subordinate dish and pillar structures are the hallmark of Facies B2 (Figure 3.10a). Large scale (>0.5 m thick) soft-sediment deformation is more abundant in Facies B4 (Figure 3.10c). There is a concentration of large-scale soft sediment deformation in the middle portion (from meter 50 to 100) of the growth strata succession (Figure 3.5). Water-escape features such as dish and pillar structures are commonly present near the top of sandstone beds where conglomerate lenses are present directly above them. Large-scale soft-sediment deformation features have high amplitudes that are nearly the entire height of the host bed. Fully preserved sand-volcano casts are present, but rare.

Despite their clast-supported fabric, conglomerate lenses within Facies B1 contain a moderate- to poorly sorted, granule and sand matrix and tend to be ungraded or normally graded. Constituent conglomerate clasts are typically subangular to subrounded clasts of friable, well-sorted, quartz arenite and rare limestone. Thin (<25 cm) mudstone units are present on the fringes of lobate sandstones, and onlap the flanks of the sandstone lenses. Small-scale, higher-angle crosss-laminations and trough cross-stratification are locally preserved between larger clasts. Deep scours, accretion sets, and along-strike changes in grain-size or sorting are generally absent in conglomerate and sandstone facies.

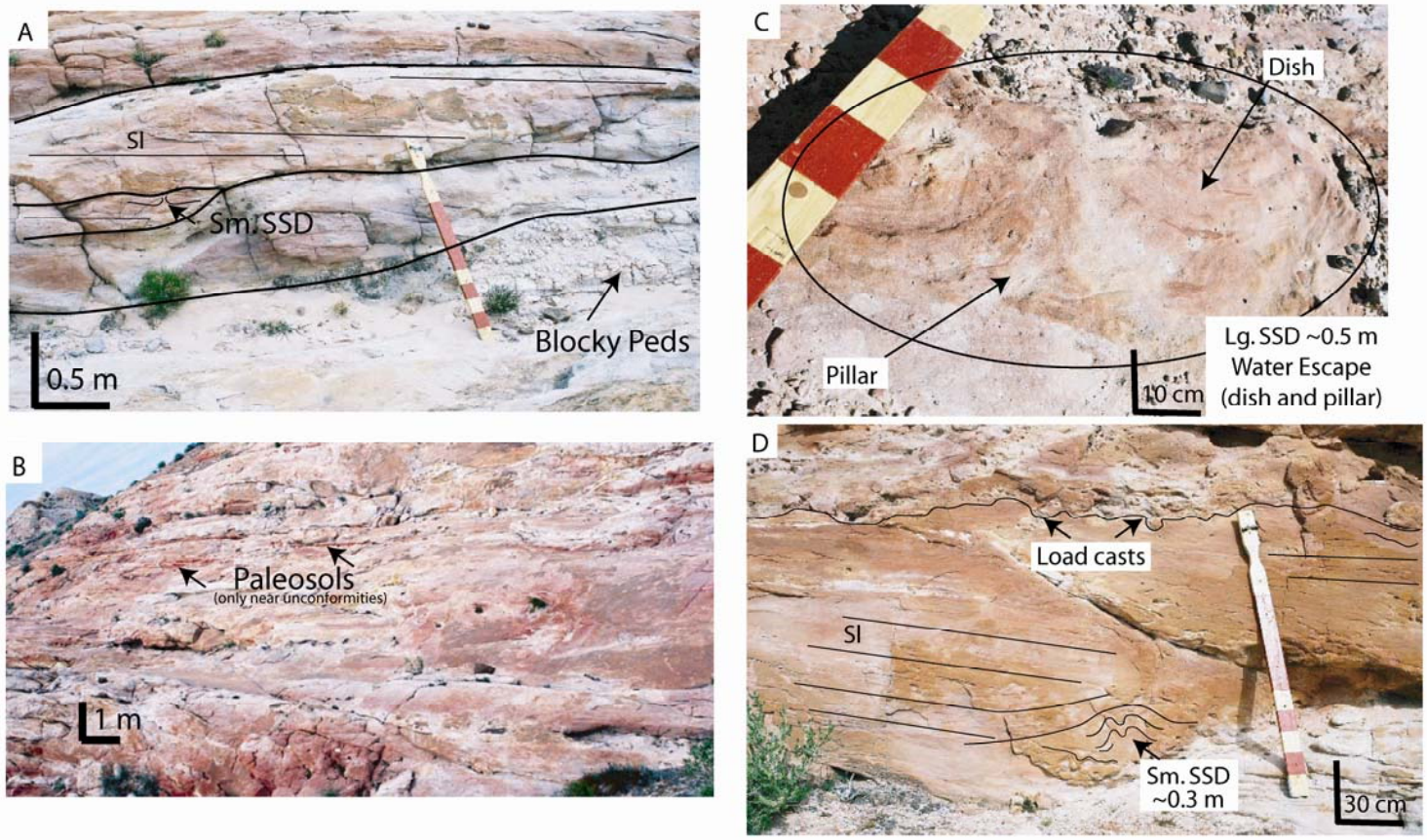

Figure 3.10 Examples of sheet-flow-dominated alluvial fan deposits. A. Sharp-based, broadly lenticular and flat-bedded, low-angle stratified sandstone bodies (Sl) that sit above chalky-white siltstone and mudstone with blocky-peds. B. Sandstone-rich facies comprising Assemblage B. C. A well-developed dish and pillar structure (large-scale soft-sediment deformation). D. An example of thick bedding character with small-scale soft-sediment deformation overlain by thickly bedded, low-angle stratified sandstone.

Interpretation

The broadly lenticular to flat-bedded style, low-angle stratification, alternation with thin lenses of pebble-cobble conglomerate, paucity of angle-of-repose bedding, and absence of deep scours suggests deposition by sediment-rich, unchannelized surface flows, such as sheetfloods. Such deposits are abundantly documented in the literature since the classic descriptions of Bluck (1967). The low-angle-stratified and planar-laminated Facies B2 is similar to the stratified pebbly sandstone facies described by Sohn et al. (1999) because both contain largely low-angle cross-stratification, and lack angle-of-repose bedding and internal scours. Blair (2000) and Sohn (1999) noted that these types of deposits are commonly produced by catastrophic, sediment-rich unconfined fluid gravity flows such as sheetfloods. It is not clear exactly how low-angle stratification is produced in these sediment-rich flows. Bridge and Best (1988) and Fielding (2006) postulate that low-angle stratification is produced by rapidly migrating, low-relief bedforms during upper-flow regime conditions that are transitional between dunes and upper plane-bed. These flow conditions are consistent with sheetfloods on an alluvial fan.

The consistency of sheetflow may have varied slightly from a grain-rich slurry (intermediate, to hyperconcentrated flow producing unlaminated facies) to a more water-laid sediment-rich flow (shallow sheetflood) capable of forming low-angle stratification and local higher-angle cross bedding. The weakly developed size stratification within conglomerates, whereby a clast-supported, coarser-grained fraction is concentrated near the base of the bed and overlain by a better sorted sandier fraction, is consistent with sheetflood deposits (Benvenuti and Martini, 2002). The bipartite character suggests that some of the conglomeratic strata were deposited by somewhat turbulent phases during

sheetflood events on an alluvial fan surface that were followed immediately by more water-rich sheetflood phases (Pierson and Costa, 1987; Costa, 1988; Sohn et al., 1999). This fabric is consistent with the sheetflood couplets described by Blair and McPherson (1994) and Blair (2000, 2003). I interpret Facies Assemblage B as the sheetflood deposits of a sheetflood alluvial fan (e.g., Blair and McPherson, 1994; Blair, 2003).

The close stratigraphic spacing of small-scale soft-sediment deformation and water-escape structures suggest that the deposits were wet and pliable at the time of successive depositional events. The deposits would need to be near the water table, or have temporally closely spaced depositional events to stay wet enough to be deformed. It is possible that slightly older, wet, sheetflood deposits were loaded by subsequent, overlying flows, perhaps during the same rainstorm. The preservation of fragile sand volcanoes, although very rare, suggests that they were not exposed to surface processes for extended periods and further supports the temporal close spacing of depositional events.

I interpret the thin mudrock units as winnowed sheetflood deposits that accumulated in low regions between active lobes on a sheetflood fan. Previous work suggests a warm, generally wet, “greenhouse” climate during the Cretaceous, and is consistent with the development of humid alluvial fans during these more humid conditions (Frakes, 1979; Barron and Washington, 1982). Fine-grained units of Facies B 3 thin toward the thickest part of sheetflood lenses suggesting that they were deposited between major sediment lobes. Flat laminations and rare ripple cross laminations suggest low energy depositional processes consistent with suspension deposition alternating with low energy depositional conditions comprising suspension deposition alternating with turbulent lower-flow regime currents. Surface runoff likely winnowed fine-grained

sediment from older sheetflood deposits that subsequently accumulated in ponds developed between depositional lobes.

CHARACTERISTICS OF SYNTECTONIC UNCONFORMITIES

Recent studies have emphasized the one-to-one, genetic relationship between kinematics and growth strata packages by using terms such as “halokinetic” (referring to salt structures) or “kinematic sequences” for the cumulative wedge sequences (Giles and Lawton, 2002; Barbeau and Geslin, 2004). Pronounced dip discordances (>10°) in conjunction with onlapping and offlapping relations are common ways to identify the syntectonic unconformities bounding these growth strata packages. However, identification of such unconformities hinges on the ability to detect subtle changes in bedding attitude through a succession. Detailed sedimentologic and stratigraphic observations provide another tool to identify subtle syntectonic unconformities and define high-resolution growth stratal packages.

Syntectonic unconformities form discordances directly adjacent to the active structure but become conformable with distance from the structure (Figure 3.2b and 3.6). Six such unconformities were identified in the Baseline Sandstone (White Member) growth strata succession. To facilitate discussion, unconformities are denoted with a “Z”, and are numbered progressively from oldest to youngest (Figures 3.4, 3.5, 3.6 and 3.11).

The largest dip discordance occurs at the lowermost unconformities, Z1 and Z2. Several small-discordance syntectonic unconformities are clustered within the upper half of the growth strata succession, Z3-Z6. I designate Traditional Type unconformities as those with major (>10°), easily discernable, angular discordances. The Traditional Type unconformities described herein are equivalent to the syntectonic unconformities with

"perceptible" dip discordance first recognized by Riba (1976), and all of the unconformities (Types A, B and C) discussed by Giles et al. (1999).

Subtle Type syntectonic unconformities are those with less apparent angular discordance, and are not widely recognized (<10°). Subtle Type unconformities are subtle surfaces found within what Riba calls a "progressive unconformity", and are not identified by Riba (1976). My view is that these progressively tilted successions consist of a series of small, subtle discordances (Subtle Type). I only interpret Subtle Type unconformities if they are mappable surfaces with small dip discordances within growth strata characterized by a suite of sedimentologic criteria defined here.

Traditional Type Syntectonic Unconformities: Sediment Accumulation << Uplift

Description

Two Traditional Type unconformities are present within the growth strata succession; these are the Z1 and Z2 unconformities (Figures 3.11a and b). The Z1 unconformity is the most extensive surface, extending 3-5 kilometers away from the structure (Figure 3.4a). This unconformity is marked by an angular discordance of as much as 17° in proximal areas (Figure 3.11a). The dip discordance decreases with increasing distance from the structure (Figure 3.2b). At a distance of ~5 km the unconformity becomes conformable. A narrow zone of cover prevents documenting the transition of the surface from angularity to conformity. The unconformity surface is characterized by an undulating, scoured morphology with local incision of up to 2 meters, and heavily oxidized or bleached zones (Figure 3.11b). Scours along the Z1 unconformity are filled with cross-stratified chert- and quartz-cemented sandstone-pebble conglomerate (recycled basal conglomerate of the Willow Tank Formation) (Figure 3.11b right). Durable clasts comprise roughly 80% of clast types found at, or just above, this

unconformity. Locally, large-scale (0.5-2 m) soft-sediment deformation features are present 0-2 m above the unconformity.

The Z2 unconformity is marked by a maximum of 26° of angular discordance (Figure 3.9c). The unconformity is traceable 0.5 kilometers from the structure, where it becomes conformable or is unrecognizable (Figure 3.9d). As with the Z1 unconformity, the dip discordance at this surface decreases with increasing distance from the structure. The Z2 unconformity is typically overlain by a massive to low-angle cross-stratified sandstone with local, large-scale soft-sediment deformation features such as dish and pillar structures and convolute bedding. Large-scale soft sediment deformation features typically occur within 2 meters of the syntectonic unconformities. A large angular discordance of about 17˚ is present between the Z1 and Z2 unconformities, the Z2a unconformitiy (Figure 3.6). This surface is locally mappable but is not well exposed and is thus not discussed in any detail.

Interpretation

The lowermost (Z1) unconformity marks the first major local hiatus in sedimentation resulting from the uplift of a local monocline or anticline in the hanging wall of the Willow Tank thrust. The large dip discordance, high degree of incision, and extensive nature (up to 5 km) of the Z1 and Z2 unconformities suggest periods when uplift rates exceed sedimentation rates. During initial stages of structural development there may not have been sufficient relief to produce large volumes of sediment. However, small relief could have diverted transverse, hinterland-sourced fluvial systems (such as those recorded by the Willow Tank and lowermost Baseline Sandstone) around this growing structure (Schmitt and Aschoff, 2004).

Structural deflection caused sediment shadow zones to develop on the leeward side (east) of the growing fold, initially starving alluvial fans of sediment. The initial sediment starvation could have accentuated early syntectonic unconformities by keeping uplift constant but decreasing sedimentation. The effects of sediment shadow-zones on the foreland side of growing folds have been recognized in the Appalachian foreland basin (Belt 1993), at Wheeler Ridge in southern California (Burbank et al., 1996), and along the wedge-top-foredeep transition of the Ecuadorian Andes foreland basin (Bes de Berc et al., 2005). Similar effects are documented on the leeward flanks of salt diapirs in the Gulf of Mexico (Camerlo and Benson, 2006), and La Popa Basin, Mexico (Aschoff and Giles, 2005; Shelley and Lawton, 2006).

The preferential location of large-scale, soft-sediment deformation features (>0.52 meters) within a few meters of Traditional Type surfaces suggests that these are linked to uplift processes responsible for the progressive rotation of bedding. Two scenarios that can explain this relationship are: (1) structural tilting and destabilizing of the depositional slope, and/or (2) liquefaction associated with earthquakes during discrete faulting events. In the first scenario, fault-motions having a significant vertical component increase the relief of the fault-related fold. As the fold grows, the depositional slope steepens, thereby ultimately causing oversteepening and internal deformation within sheetflood deposits. Nigro and Renda (2004) show that tilting of the limb (and hence, depositional surface) of contractional folds gives rise to soft-sediment deformation by remobilizing unlithified sediments. In the second scenario, earthquakes shake unconsolidated sheetflood deposits (Moretti et al., 2002) above a well-indurated basal seal.

Subtle Type Syntectonic Unconformities: Sediment Accumulation ~/< Uplift

Description

Unconformities Z3, Z4, Z5, and Z6 have minor (<10°) dip discordances. The cumulative effect of many minor dip-changes up-section results in a diffuse stratigraphic zone (~50 to 80 m) over which bedding progressively and subtly flattens (Figures 3.9a, f). The entire diffuse zone would be termed a "progressive unconformity" (sensu Riba, 1976). Small but measurable dip discordances comprise the progressive unconformity, and accommodate the up-section flattening. Recognition of the Subtle Type surfaces may be facilitated using sedimentologic criteria, and careful mapping of facies and surfaces.

The Z3, Z4, and Z5 unconformities have dip discordances of 2° to 4°, are developed within sheetflood-dominated alluvial fan deposits of Facies Assemblage B, and are less extensive than the Z1, Z2, and Z6 unconformities. Locally, the unconformity surfaces have relief of up to 1.0 m, but such incision is uncommon. Large-scale, (.5-2 m) soft-sediment deformation and water-escape structures are locally developed in sandstones directly above several unconformities. Evidence of paleosol development including blocky texture (Figure 3.11a), root traces, and bleaching or oxidation is found only within a few meters above small-scale discordance surfaces (Figure 3.11b) (Figures 3.11a, b).

The Z6 unconformity is the youngest and has a dip discordance of only 2°. Interestingly, this surface marks a major change in deposition and abrupt grain-size increase from sand- and pebble-rich deposits to boulder-rich deposits (Figures 3.11a, f, g). Strata below this unconformity are dominantly sheetflood deposits, whereas the strata

above record proximal debris-flow alluvial fan deposition. Although the unconformity surface is sharp, it is generally flat with little or no incision present (Figure 3.11e).

Interpretation

The small, but cumulative nature of dip changes within the stratigraphic intervals containing Subtle Type unconformities suggests that this portion of the section was progressively tilted during deposition. This is characteristic of progressive unconformities. The slight angular discordance is evident by increased winnowing of older deposits, incipient paleosol development, local erosion/incision, and large-scale, soft-sediment deformation. The well-sorted nature of unconformity-mantling, conglomeratic lenses suggests that there was more surface reworking, or winnowing occurring at these surfaces than in underlying and overlying deposits.

The preponderance of friable, Aztec Sandstone clasts within Subtle Type unconformity-mantling conglomerates suggest that the duration of exposure was less than that of Traditional Type unconformities, since these constituents would have been destroyed if exposed for very extended periods. Paleosol development typically requires a minimum of tens of thousands of years for pedogenic features to become noticeable; hence, I interpret zones that have numerous, or clustered paleosol horizons as evidence of increased residence time. Paleosols are rare except within a few meters above dip discordances, where they tend to cluster. Increased reworking and local incision at unconformity surfaces, coupled with preferential paleosol development adjacent to unconformities, suggests that these surfaces were exposed longer than other intraformational surfaces.

The high amplitude of large-scale soft-sediment deformation features and relatively thin, overlying beds (less than a few meters) suggests that the overlying (thin)

sandstones were insufficient to load and deform the underlying beds. Such soft-sediment deformation features are best explained by earthquakes, or slope destabilization by uplift (Nigro and Renda, 2004). By contrast, the small-scale soft-sediment deformation features could easily be generated during rapid successive depositional events.

I suggest the following features to identify Subtle Type syntectonic unconformities:

(1) stratigraphic position within an interval, or zone, where dips fan upward,
(2) presence of a small, but measurable dip discordance within a zone where dips appear to change (generally 2-10 degrees),
(3) mappable erosion surfaces with local incision that are of greater lateral extent than a single channel or gully feature,
(4) lenses of better-sorted, cobble- to pebble conglomerate that mantle unconformity surfaces and infill local undulations on the unconformity surface,
(5) presence of large-scale, (>0.5 m) soft sediment deformation and water-escape structures within sandstones stratigraphically above unconformity surfaces, and
(6) massive sandstones with better-developed paleosols and evidence of incipient cementation directly adjacent to unconformity surfaces.

Mapping and stratigraphic correlation show that the sedimentologic criteria I propose are remarkably consistent as a guide to interpreting syntectonic unconformity types (Figures 3.4a and 3.6). However, I caution that Subtle Type surfaces should only be interpreted with multiple criteria because many of these features alone can be intrinsic to the host depositional system. For this reason it is critical that the depositional context of the features be considered before interpreting a Subtle Type surface.

Riba (1976) suggested that angular unconformities become conformable with distance away from a given structure. Conceptually, Traditional Type unconformities should change into Subtle Type with increasing distance from the paleo-uplift because the amount of rotation/uplift incrementally decreases with distance. My mapping and correlation of syntectonic unconformities is generally consistent with this view. Traditional Type syntectonic unconformities correlate basinward to a single Subtle Type

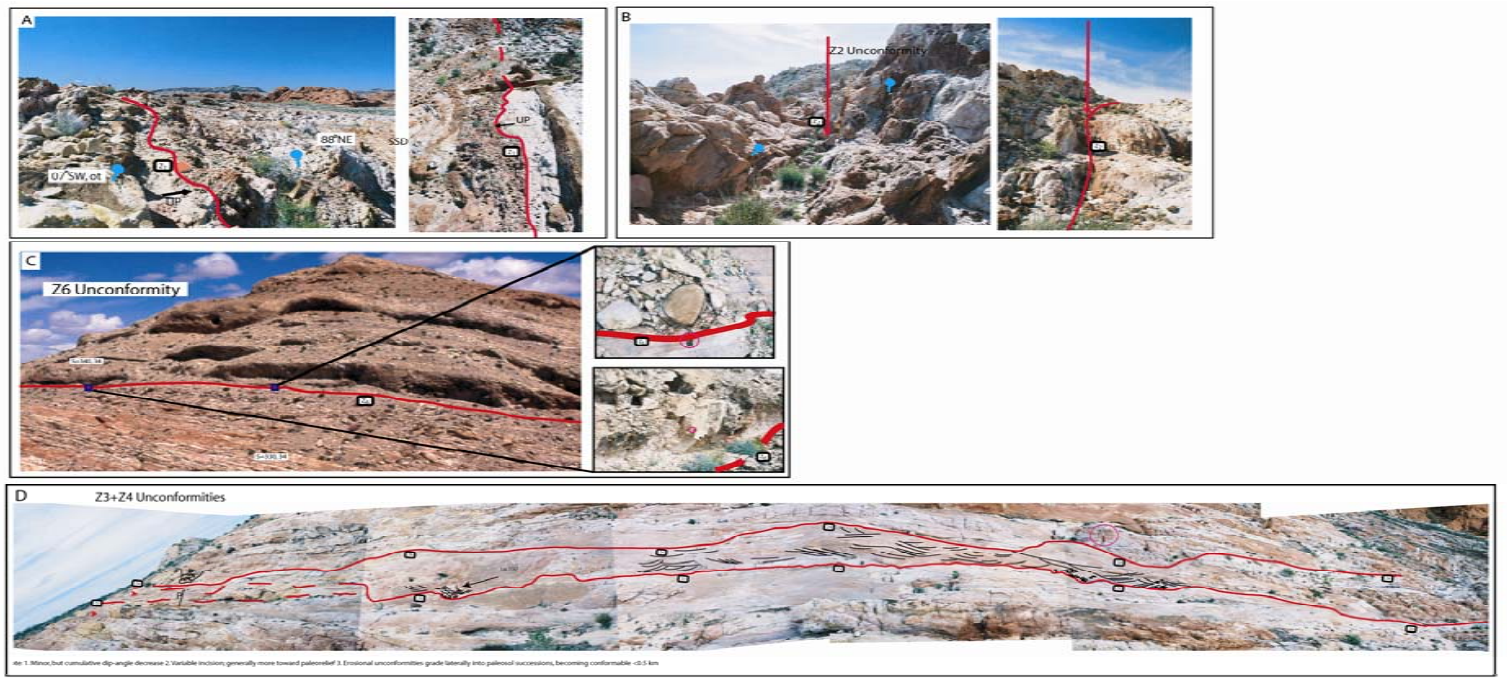

Figure 3.11 A. The Z1 syntectonic unconformity (Traditional Type) with obvious dip discordance, erosion and concentration of harder clast types. B. The Z2 syntectonic unconformity (Traditional Type) with obvious dip discordance and mappable surface of erosion. C. The Z6 syntectonic unconformity (Subtle Type) showing subtle dip discordance (<10 degrees), mappable surfaces of erosion, sharp increase in grainsize and change in depositional facies. D. The Z3 and Z4 syntectonic unconformities (Subtle Type). Both surfaces have subtle dip discordance (<10 degrees), a mappable erosion surface with local incision, lenses of better-sorted, cobble conglomerate, large-scale, (>0.5 m) soft sediment deformation and water-escape structures within sandstones above unconformity surfaces, and clustered paleosols.

unconformity, or a stratigraphic succession with clustered Subtle Type unconformities (Figure 3.6). This transition is best developed along the Z2 and Z2a unconformities; however, exposures are insufficient to determine the exact nature of the transition. Subtle Type syntectonic unconformities correlate basinward to conformable stratigraphic successions (Figure 3.6).

DISCUSSION

Some of the criteria used to identify Subtle Type unconformities, such as the presence of large soft-sediment deformation, increased reworking at unconformity surfaces, local incision, and clustered paleosol development, are the same as criteria used to identify Traditional Type unconformities. Similarities are expected if both surface type were subjected to tilting of the depositional surface, seismicity, local erosion and paleosol development.

Key differences between the two types of surfaces are the amount of dip discordance, lateral extent, and degree of reworking on the surface. Traditional Type unconformities have greater discordances, more evidence of erosion, more reworking at or near the surface of discordance and are more extensive than Subtle Type. Subtle Type unconformities have smaller, but measurable discordances (<10°) that correspond with large-scale soft-sediment deformation structures, clustered paleosols and greater incision. Used alone, the presence of soft-sediment deformation structures, paleosols, or evidence of longer residence time does not indicate a Subtle Type unconformity. Such criteria are subjective, and should be combined with bedding attitude, depositional context and other criteria described here.

Analyses of the Sant Llorenç de Morunys growth strata note a continuous up-section decrease in bedding dip (i.e., progressive unconformity) but no discordances within the progressive unconformity (Suppe et al., 1997 and Ford et al., 1997). My study suggests that Subtle Type unconformities are locally present within some flattening-upward successions, depending on the interplay of sediment supply, and local (structural) and regional accommodation. If regional accommodation and sediment supply greatly outpace local uplift a progressive flattening-up succession without Subtle Type syntectonic unconformities may form; this may be the case in Sant Llorenç de Morunys growth strata. Defining Subtle Type and Traditional Type unconformities extracts more information from growth strata, especially for strata formed during high sediment supply and regional accommodation creation. Figure 3.12 shows a hypothetical succession that compares growth strata interpretations using only Traditional Type unconformities, and using both Traditional Type and Subtle Type unconformities. As this example suggests, additional information can be extracted from monotonous flattening-up intervals by identifying both types of syntectonic unconformities.

Numerical models predict variation in growth strata geometries and syntectonic unconformity development under different fold accommodation space efficiency (FASE) conditions; these models consider local and regional accommodation space on growth strata geometries (Patton, 2004). For example, a monocline growing during base-level rise will have space available for sediment accumulation across its crest. In this scenario, local uplift destroys local accommodation space, but regional accommodation allows sediment accumulation across the crest of the structure, thereby producing growth strata with a progressive, up-section decrease in dip. By contrast, a monocline growing at the same rate as the previous example when base-level is low would have less space

available for sediment accumulation across its crest. In the latter scenario, the uplift destroys local accommodation space, and regional accommodation is low, thus causing non-deposition and/or incision across the crest of the structure.

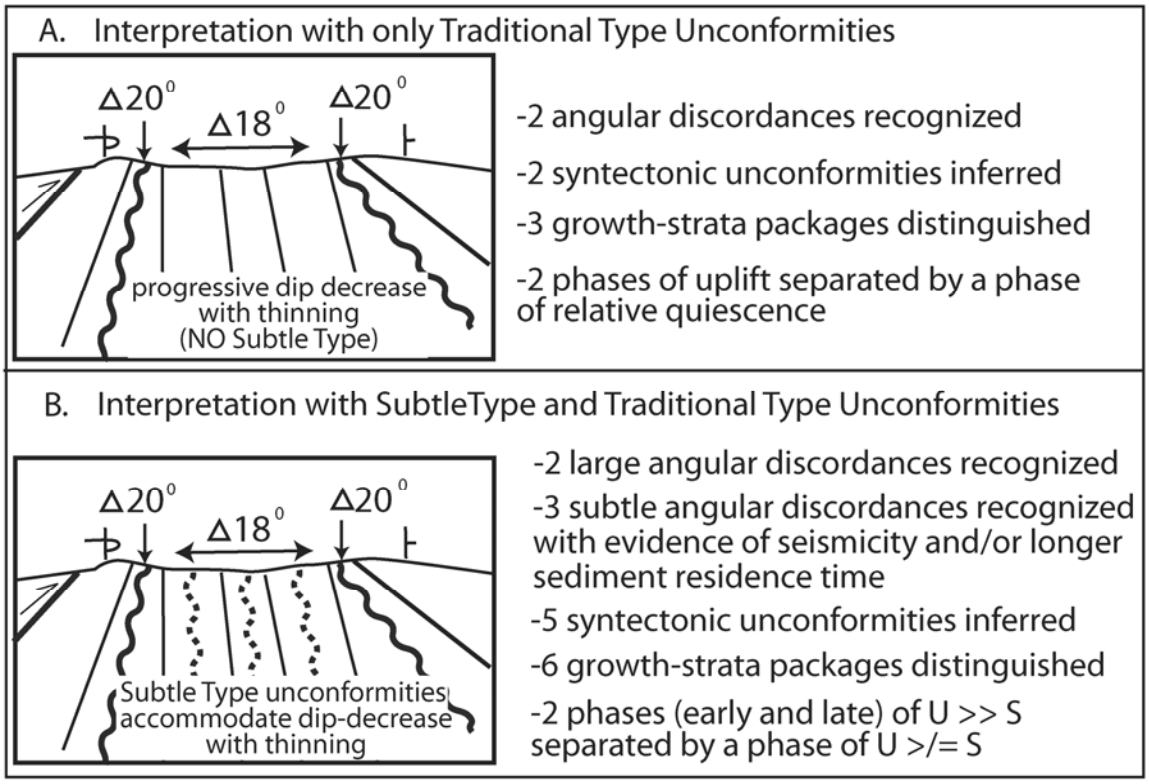

Figure 3.12 Schematic illustration showing potential differences in growth strata interpretations: (a) if only Traditional Type unconformities are used (a), and if both Traditional Type and Subtle Type unconformities are used (b). Note that 3 additional phases where uplift>sedimentation are identified.

I speculate that increases in sediment supply and regional accommodation space creation are responsible for the up-section change from Traditional Type to Subtle Type unconformities. Punctuated aggradation across the structure is suggested by the restricted lateral extent and small dip-discordance of each Subtle Type unconformity. Closely spaced, pervasive, small-scale soft-sediment deformation features, a general dearth of paleosol development except above unconformity surfaces, and greater thickness (>70 m) of the deposits suggest sediment accumulation was generally higher compared to older strata. A provenance of easily eroded, sand-producing Jurassic Aztec Sandstone is consistent with this inference. Erosion of the friable sandstone unit is conducive to producing abundant sediment. Assuming sufficient regional accommodation space to preserve the deposits, an increase in sediment supply, while keeping local uplift rate constant, could explain the change from Traditional Type to Subtle Type unconformities.

Alternatively, the up-section change from Traditional Type to Subtle Type unconformities could be explained by a decrease in the uplift rate, whereby less accommodation is locally destroyed by uplift. If constant sediment supply and regional accommodation is assumed, higher uplift rates are then necessary to cause incision and longer residence times at syntectonic unconformities. It is not possible to unequivocally determine rates of sedimentation due to lack of age constraints.

The Z6 unconformity is anomalous because it lacks a well-defined angular discordance, but unlike the other unconformities, it marks a significant change in depositional style despite compositional similarities (i.e., sourced primarily from the Aztec Sandstone) to underlying strata. The sharp facies change from sheetflood dominated to debris-flow dominated deposits does not coincide with a major angular discordance. The sharp facies change could be due to some drainage-basin threshold

whereby sheetflood fans were replaced by debris-flow fans, or because the dip discordance is masked by high sedimentation rates. Sharp up-section facies changes and grain-size increase should not be assumed to be of tectonic origin, they must be placed in context. Understanding the controls on abrupt upward facies changes requires more study of the controls on coarse clastic sediment production and deposition.

CONCLUSIONS

Two types of syntectonic unconformities are defined based on new data from Upper Cretaceous growth strata exposed in southeastern Nevada. Traditional Type syntectonic unconformities develop when sedimentation rates lag behind uplift; these are the traditionally recognized surfaces with distinct angular discordances (>10°) within growth strata. These surfaces are probably analogous to angular syntectonic unconformities sensu Riba (1976). Subtle Type syntectonic unconformities (2° to 10°) develop when sedimentation keeps pace with, or exceeds, uplift rate. This results in several subtle small-angle discordances that accumulate throughout a flattening-up stratigraphic interval. These surfaces are subtle discordances found within “progressive syntectonic unconformities” sensu Riba (1976).

Subtle Type syntectonic unconformities can be located using a suite of criteria including: (1) identification of small angular discordances within a flattening-up stratigraphic succession, (2) clustering of large-scale (>1 m) soft sediment deformation features (possible seismites), (3) clustering of semi-continuous erosional surfaces (these are more laterally extensive than the autocyclic erosional surfaces characteristic of the facies they occur in), (4) clustering of paleosols, (5) sharp increase in grain-size, and (6) changes in facies and detrital composition. I recommend that they be identified as such using multiple criteria, and always in context. This classification enhances growth strata

studies because it provides information from growth strata intervals with muted unconformities.

I cannot rule out the possibility that a reduction in uplift rates (increasing local accommodation) were responsible for a switch from Traditional Type to Subtle Type unconformity development, but qualitative observations suggest higher sediment supply as a primary cause. Sediment supply is controlled by climate, drainage basin size/relief and source area lithology. I postulate that (1) decreasing the uplift/sedimentation ratio by increasing sediment supply, in the presence of positive net accommodation, can mask syntectonic unconformities and form syntectonic discordances with less angularity (Subtle Type) and (2) failure to recognize Subtle Type unconformities can lead to biased interpretations of uplift history.

Chapter 4: Anomalous Clastic Progradation in the Cordilleran Foreland Basin: Implications for the Sevier-Laramide Transition

ABSTRACT

A new, high-resolution regional correlation and isopach maps provide evidence that (1) Laramide deformation began as early as ca. 77 m.a. in central Utah, and (2) anomalously extensive, internally complex clastic-wedge (Wedge B) development was caused by interference of Laramide-style uplift (San Rafael Swell) on the foreland flexural profile, and possibly enhanced by reduced dynamic subsidence. Three Campanian, alluvial-to-marine, clastic wedges traversed 250-400 km eastwards across the Utah-Colorado segment of the Cordilleran foreland basin. Wedges A and C are thick (600-1000 m) successions with a rising-trajectory shoreline stacking pattern (Blackhawk Formation and lower Castlegate Sandstone; Bluecastle Tongue and Rollins Sandstone) that reflect slower progradation of narrow (10-20 km wide), wave-dominated shorelines. In contrast, Wedge B consists of thinner (200-300 m) successions with a flat-to-falling shoreline stacking pattern (middle Castlegate Sandstone, Sego Sandstone, Neslen Formation, Corcoran and Cozzette Members of the Iles Formation) that reflects rapid progradation of embayed (60-80 km wide), tide-influenced shorelines. Wedges A and C prograded 200-250 km in more than ca. 5 My, whereas Wedge B prograded 340-400 km in just ca. 2 My (~170 km My^{-1}). Stratigraphic relations indicate development of Wedge B coeval with both Sevier- and Laramide-style deformation. Uplift of the basement-cored San Rafael Swell in the foredeep may have altered the flexural profile of the foreland basin, reduced net subsidence and accommodation in a broad (~200 km wide) intrabasin region, and caused anomalous clastic wedge development. Additionally,

reduced dynamic subsidence may have reduced accommodation throughout the basin and catalyzed progradation of Wedge B.

INTRODUCTION

Foreland basin models rely on clastic progradation and basin-fill architecture to interpret patterns of uplift and subsidence (Beaumont, 1981; Flemings and Jordan, 1981; Jordan, 1981). Despite more than 20 years of research, the spatial and temporal relationships between tectonics, clastic progradation and stratigraphic architecture remains unclear (Burbank et al., 1988; Heller et al., 1988; Horton et al., 2004). In particular, the temporal relationship between progradation and tectonics is debated (e.g., coeval with uplift or isostatic adjustment) (Heller et al., 1988; Burbank et al., 1988; Flemings and Jordan, 1990; Marzo and Steel, 2000; Horton et al., 2004; Jones et al., 2005). Lack of consensus about the stratigraphic signature of tectonics is partly due to a dearth of detailed, regional stratigraphic studies that link basin-margin growth-strata with distal foreland basin successions.

Progradation of the lower Castlegate Sandstone has been the focus of debate because of its unique sheet-like character and great extent (~200-240 km). Spieker (1946) first interpreted the Castlegate Sandstone as an indicator of uplift in the Sevier fold-thrust belt. Horton et al. (2004) established that thrust-belt motion (Charleston-Nebo thrust) was coeval with progradation of the Castlegate Sandstone by linking growth-strata with the Castlegate Sandstone using biostratigraphy and lithostratigraphy.

Undoubtedly, there is considerable net progradation of the Castlegate Sandstone into the basin, with an average progradation rate of 67-80 km My^{-1} (based on total wedge length/ duration). Yet, nearly *twice as much* net progradation (~340 km) occurred within the overlying clastic wedge (Wedge B), including the Sego Sandstone, Neslen Formation,

and Corcoran and Cozzette Members of the Iles Formation in just ca. 2 My (+/- 0.28 My). Additionally, previous work highlights the complex architecture and tide-influenced facies in this interval (Willis and Gabel, 2003). Progradation within the Sego-Neslen-Corcoran-Cozzette wedge was anomalously fast and far, with an usually complex architecture. Understanding the controls on anomalous wedge development (Wedge B) is important to resolve links between tectonics and progradation.

New data links uplift of Sevier thrust-belt and a Laramide structure, to anomalous clastic wedge development using a detailed, down-dip, sequence-stratigraphic correlation and biostratigraphically constrained isopach maps. The correlation is constrained by (1) five radiometrically dated ammonite zones that correspond to flooding surfaces and/or transgressive intervals in marine strata, (2) palynology in non-marine strata, (3) marine flooding surfaces that correlate with tidally influenced intervals, and (4) field-validation. Progradation rates are based on stratigraphic data in this, and previous studies, and high-resolution ammonite biostratigraphy that is calibrated with radiometric dates of interbedded tuffs with errors between 0.11-0.45 My (Cobban et. al., 2006 and references therein). The correlation presented here is the most comprehensive and most detailed correlation to date.

GEOLOGIC CONTEXT

The Cordilleran foreland basin is an elongate, NW-SE trending retroarc foreland basin that developed from Jurassic(?) to Cretaceous time along the eastern margin of the Sevier fold-thrust belt (DeCelles, 2004) (Figure 4.1). The basin formed by a combination of downward crustal flexure adjacent to the Sevier fold-thrust belt, dynamic subsidence and sediment loading. It parallels the Sevier fold-thrust belt, and spans much of the length of western North America, arguably from Canada to Mexico (Jordan, 1981;

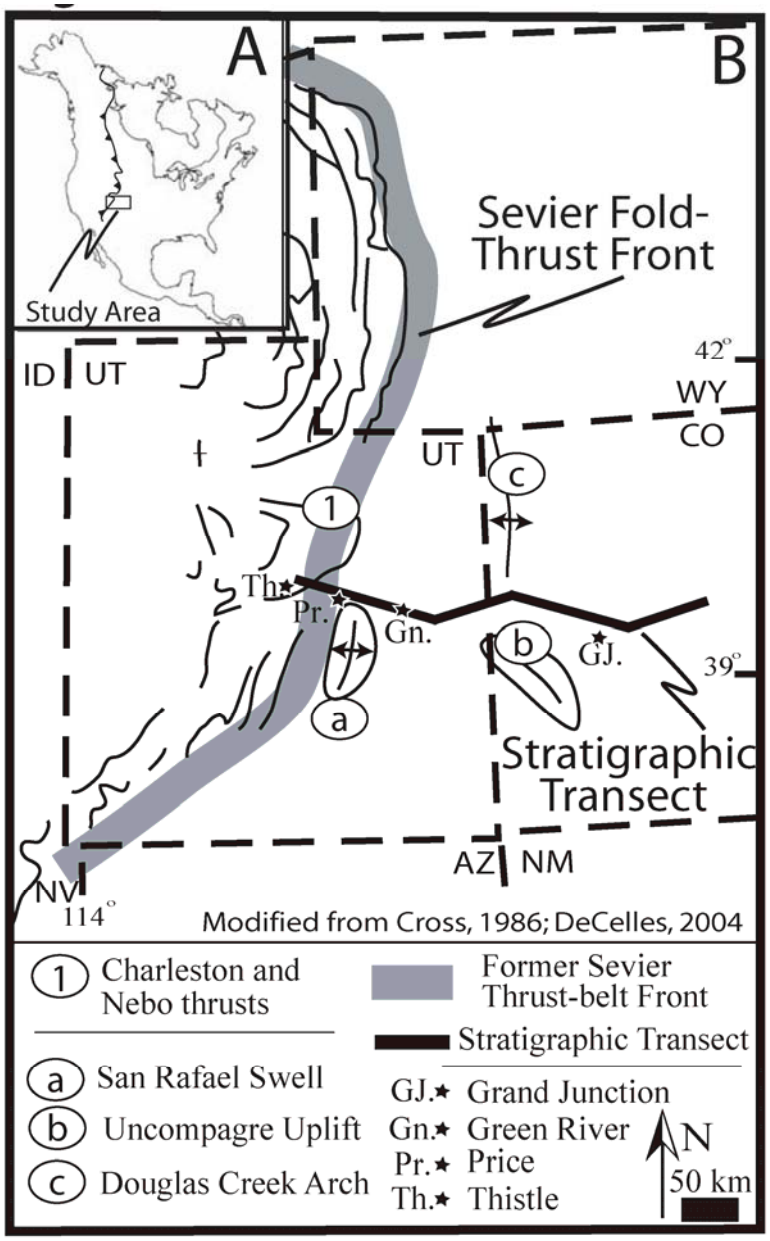

Figure 4.1 A. General location of the study area. B. Geologic context and location of study area and position of the Sevier Fold-thrust front.

Beaumont, 1981; Dickinson, 1993). As early as latest Campanian and continuing through the Paleocene, the foreland basin was segmented by basement-involved (Laramide-style) uplifts (DeCelles, 2004). Changes in subduction dynamics at the western US margin are cited as causes for the transition from Sevier- to Laramide-style deformation. Most notable is the proposed relationship between flat-slab subduction and Laramide-style deformation (Dickinson and Snyder, 1978; Jordan and Allmendinger, 1986). However, the timing of this transition is not well constrained and varies along strike of the Sevier fold-thrust belt.

Upper Cretaceous strata constitute much of the Cordilleran foreland basin fill, and record fold-thrust belt and Laramide-style deformation. Excellent, near-continuous exposures of Upper Cretaceous strata are present on the former, leading edge of the Sevier fold-thrust belt (i.e., present-day eastern Wasatch Plateau) and along the length of the Book Cliffs from Utah to Colorado. This study uses an east-west stratigraphic transect that bisects the Cordilleran foreland basin from the fold-thrust belt to the distal part zones of the foreland basin. The transect crosses fold-thrust belt in the west, and an intra-basinal, Laramide-style uplift (Figure 4.2). Frontal thrust-belt structures are imaged in a 2D seismic line at the western margin of the study area (Horton et al., 2004). Sevier fold-thrust belt highlands in the west provided sediment to the basin fill. Depositional systems transported this detritus in a general eastward direction into the Western Interior Seaway.

The thickness, stratigraphic architecture and depositional facies of basin fill are controlled by the relative rates of accommodation creation (sea-level rise and subsidence) and sediment supply; however, subsidence is thought to be the main driver of accommodation in foreland basins (Jordan, 1981; Shanley and McCabe, 1996; Porebski

and Steel, 2006; Yoshida et al, 2007). Widely recognized subsidence mechanisms in foreland basins include: (1) mega-regional dynamic subsidence, caused by asthenospheric backflow at the subduction zone (Gurnis, 1992; Catuneanu et al., 1997; Liu et al., 2005), (2) regional flexural subsidence, caused by thrust-belt loading (Beaumont, 1981; Jordan, 1981), and (3) local sediment loading (Dickinson, 1993). Additionally, intrabasinal (Laramide) uplifts could reduce flexural subsidence and influence stratigraphic patterns, notably thinning and erosion patterns during the transition between thin- and thick-skinned styles of deformation. The relative contributions of subsidence mechanisms, the time scales at which they operate, and how they are recorded in Cordilleran Basin fill are largely unresolved (DeCelles, 2004).

METHODS

I present (1) a >400 km-long transect that correlates progressively deformed, growth-strata at the Sevier fold-thrust belt to foreland basin fill and (2) high resolution isopach maps that illustrate spatial patterns in sediment accumulation. The stratigraphic cross section provides a 2D perspective, supplemented by isopach maps that add a 3D perspective of the units correlated in the cross-section (Wedge B). The dataset consists of forty-eight new, detailed stratigraphic sections, and 70 published well logs and sections (Figure 4.2). Growth strata were correlated out to foreland basin strata using the occurrence of tidal/brackish-water markers (flooding surfaces), facies stacking patterns, grain-size trends and biostratigraphy (see also Horton et al., 2004). Recognition of tidal influence (within estuaries) that penetrates back into non-marine strata during shoreline transgression and base-level rise is crucial for correlation of marine and non-marine successions (Shanley et al., 1992; McLaurin and Steel, 2000; Plink-Björklund, 2005).

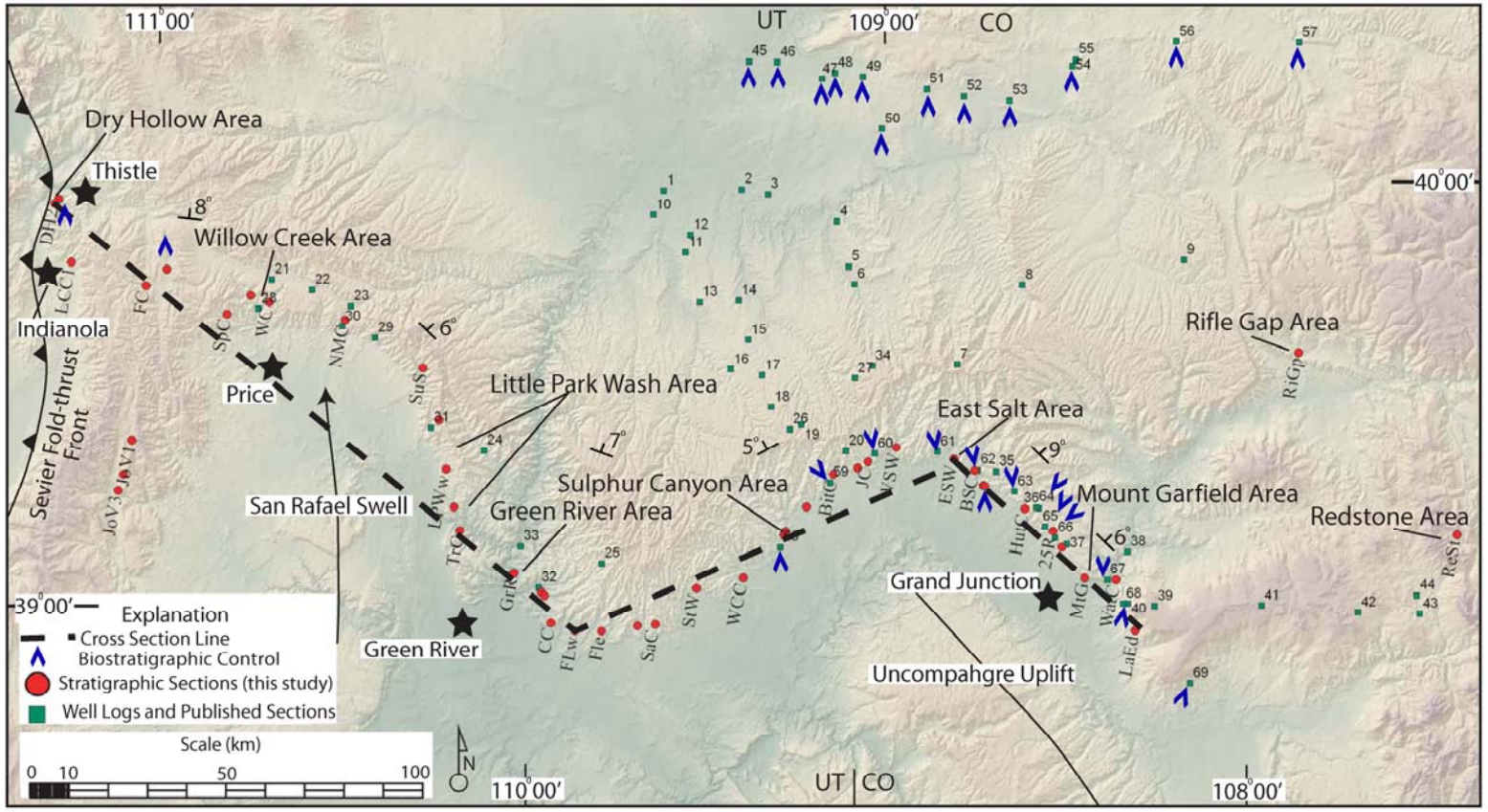

Figure 4.2 Shaded relief map of the study area showing location of cities (stars), key structures (Sevier fold-thrust belt and Laramide structures), new stratigraphic profiles (circles), published stratigraphic and well-log data (squares) and published biostratigraphic data (arrows). Detailed information and list of data sources provided Appendix A, B and C.

Using this method, correlation of the flooding surface at the base of the Anchor Mine Tongue to tidally influenced in the Middle Castlegate to the west was possible.

Sequence stratigraphy has been successfully applied in countless studies in the last 25 years, and is now a well-accepted and accurate means of correlation. However, correlation uncertainty was further-reduced by integrating palynology, ammonite biostratigraphy and radiometric dates available for ammonite zones with the sequence-stratigraphic framework. Six ammonite zones, published palynology, detailed photomosaics, airplane-shot photomosaics of the entire Book Cliffs, a published seismic line and on-ground mapping of stratigraphic surfaces were used to constrain the regional correlation. Sections were measured between previously published sections and at 3-10 mile spacing whenever possible. Ammonite zones constrain the medial and distal zones (> 100 km) of the stratigraphic correlation to within ca. 200 Ky, and palynomorph zones constrain the proximal zones (<25 km) to within ca. 1 My.

UPPER CRETACEOUS CLASTIC WEDGES IN THE CORDILLERAN FORELAND BASIN

Thick (>600 m), Wave-influenced Packages with Rising Shoreline Stacking Patterns

Clastic Wedge A includes the Emery and Star Point Sandstones, Blackhawk Formation and lower Castlegate Sandstone (Figure 4.3) (Hettinger and Kirschbaum, 2002). Wedge A is up to 800 m thick and extends 200-250 km from the Wasatch Plateau to eastern Utah. Its extent west of Indianola is uncertain because it has been cannibalized by eastward migration of the Sevier fold-thrust belt. This clastic wedge consists of 6-10 smaller-scale sandstone tongues that stack into a steeply rising, eastward-stepping succession. The tongues consist of marine shoreface or wave-dominated delta deposits that grade westward into coaly coastal-plain and fluvial deposits, and eastward into marine mudstones (Kamola and Van Wagoner, 1995; Dubiel, 2000).

The upper clastic wedge (Wedge C) is ~650 m thick and extends 175-250 km from Cottonwood Canyon, Utah area to Snowmass, Colorado (Figure 4.3). Its extent east of Snowmass is uncertain because it is eroded from the crest of younger Laramide uplifts. This stratigraphic interval includes the Bluecastle Tongue, lower Williams Fork Formation, Rollins Sandstone and Bowie Shale. Numerous smaller-scale sandstone tongues also constitute Wedge C; each of these tongues consist of marine shoreface or wave-dominated delta sandstones that grade westward into fluvial and coastal-plain deposits, and eastward into marine mudstones.

Wedges A and C consist of numerous, short-length (< 30 km), vertically offset-stacked, short-duration (< ca. 100 k.a.), wave-influenced, regressive-transgressive shoreline sandstone tongues (Figure 4.3). The shorter sandstone tongues interfinger landwards (NW) with coastal plain and fluvial sandstones, and seawards (SE) with marine shale (Figure 4.2). The regressive part of each tongue represents progradation of a single shoreline. Successive paleo-shorelines outline the "shoreline trajectory" within *a single tongue*. The track and maximum extent of successive paleo-shorelines outlines the shoreline trajectory or stacking pattern for *the succession of tongues in the clastic wedge* (Figure 4.2). Wave-generated facies (hummocky/swaley cross strata) constitute the tongues indicating wave-dominated, linear to cuspate shorelines. The high-frequency shoreline tongues stack in a basinward-stepping, steeply rising-trajectory stacking pattern that is characteristic of Wedges A and C (Figure 4.3).

Wedge A spans ca. 4-5 My (88.55 -77 My +/- 1 My) based on the time separating ammonite zones *Scaphites ventricosus* and *Baculites perplexus* (Figures 4.3, 4.4) (Cobban et al., 2006). The average progradation rate for the clastic wedge is 17.3-21.6 km My^{-1}. The duration of Wedge C is ca. 3 My based on the span *Exiteloceras jenneyi*

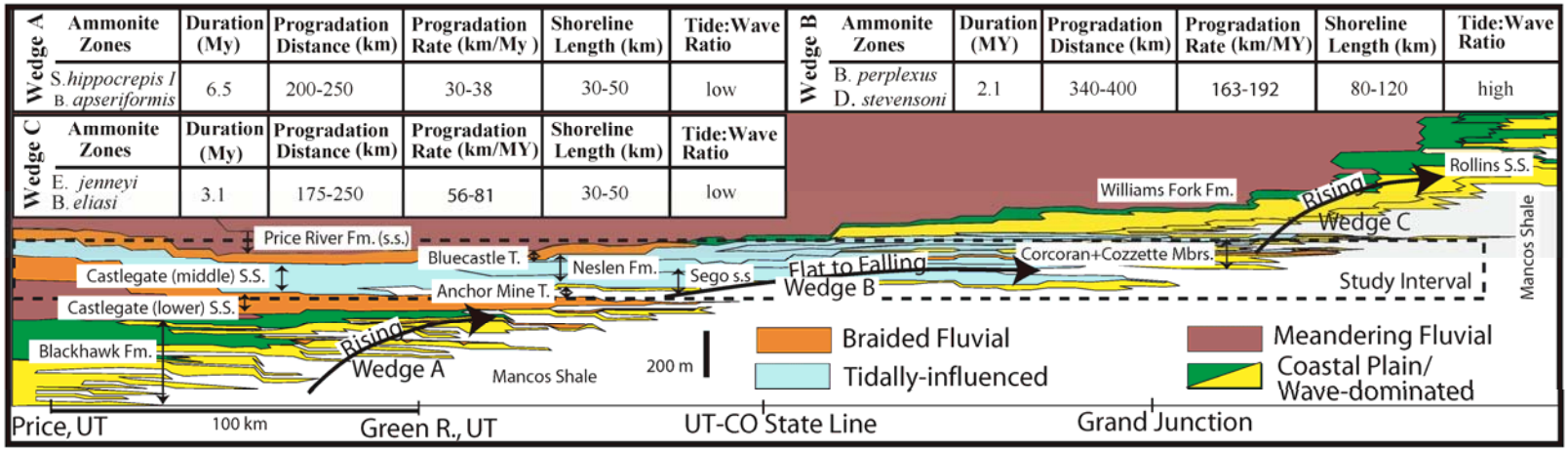

Figure 4.3 Generalized stratigraphic correlation for three Campanian clastic wedges in the Cordilleran foreland basin showing stratigraphic units, trajectories of shoreline stacking patterns, facies and average clastic wedge progradation rates. Correlation modified from Hettinger and Kirschbaum, 2002.

and *Baculites eliasi* (ca. 75.08-71.98 m.a.) (Figures 4.3, 4.4) (Cobban et al., 2006). The average progradation rate for Wedge C was 58-83 km My^{-1}. Progradation rates calculated for Wedges A and C are average rates based on the cross-sectional length of the clastic wedge divided by the time-duration of the wedge. Shoreline progradation rates for individual sandstone tongues comprising the clastic wedges are more difficult to estimate because age-constraints are scarcer, yet these rates would be considerably faster than the average progradation rate of the entire wedge.

Wedge B: Thin (200-300 m), Internally Complex, Tide-influenced Package with Flat Shoreline Stacking Patterns

The middle clastic wedge (Wedge B) is strikingly different from Wedges A and C. Wedge B prograded >1.5x farther than Wedges A and C, and had an anomalously fast progradation rate (163- 192 km/My) (Figure 4.2). Wedge B extends from Thistle, Utah to east of Redstone Colorado, is 200-300 m thick and has a total progradation distance of 340-400 km (Figure 4.3, 4.4). The wedge includes strata between the Buck Tongue and Rollins Sandstone maximum flooding surfaces (Figures 4.3, 4.4)- i.e., the Buck Tongue, Sego Sandstone, m. Castlegate Sandstone, Neslen Formation, and Corcoran an d Cozzette Members of the Iles Formation.

Wedge B consists of numerous, long-transit (> 80 km), short-duration (< ca. 100 k.a.), regressive-transgressive sandstone tongues. Constituent tongues are amalgamated with abundant incisions and pervasive tidal facies (Figure 4.5). The complex architecture and facies of Wedge B has been documented in the Sego Sandstone (Willis and Gabel, 2003; Wood, 2004) and in the Neslen Formation (Kirschbaum and Hettinger, 1998; McLaurin and Steel, 2000; Kirschbaum, 2004). As in Wedges A and C, the constituent sandstone tongues interfinger landward (to the E-NE) with coastal plain and fluvial sandstones, and seaward (to the SE and E) with marine mudstone (Figures 4.4, 4.5). The

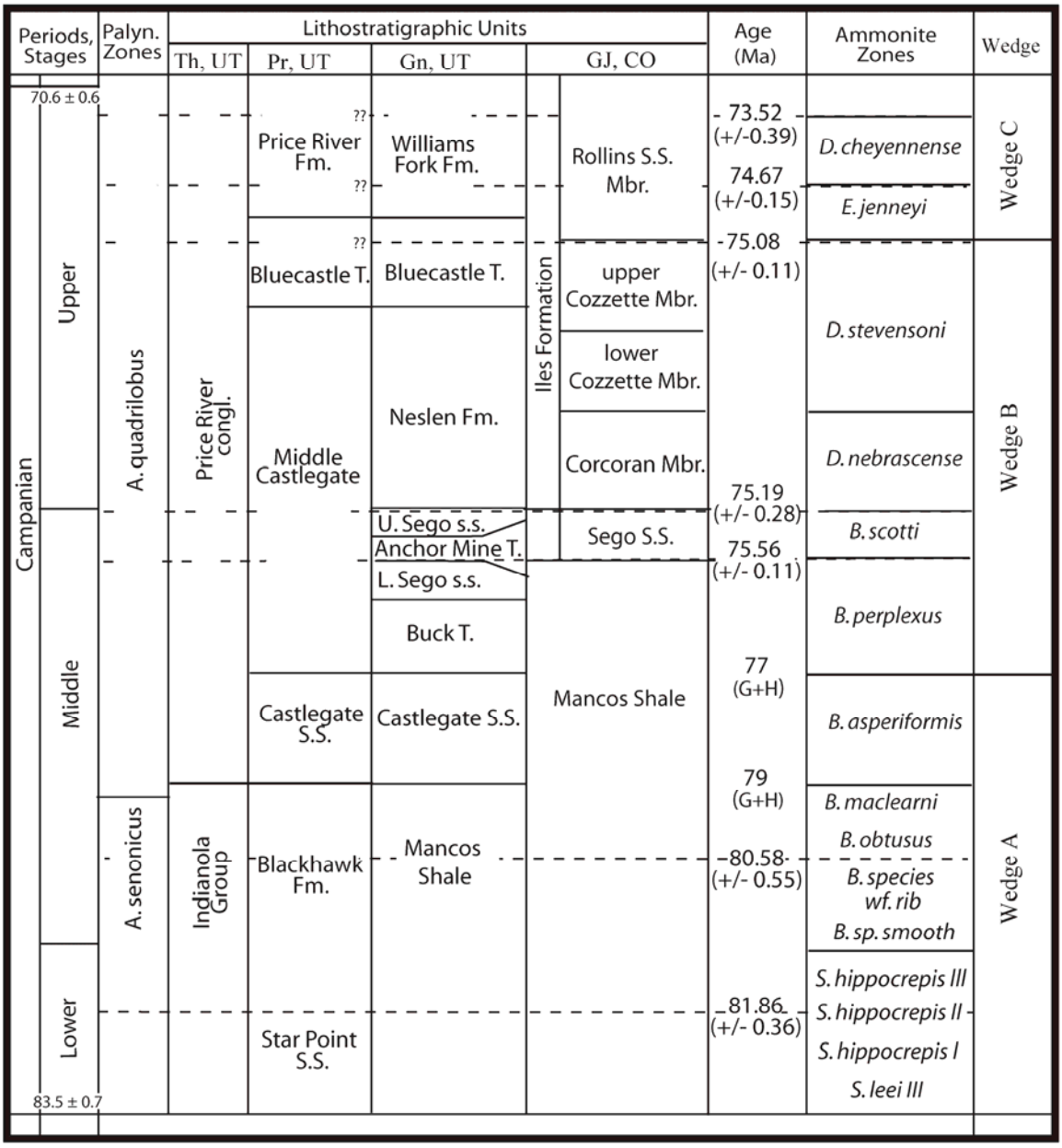

Figure 4.4 Correlation chart for three Campanian clastic wedges in Cordilleran foreland basin fill, Utah and Colorado, USA. Ammonite biostratigraphy and ages are summarized from Cobban et al. (2006). See Figure 2 and Appendix B for detailed ammonite localities and references.

regressive-transgressive tongues in Wedge B are often >2x as long, and of shorter duration, than those in Wedges A and C. Numerous incisions truncate the upper portions of many regressive-transgressive tongues, and make it difficult to determine the full extent of the sandstone tongues. These regressive parts of the tongues record progradation of high-frequency shorelines that transited more than 80 km in less than 100 Ky each (Figures 4.3, 4.5).

Internally, Wedge B is much more complex than Wedges A and C. A wide array of depositional facies constitute Wedge B. Shoreface sandstones, tidal-fluvial channel, bay-head delta, and tidal-channel deposits are commonly overlain by thin, coaly, mud-prone and tidally influenced intervals (proximally), and thin transgressive marine shale units (distally) (Figure 4.5). Marine transgressive-regressive tongues of Wedge B are more heavily bioturbated than those of Wedges A and C. Abundant tide-dominated facies (inclined, thin-bedded, ripple cross-laminated sandstones with double mud drapes, sigmoidal bedding and bi-directional, rippled sandstones) comprising the T-R tongues indicates that most of the shorelines were overall tide-dominated, and likely embayed. The high-frequency, tide-dominated shorelines form an amalgamated succession with flat-to-falling shoreline stacking pattern that is unique to Wedge B.

Wedge B developed in ca. 2.08 My (+/- 0.28 My), and is constrained by *Baculites perplexus*, *Baculites scotti*, *Didymoceras nebrascense* and *Didymoceras stevensoni* ammonite zones (Figures 4.2, 4.3) (Cobban et al., 2006). The average progradation rate of Wedge B is 163-192 km My^{-1}. This progradation is anomalously far and fast compared to the other clastic wedges in the Utah-Colorado segment of the Cordilleran foreland basin.

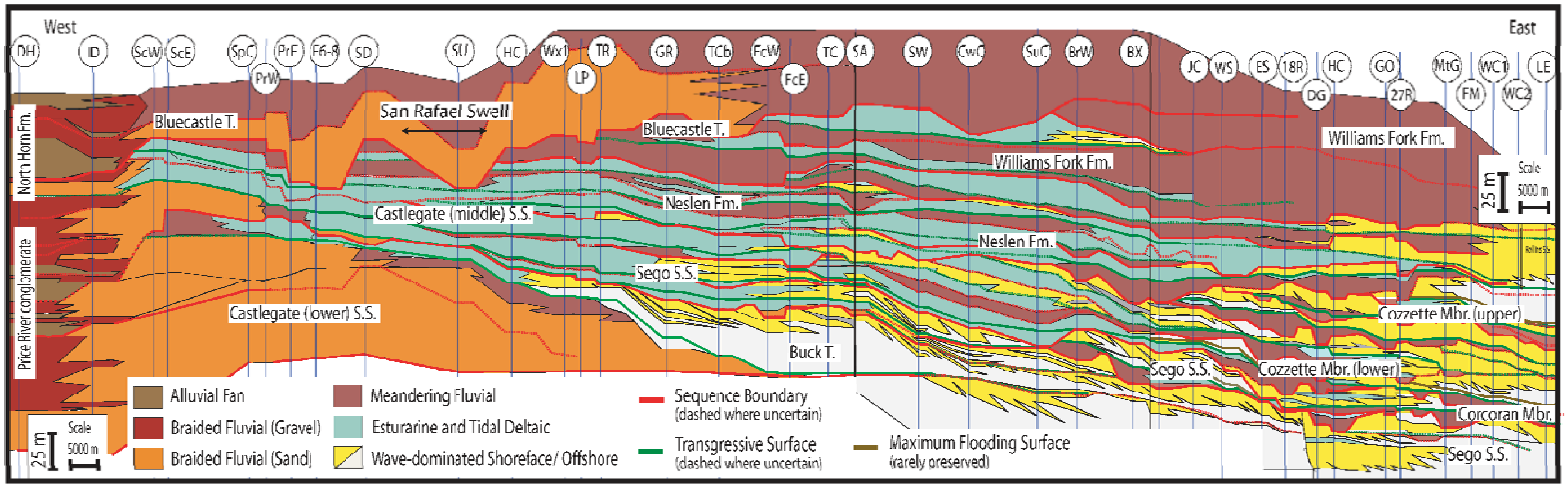

Figure 4.5 Sequence stratigraphic correlation and facies architecture of the anomalous clastic wedge (Wedge B). Section abbreviations: DH, Dry Hollow; ID, Indianola; ScW, West Scofield Reservoir; East Scofield Reservoir, SpC, Spring Canyon; PrW, West Price River (along Rt.6); PrE, East Price River (Willow Creek); F6-6, Federal-6 public well-log; SU, Sunnyside; HC, Horse Canyon; Wx1, Wilcox-1 public well-log; LP, Little Park Wash; TR, Trail Canyon; GR, Green River; TCb, East Tusher Canyon; FcW, West Floy Canyon; FcE, East Floy Canoy; TC, Thompson Canyon; SA, Sagers Wash; SW, Strychnine Wash; CwC, Cottonwood Canyon; SuC, Sulphur Canyon; BrW, Bryson Wash; BX, Bar-X Canyon; JC, Jim Canyon; WS, West Salt Creek; ES, East Salt Creek; 18R, 18-Road; HC, Hunter Canyon; GO, Grasso Section from Hettinger and Kirschbaum (2002); 27R, 27-Road; MtG, Mount Garfield; FM, Farmers Mine from Hettinger and Kirschbaum (2002); WC1,Watson Creekfrom Gill and Hail (1975); WC2, East Watson Creek; LE, Land's End. Detailed section locations are provided in Appendix A.

RELATIONSHIP BETWEEN ANOMALOUS PROGRADATION AND THRUST-BELT DEFORMATION

Thrust-related growth strata (i.e., progressive unconformities) constrain basin-margin kinematics. Such strata form by progressive tilting, or deformation, by an adjacent structure (Riba, 1976). Although growth *strata* can be associated with growth *faults*, the two features are very different and should not be confused. The former are flattening-upwards, *stratigraphic* packages that are an integral part of reconstructing structural histories. The latter are syndepositional *faults* that generally form near the edge of continental shelves where sedimentation rates are exceptionally high. There are no growth faults identified in the Upper Cretaceous basin fill. However, growth strata provide information about the kinematics of active thrust-belt structures on the margin of the Cordilleran foreland basin.

Growth strata were identified by Horton et al. (2004) in (1) outcrop at Dry Creek, near Thistle, Utah (west end of Figure 4.5) and (2) in seismic data east of Thistle, Utah. General stratigraphic relations and palynologic data collected from these locales indicate that the motion of the frontal-most thrust-belt structure, the Charleston-Nebo thrust, was coeval with deposition of the Castlegate Sandstone (Horton et al., 2004). However, their study did not extend the correlation east of Price, Utah, and only provided a general sense that growth strata correlate with the "Castlegate Sandstone", sensu Young (1955), which includes the "middle Castlegate Formation" and "Bluecastle Tongue", and their down-dip equivalents (sensu Olsen et al., 1995; McLaurin and Steel, 2000). My correlation provides this needed detail by correlating growth strata to their basinal equivalents within a sequence-stratigraphic context.

Pre- and post-growth strata include the Indianola Group and much of the North Horn Formation, respectively (Figure 4.5). These successions developed just prior to, and following the motion of the Charleston-Nebo thrust. Syn-growth strata involve conglomerates of the Price River Formation and lowermost North Horn Formation. I herein refer to the conglomerates of the Price River Formation exposed near Lake Creek as the "Price River conglomerate" to distinguish it from the older, sandstone-dominated Price River Formation that crops out near Price, Utah (Olsen et al., 1995; Robinson and Slingerland, 1998).

In the Dry Hollow area ("DH" Figure 4.5), I define four unconformity-bounded packages in growth strata. Angular unconformities within the growth strata are 5 to 20 degrees, and typically correspond with changes in detrital composition and grain-size increase. A fine-grained stratigraphic interval splits the Price River conglomerate, and growth strata, into two units. The fine-grained interval, and corresponding back-stepping facies pattern, is quite distinctive and has been recognized in two other, independent studies (Robinson and Slingerland, 1998; Horton et al., 2004). I correlate this fine-grained unit to a transgressive, brackish-marine interval in the Middle Castlegate Sandstone (McLaurin and Steel, 2000), the Anchor Mine Tongue (Figure 4.4), and use the base of the interval as regional datum.

Baculites scotti is present in the Anchor Mine Tongue near Sulphur Canyon ("SC" on Figure 4.4), roughly 20 m below the flooding surface I correlate to the fine-grained growth-strata interval (Gill and Hail, 1975). This suggests that the surface is younger than 75.56 My (+/- 0.11 My) (Gill and Hail, 1975; Cobban et al., 2006). The regional flooding surface is older than 75.19 (+/- 0.28 My), as constrained by the presence of *Didymoceras nebrascense* ~20 m below the flooding surface. Here,

Didymoceras nebrascense was found in the shale just above the Corcoran Member of the Mount Garfield Formation near Grand Junction, Colorado (Gill and Hail, 1975). If I assume a reasonable correlation error of 10 m, the flooding surface I use as a datum must still be between 75.56 and 75.19 My because the surface is located between the *Baculites scotti* and *Didymoceras nebrascense* ammonite zones.

Paleocurrent analysis and published petrographic data provide conjectural evidence that supports the correlation. Correlative depositional systems should have roughly consistent paleocurrent directions and composition, as river systems feed deltas that prograde in a similar direction with sediment from similar source areas. Paleocurrent directions are southeasterly in the upper part of the Lower Castlegate Sandstone and northeasterly in Bluecastle Tongue, defining a consistent up-section change in paleocurrent direction. This up-section change in paleocurrent direction is well-defined from Dry Creek to Horse Canyon, but is less defined in more distal areas as tides and waves influence the paleocurrents. Between Dry Creek and Horse Canyon my correlation is consistent with this up-section change in paleocurrents, and correlates sequences with roughly similar paleocurrent directions (Plate 1).

Lawton (1983) defined stratigraphic trends in sandstone composition for upper Campanian through lower Paleocene strata in the Book Cliffs. Most notably, these stratigraphic trends indicated that younger stratigraphic units (uppermost Campanian through Paleocene) are more lithic-rich than older Campanian units. In addition, the Neslen Formation (and updip equivalents) was slightly more lithic-rich than the Lower Castlegate sandstone and Bluecastle Tongue. My correlation is consistent with the aforementioned compositional trends such that each depositional sequence has a similar detrital composition.

The new regional correlation (Figure 4.5) shows that: (1) the lowermost growth-strata unit corresponds to the main body of the Castlegate Sandstone, (2) the second and third growth-strata units correlate with the anomalous clastic wedge B described above, and (3) the upper growth-strata unit corresponds with the Bluecastle Tongue in the Green River (medial) area and Rollins Sandstone in the Grand Junction (distal) area.

RELATIONSHIP BETWEEN ANOMALOUS PROGRADATION AND LARAMIDE DEFORMATION

The San Rafael Swell is one of several Colorado Plateau uplifts interpreted as basement-cored, Laramide-style uplifts (Figure 4.1 and 4.2) (Bump and Davis, 2003). Stratigraphic evidence constraining motion of the San Rafael Swell includes stratal thinning trends, paleocurrent shift, incision on the San Rafael crest, and down-basin changes in fluvial architecture. Though disputed, previous stratigraphic studies suggest San Rafael Swell uplift began < ca. 74 m.a., (Lawton, 1986; Robinson and Slingerland, 1997).

New high-resolution isopach maps are based on ammonite zones and flooding surface correlation (i.e., base of ammonite-bearing shales). The maps were created using a dataset of 69 datapoints derived from published stratigraphic sections tied directly to ammonite locales, well-logs and new stratigraphic sections (Figure 4.2). Well-logs were correlated with outcrop data using flooding surfaces, facies stacking patterns and regional unconformities. Because ammonites are commonly found in condensed sections at, or very near marine flooding surfaces, it was possible to establish a direct relationship between ammonite biostratigraphy and sequence stratigraphy.

The isopach maps show distinct thinning across the San Rafael Swell (Figure 4.6) as early as ca. 77 m.a. (B. *perplexus* biozone). Thickness trends of strata within the B. *asperiformis* show a distinct thickening adjacent to the front of the thrust-belt. No

obvious thinning trends are observed in the vicinity of the San Rafael Swell during B. *asperiformis*. Thrust-belt proximal strata are thinner, and the foredeep depozone is less developed during the B. *perplexus* interval. Furthermore, obvious thinning trends are developed across the San Rafael Swell. Finally, the isopach map including the youngest strata shows a prominent thinning trend across the San Rafael Swell.

The stratigraphic correlation corroborates the interpretation of increasing influence of the San Rafael Swell on depositional patterns. The correlation shows a clear up-section increase in the number, depth, and lateral extent of incisions across the San Rafael Swell. As much as 50 m of incision on the San Rafael Swell crest is present at the base of the Bluecastle Tongue. Thinning and crestal incision indicate that structural growth of the San Rafael Swell influenced sedimentation as early as middle Campanian, and had relief by latest Campanian. Thinning patterns suggest that the San Rafael Swell influenced sedimentation as early as ca. 77 m.a., 2-3 My earlier than previously reported.

The north-south trending thick zone is interpreted as the former foredeep depozone developed during the B. *asperiformis* interval. This depozone is less developed up-section, and is increasingly overprinted by the uplift of the San Rafael Swell. The onset of San Rafael Swell-related thinning, during B. *perplexus* (ca. 77 m.a.) is coeval with development of the anomalously extensive, architecturally complex clastic Wedge B. The close relationship between anomalous clastic wedge progradation and uplift of the San Rafael Swell suggests that uplift of the Laramide-style structure, or regional tectonic processes associated with these structures, influenced development of this wedge.

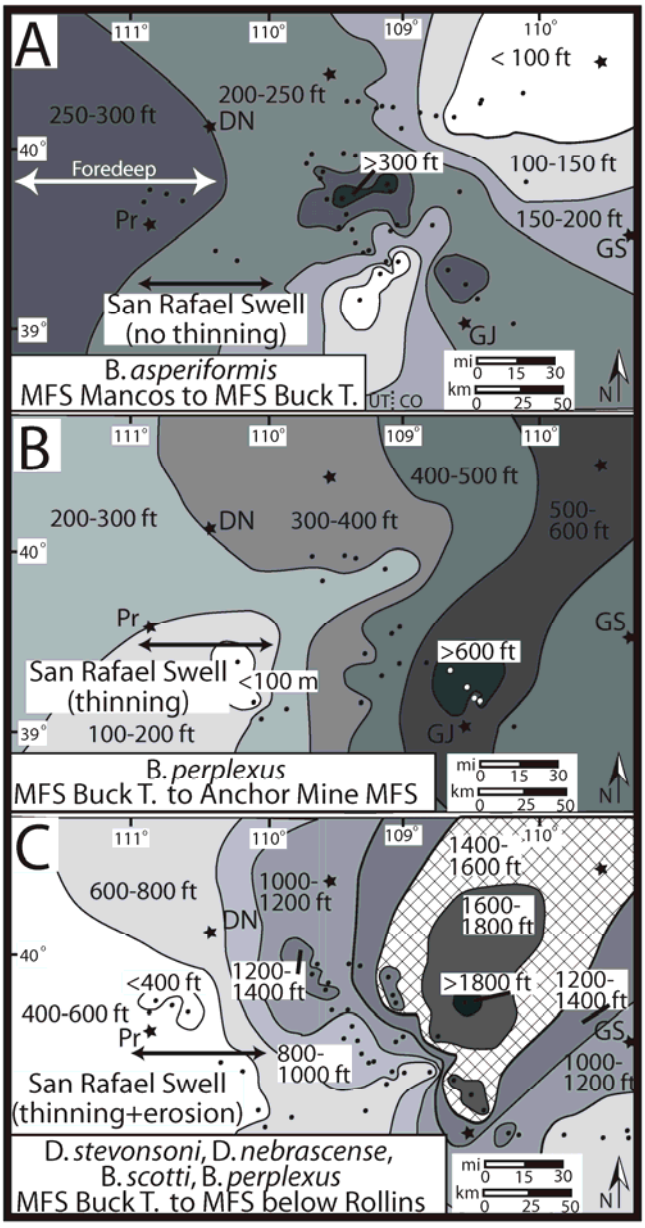

Figure 4.6 Isopach maps for the B. *asperiformis* (A), B. *perplexus* (B) and B. *perplexus* to D. *stevensoni* ammonite zones (C). Maps are not decompacted and are based on direct correlation between published stratigraphic sections with biostratigraphic data to flooding surfaces on well-logs and new stratigraphic sections.

DISCUSSION

Correlation uncertainty can be a concern for regional stratigraphic correlations. Regional sequence-stratigraphic correlations generally assume that: (1) marine flooding surfaces can be traced up-dip into tidally influenced, fluvial successions and (2) shoaling-upwards, and coarsening-upwards, packages in proximal areas correlate with similar packages in medial parts of the basin. Correlation uncertainty associated with these assumptions was reduced by integrating palynology, ammonite biostratigraphy, radiometric dates, and trends in paleocurrent directions and detrital composition with the sequence-stratigraphic framework. Ammonites are most abundant in condensed sections at marine flooding surfaces; this provides a one-to-one match between the ammonite biostratigraphy and the sequence-stratigraphic correlation. Furthermore, stratigraphic trends in sandstone composition (Lawton, 1983) and paleocurrents guide the correlation, whereby sandstone composition must be similar between units within the same depositional sequence. This assumes that up-section patterns in detrital composition and paleocurrent direction are spatially consistent. The resultant correlation was completely compatible with biostratigraphic constraints and, paleocurrent and compositional trends. I estimate a maximum stratigraphic correlation uncertainty of no more than 10 m, vertically. A correlation uncertainty of ~10 m does not change the 3rd and 4th order sequence-stratigraphic correlation or growth-strata linkage does not change.

Steeply rising, basinward-stepping shoreline stacking patterns develop when accommodation and sediment supply are subequal and high (Jervey, 1988; Shanley and McCabe, 1991). By contrast, lower accommodation and higher sediment supply favor flat-to-falling patterns (Helland-Hansen and Martinsen, 1996; Porebski and Steel, 2003). The steeply rising shoreline stacking pattern in Wedges A and C suggest that sediment

supply barely exceeded accommodation creation (Figure 4.3). The flat-to-falling shoreline stacking pattern and abundant erosion within Wedge B (Figures 4.3, 4.5) suggest that sediment supply exceeded accommodation.

Constituent short-transit, wave-dominated shoreline tongues comprising Wedges A and C suggest regression of wave-influenced shorelines when base-level was continuously rising. Longer-transit, valley-incised, tide-dominated shorelines of Wedge B indicate repeated, forced regression of tide-influenced (embayed) shorelines, during repeated base-level fall. In contrast to Wedges A and C, the amalgamated, incised architecture of Wedge B suggests that shoreline regressions were accommodation-driven rather than supply driven.

If tectonic factors are held constant, extensive progradation can be caused by increased sediment supply, or repeated, high-amplitude sea-level falls (Galloway, 2001). If sediment supply is held constant, progradation can be driven by reduced accommodation due to: (1) reduced flexural subsidence, (2) isostatic rebound, (3) uplift of Laramide structures, (4) reduction of dynamic subsidence, or (5) some combination of these. Figure 4.7 summarizes the relative contribution of subsidence mechanisms to accommodation space in the foreland basin.

Cretaceous greenhouse climate conditions and active Cordilleran/hinterland uplift favor high sediment supply conditions. Climatic and uplift conditions in the Cordilleran foreland basin during the Cretaceous therefore favored high sediment supply. Fluvial megafans are highly efficient, transverse-oriented sediment delivery systems (Horton and DeCelles, 2001). Fluvial megafan deposits, such as those of the Cretaceous-Paleogene Wildhorse conglomerate complex (sensu Lawton et al., 1994), further suggest that high-supply depositional systems existed throughout the Campanian. Given consistent

greenhouse climate conditions and stratigraphic record of high-supply depositional systems throughout the Campanian, a marked change in sediment supply is unlikely. A change in sediment supply is a poor explanation for Wedge B development because high sediment supply was common to all three wedges; changes in accommodation are thus needed.

The new correlation of growth strata to basin fill (Figure 4.5), and previous work by Kamola and Huntoon (1995), Yoshida et al. (1996), Houston et al. (2000); Horton et al. (2004), indicate that Wedges A and B were coeval with thrust-belt development. Active thrust-belt deformation causes thickening of the orogenic wedge, which, in turn increases flexural subsidence. This results in higher accommodation, in the adjacent basin, producing patterns akin to those characteristic of Wedge A (Jordan, 1981). Wedges A and B developed coeval with thrust-belt motion. Conceivably, subsidence rates should be high for both wedges if the orogenic wedge is actively building (i.e., increasing load), and if sediment supply is the same for both wedges they should both have similar architectures and progradation rates; yet this is not the case. Changes in flexural subsidence related *only* to the thrust-belt are unlikely However, and *alone* is a poor explanation for anomalous progradation of Wedge B because the thrust belt was active for both intervals. .Conceivably, the low-accommodation patterns characteristic of Wedge B is compatible with isostatic rebound; yet, evidence of coeval thrust-belt development precludes this. Isostatic rebound is a poor explanation for Wedge B progradation because the thrust-belt was active during its development; greater loading and flexure is expected during thrust-belt culmination, not rebound (Flemings and Jordan, 1990).

Global sea-level was generally high in the Campanian and eustatic sea-level fluctuations were quite small (Kaufmann, 1993). Fourth-order (~500 Ky) sea-level fluctuations of only a few 10's of meters, and third-order (~2-3 My) of a few meters, are expected during greenhouse conditions characteristic of the Cretaceous (Wilson, 1988; Tucker, 1993; Galloway, 2001). Because the amplitude of sea-level fall is quite small, sea-level fluctuation alone is an unlikely cause for such extensive (>100's of km) progradation.

Thinning and stratigraphic relations indicate that *both* Laramide and Sevier structures were active during Wedge B development (Figures 4.5, 4.6). However, only Sevier deformation was active for Wedge A in the study are, and only local Laramide deformation was active for Wedge C, although Wedge C has not been thoroughly studied. Using an example from the Karoo foreland basin, Catuneanu, (2004) suggested that uplift of a basement-cored structure in the forebulge depozone can alter the flexural profile of the basin and influence deposition. Uplift of a Laramide-style structure in the subsiding Cordilleran foredeep could have a similar effect; this could widen the forebulge zone and reduce accommodation space during the Sevier to Laramide transition when both types of structures are interacting. Based on new structural-stratigraphic relationships I propose that uplift of the San Rafael Swell reduced local subsidence (and accommodation), and allowed extensive clastic progradation (Wedge B). However, more work is needed to determine *how* the uplift of this structure may have influenced basin dynamics.

Dynamic subsidence (mega-regional subsidence), or development of dynamic topography (regional uplift) are other potential accommodation drivers. Such regional processes are linked to viscous corner-flow of the asthenosphere above a subducting slab

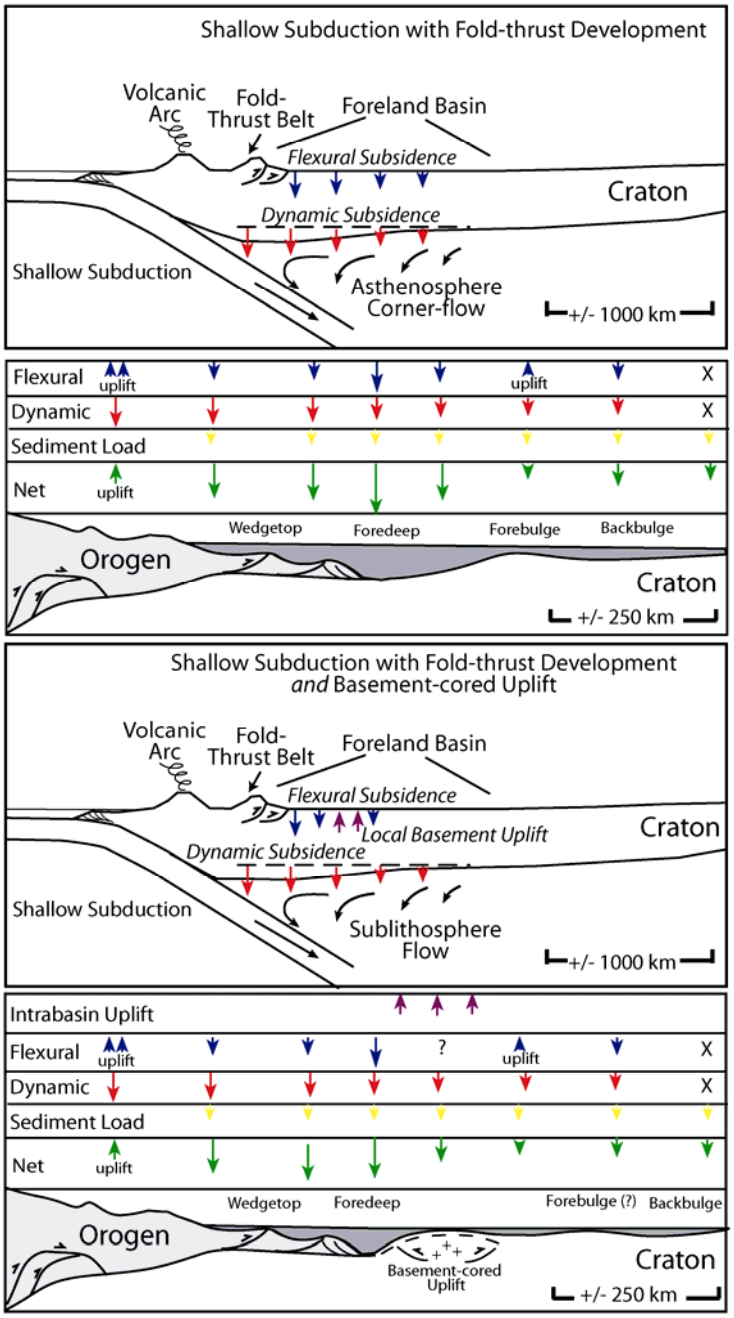

Figure 4.7 Summary of subsidence mechanisms in foreland basins during shallow angles of subduction. Note that the contribution of "dynamic" subsidence is predicted to be greater during shallow angles of subduction than during steep subduction (Gurnis, 1992; Catuneanu, 1997).

(Catuneanu et al., 1997). The corner-flow can cause long-wavelength subsidence, or uplift, that is superimposed on the shorter-wavelength flexural profile of a foreland basin. Numerical models and stratigraphic studies suggest dynamic subsidence rates can be >100 m My^{-1}, and sediment accumulation can be > 600 m (Gurnis, 1992; Liu and Nummedal, 2005). Several authors link flat-slab subduction to the switch from thin- to thick-skinned deformation (Dickinson and Snyder, 1978; Jordan and Allmendinger, 1986). Models predict that flat-slab subduction is conducive to *higher* dynamic subsidence rates (more accommodation) (Gurnis, 1992). Dynamic topography, not subsidence, is therefore needed to reduce accommodation and catalyze progradation. However, steeper subduction angles are predicted to cause creation of dynamic topography. This study documents Laramide deformation *with reduced* regional accommodation for Wedge B development; this is inconsistent with inferred flat-slab subduction at the onset of Laramide-style deformation.

CONCLUSIONS

I define three clastic wedges within a late Campanian interval of the Cordilleran foreland basin. The upper and lower clastic wedges (Wedges A and C) are thick (>600 m), wave-dominated shoreline successions with a characteristic stratigraphic rise and basinward stepping through time. The middle wedge (Wedge B) is strikingly different, and is characterized by a complex internal architecture with numerous incisions, extensive tide-dominated shoreline progradation and flat-to-falling shoreline trajectories.

Radiometrically constrained, high-resolution biostratigraphy allows calculation of clastic wedge progradation rates for the wedges. Wedges A and C prograded 200-250 km in more than ca. 5 My (roughly 17-80 km/My), whereas Wedge B prograded 340-400

km in just ca. 2 My (~170 km My^{-1}). The great extent, rapid progradation rate and internally complex architecture make the middle wedge (Wedge B) anomalous in this segment of the Cordilleran foreland basin, with important implications for foreland basin models.

The 400 km long regional sequence-stratigraphic correlation and high-resolution isopach maps presented here relate anomalous clastic wedge progradation (Wedge B) with the Sevier-Laramide transition in Utah. In conclusion, these new data indicate (1) Anomalous progradation and architecture of the Neslen-Sego-Corcoran-Cozzette clastic wedge (Wedge B) was coeval with an overlap, or transition, from thin- to thick-skinned deformation; (2) Uplift of a basement-cored structure (San Rafael Swell) in the subsiding foredeep reduced net subsidence and catalyzed clastic progradation and complex wedge architecture (Wedge B).

Chapter 5: Anatomy of a Low-accommodation Clastic Wedge, Upper Cretaceous, Cordilleran Foreland Basin, USA

ABSTRACT

Clastic wedge architecture provides insight into the relative roles of tectonics, basin dynamics, climate and eustasy on basin fill. Two main types of clastic wedges have been identified in Cretaceous Cordilleran foreland basin fill: (1) thick, vertically stacked, high aspect ratio wedges and (2) thinner, more extensive, low aspect ratio wedges. Low-aspect-ratio wedges are relatively rare in the Cordilleran foreland basin, and record a complex interplay of tectonic styles, climatic conditions and eustatic processes. Low aspect-ratio wedges typically consist of numerous incomplete, amalgamated and offlapping sequences with longer shoreline tongues that stack in a flat to falling pattern; these characteristics are the hallmarks of a low-accommodation setting. Detailed analysis of the external geometry, internal sequence architecture and facies assemblages for a low-aspect-ratio wedge in the Utah-Colorado segment of the Cordilleran foreland basin indicates a strong tectonic control on the development of these unique wedges. This clastic wedge consists of twenty-five facies assemblages and six key parasequence types that stack into 3rd-, 4th- and 5th-order sequences and sequence sets. High-order sequences stack in a striking offlapping pattern and contain a high proportion of tidally influenced facies with numerous incisions. Sequence-stratigraphic and biostratigraphic correlation, coupled with thinning trends indicate that the wedge developed coeval with Sevier- *and* Laramide-style deformation. The unique, low aspect ratio clastic wedge records a key overlap in deformation style that may have interfered with the normal (e.g., thrust-belt-controlled) flexural wavelength of the foreland basin,

thereby influencing accommodation patterns and wedge type. Recognition and analysis of these unique, low-aspect-ratio (i.e., low accommodation) clastic wedges may be useful indicators of change in tectonic style and basin dynamics.

INTRODUCTION

Foreland basin models were originally developed using the North American Cordilleran foreland basin. Early models compared basin fill patterns to models that predicted gross stratal geometries under a variety of load, flexure and rigidity parameters (Beaumont, 1981; Jordan, 1981). The models consider the gross depositional geometries of the basin fill, but fail to distill details within the basin fill that can provide additional information about basin dynamics. Detailed stratigraphic studies of Cordilleran foreland basin fill are abundant, but typically focus on the details of a single stratigraphic unit and/or in a geographically restricted area. Focus on either generalized regional approaches, or detailed local approaches leave many details about foreland basin development unresolved. Details of internal clastic wedges architecture, and the stratigraphic connection (or disconnection) to basin-margin structures is key to establishing a one-to-one linkage between tectonics and the basin fill.

The Cordilleran foreland basin is one of the best-dated foreland basins in the world. Superb age control is possible due to numerous bentonites and ashes that allow dating of numerous ammonite biozones. Ammonites that inhabited the Western Interior Seaway were abundant, widely dispersed and evolved quickly; this allows ammonite zones to be correlated relatively easily over long distances with high precision. In addition to the superb age control, excellent exposures of the thick basin fill make the Cordilleran foreland basin one of the best places to study foreland basin development. Moreover, it may be the only place where an entire clastic wedge can be traced (walked

out) and described in detail from the fold-thrust belt front for 100s of km to the distal part of the basin.

This paper highlights important details within the Cordilleran foreland basin fill at a regional scale (>400 km) and provides a high-resolution stratigraphic connection between basin-margin thrust-related growth strata and adjacent basin fill. This study defines 3 clastic wedges in Cordilleran foreland basin fill, and present a detailed sequence stratigraphic correlation, isopach maps and architectural analysis of one of the wedges.

The goals of this paper are to:
1) describe the internal and external geometry of a unique, low-accommodation clastic wedge, spanning some 2my between ammonite zones base E.jenneyi to base *B. perplexus.*
2) illustrate the relationship of the clastic wedge development to a key tectonic transition from thin- to thick-skinned style deformation in the Cordilleran foreland basin, and
3) postulate that external clastic wedge geometry can be used as an indicator of tectonic transitions tectonic in other foreland basins.

GEOLOGIC CONTEXT

The North American Cordilleran foreland basin is a north-south trending, roughly 3,000 km-long, 300-600 km-wide basin that spans the length of North America (Figure 5.1). The basin developed from the Jurassic(?) through Paleocene on the eastern side of the Sevier fold-thrust belt due to downward flexure of the crust adjacent to the lithospheric load created by an internally thickened fold-thrust belt. The close linkage between fold-thrust belt ("thin-skinned") loading and basin development is reflected in the gross geometry of basin fill. From latest Cretaceous through Paleocene time the contiguous Cordilleran foreland basin was punctuated by local, basement-involved structures. Basement-involved deformation throughout North America is termed "Laramide-style", or "thick-skinned" deformation, whereas fold-thrust deformation is

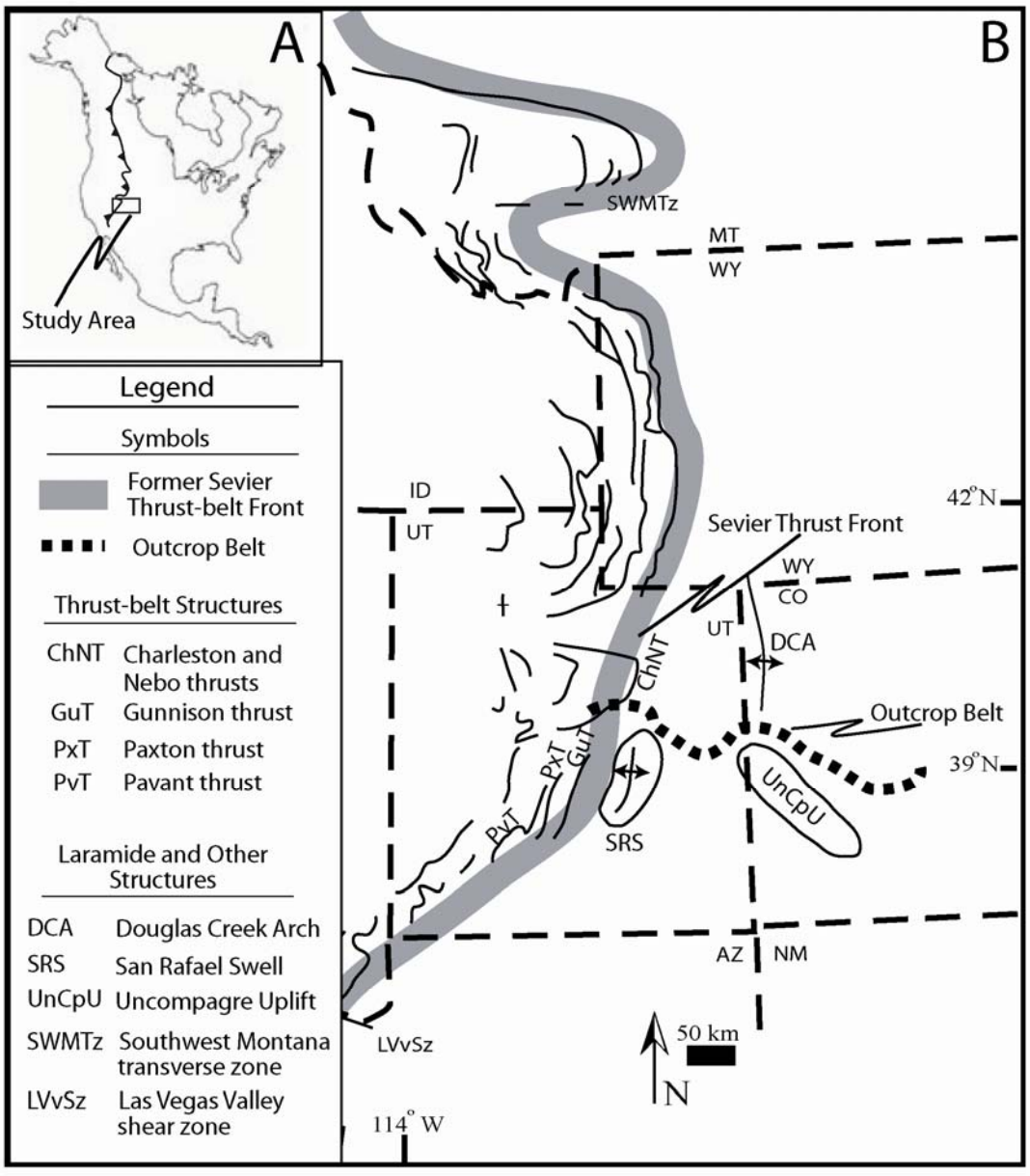

Figure 5.1 Location and geologic context of the study area.

termed “Sevier-style” or “thin-skinned” deformation. Although many workers refer to “Laramide deformation” as a time interval, I refer to it only as a structural style because the timing of Laramide-style deformation varies greatly along the length of the Cordilleran foreland.

Subduction of the Faralon plate at the western margin of North America is interpreted to have caused shortening within the Sevier fold-thurst belt and Laramide structures (Dickinson and Snyder, 1978; Jordan and Almendinger, 1986). The observation in South America that the latitudinal extent of shallow subduction corresponds to the latitudinal extent of Laramide-style structures prompted North American geologists to interpret a genetic link between subduction angle and deformation style (Jordan and Allmendinger, 1986). By comparison with the modern example in South America, the transition from thin- to thick-skinned deformation in North America is interpreted to have been caused by a shallowing of the subducting slab on the western margin of North America. However, the cause of the transition from thin- to thick-skinned deformation is hotly debated, and many questions remain unanswered. Among these questions is the precise timing of the onset of Laramide-style deformation in the Cordilleran foreland, and the potential influence of convergence rate on deformation styles.

Cretaceous strata comprise much the Cordilleran foreland basin fill, and record details of fold-thrust belt and Laramide-style deformation. Sevier fold-thrust belt highlands in the west provided the main sediment to the basin fill. Depositional systems transported detritus generally from west to east into the Western Interior Seaway, although there was local sediment contribution from early rising Laramide uplifts such as the Wind River Range (Martinsen et al., 1999). Excellent, near-continuous exposures of

Upper Cretaceous strata are present on the former, leading edge of the Sevier fold-thrust belt (i.e. present-day eastern Wasatch Plateau) and along the length of the Book Cliffs from Utah to Colorado. This study uses a 400 km east-west stratigraphic transect that bisects the Cordilleran foreland basin to establish a more precise link between fold-thrust belt kinematics, early Laramide deformation and clastic wedge development in the adjacent foreland basin (Figure 5.1). The transect crosses fold-thrust structures in the west, and an intra-basinal Laramide uplift (San Rafael Swell).

STRATIGRAPHY AND PREVIOUS WORK

Cretaceous stratigraphy and east-prograding clastic "tongues" were first described by Speiker (1949), Young (1955), Fisher (1960), Armstrong (1968) and Van de Graff (1972). West of the Green River, Fisher et al. (1960) assigned the strata above the coal-bearing Blackhawk Formation to the Castlegate Sandstone and Price River Formation to Cretaceous strata overlying the Castlegate Sandstone. East of the Green River, Fisher et al. (1960) divided the Cretaceous stratigraphy into the Castlegate Sandstone, Buck Tongue of the Mancos Shale, Sego Sandstone, Neslen Formation, Farrer Formation and Tusher Formation. This nomenclature was modified by Fouch (1983) and Lawton (1986), who split the Castlegate Sandstone into three units: (1) the lower Castlegate Sandstone for the extensive, cliff-forming sandstone above the coal-bearing Blackhawk Formation, (2) the upper Castlegate Sandstone for the recessive, siltstone- and mudstone-rich interval above the lower Castlegate Sandstone, and (3) the Bluecastle Tongue for the massive, cliff-forming sandstone above the recessive Upper Castlegate Sandstone. Fouch et al. (1986) and Olsen et al. (1995) use "Castlegate Formation", and split the Castlegate Formation into a lower unit, middle unit and Bluecastle Tongue. Robinson and Slingerland (1998), and McLaurin and Steel (2000) use "lower Castlegate sandstone",

"middle Castlegate sandstone" and "Bluecastle Tongue. The name assigned to the recessive, siltstone- and mudstone-rich interval is the chief difference in the proposed stratigraphic divisions. In this study I use "middle Castlegate Sandstone" for the recessive, middle interval within the Castlegate Sandstone. Figures 5.2 and 5.3 summarize the nomenclature used in this study.

Correlation of Cretaceous sandstones and shale from the Book Cliffs westward to conglomeratic strata exposed on the eastern margin of the Wasatch Plateau was unclear until palynologic data and new subsurface data were published by Robinson and Slingerland (1998), and Horton et al., (2004). Early studies suggested that quartziticconglomerates in the Wasatch and Gunnison Plateaus were equivalent to the lower part of the Castlegate Sandstone (lower Castlegate Sandstone). Using copious palynologic data, Robinson and Slingerland (1998) determined that conglomerate units exposed in the Bennion Creek area (eastern Wasatch Plateau), although assigned to the Price River Formation, are not time-equivalent to the sandstone-dominated Price River Formation exposed near Price, UT. Conglomeratic units exposed at the eastern margin of the Wasatch Plateau are (herein referred to as Price River conglomerate) are equivalent to the Castlegate Sandstone, including the lower Castlegate Sandstone, middle Castlegate Sandstone, and Bluecastle Tongue.

Conglomeratic growth strata are developed in the Price River conglomerate and record contractional deformation at the former front of the Sevier fold-thrust belt (Horton et al., 2004). The conglomerates intertongue down-dip with sandstones, siltstone, mudstone and shale exposed in the Book Cliffs. Previous work using subsurface correlation and palynologic data suggests that the conglomeratic growth strata correlate with the Castlegate Sandstone, but the precise connection of basin-margin growth strata

to individual Castlegate Sandstone units and Bluecastle Tongue was still unclear (Robinson and Slingerland, 1998; Horton et al., 2004). The present study pursues this problem, but also greatly extends the tectonic response arena out to the middle Castlegate Sandstone, Bluecastle Tongue, Buck Tongue of the Mancos Shale, Sego Sandstone, Neslen Formation, Anchor Mine Tongue of the Mancos Shale, Corcoan Member and Cozzette Member of the Iles Formation (Figures 5.2, 5.3).

Six, radiometrically dated ammonite zones and two palynomorph zones constrain the stratigraphic correlation and isopach maps of Middle and Upper Campanian strata in this study (Figure 5.3) (Obradovich, 1994; Izett et al., 1998; Cobban et al., 2006). The ammonite zones span from 79 Ma (base of B. asperiformis) to 75.08 Ma (base of E. jenneyi). Particularly high ammonite resolution is present from B. scotti to E. jenneyi, spanning only 600,000 years, with dating errors between 100,000 to 280,000 years (Izette et al., 1994). Ammonites are common in shales, and are particularly common along marine flooding surfaces where fossils are typically concentrated (Gill and Hail, 1975). This is very useful for enhancing outcrop to subsurface stratigraphic correlation and building biostratigraphically constrained isopach maps.

METHODS

This study presnets (1) a >400 km-long transect that bisects the Cordilleran foreland basin, extending from the former front of the Sevier fold-thrust belt to distal zones (>300 km) of the basin, (2) high resolution isopach maps and (3) detailed descriptions of the architecture of an anomalous clastic wedge. The dataset consists of forty-eight detailed stratigraphic sections and sixty eight published well logs and sections (Figure 5.4). Six ammonite zones, published palynology, detailed photomosaics, airplane-shot photomosaics of the entire Book Cliffs and on-ground mapping of key

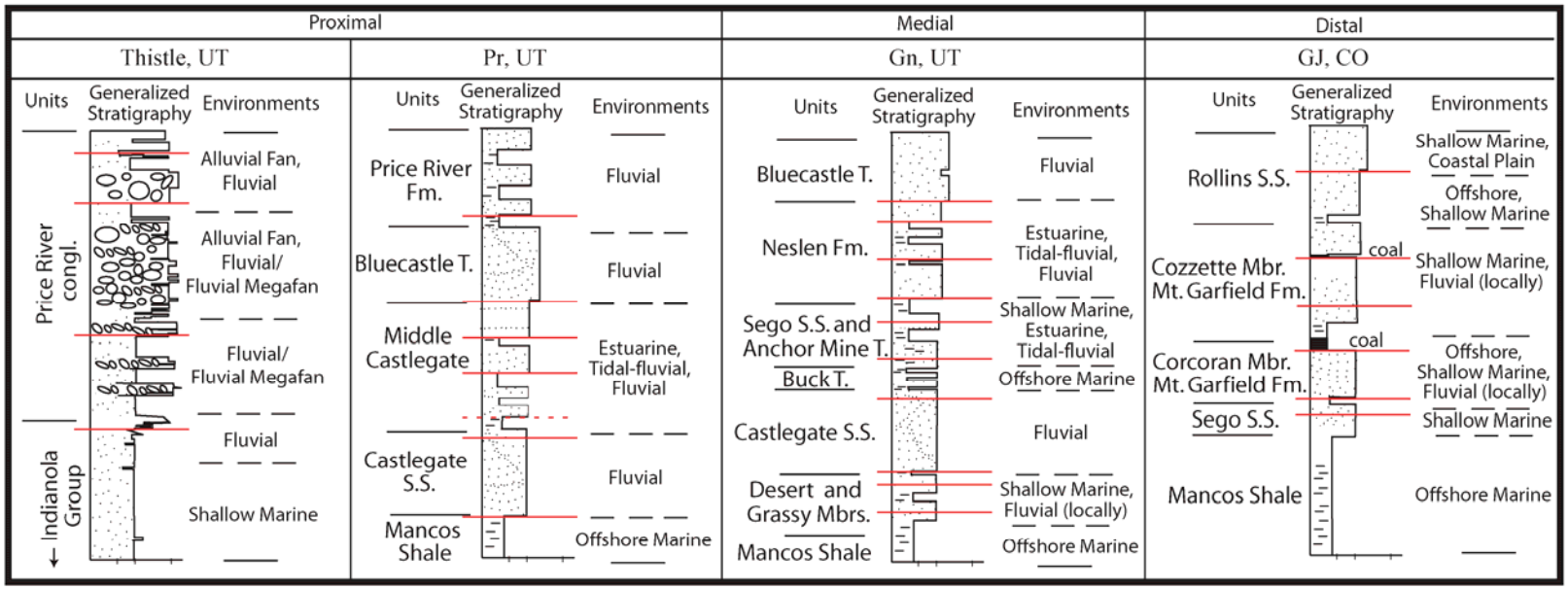

Figure 5.2 Generalized stratigraphic columns for the proximal (0-100 km), medial (100-250 km) and distal (250-500 km) areas of foreland basin fill showing the unit names and distribution of facies in each zone.

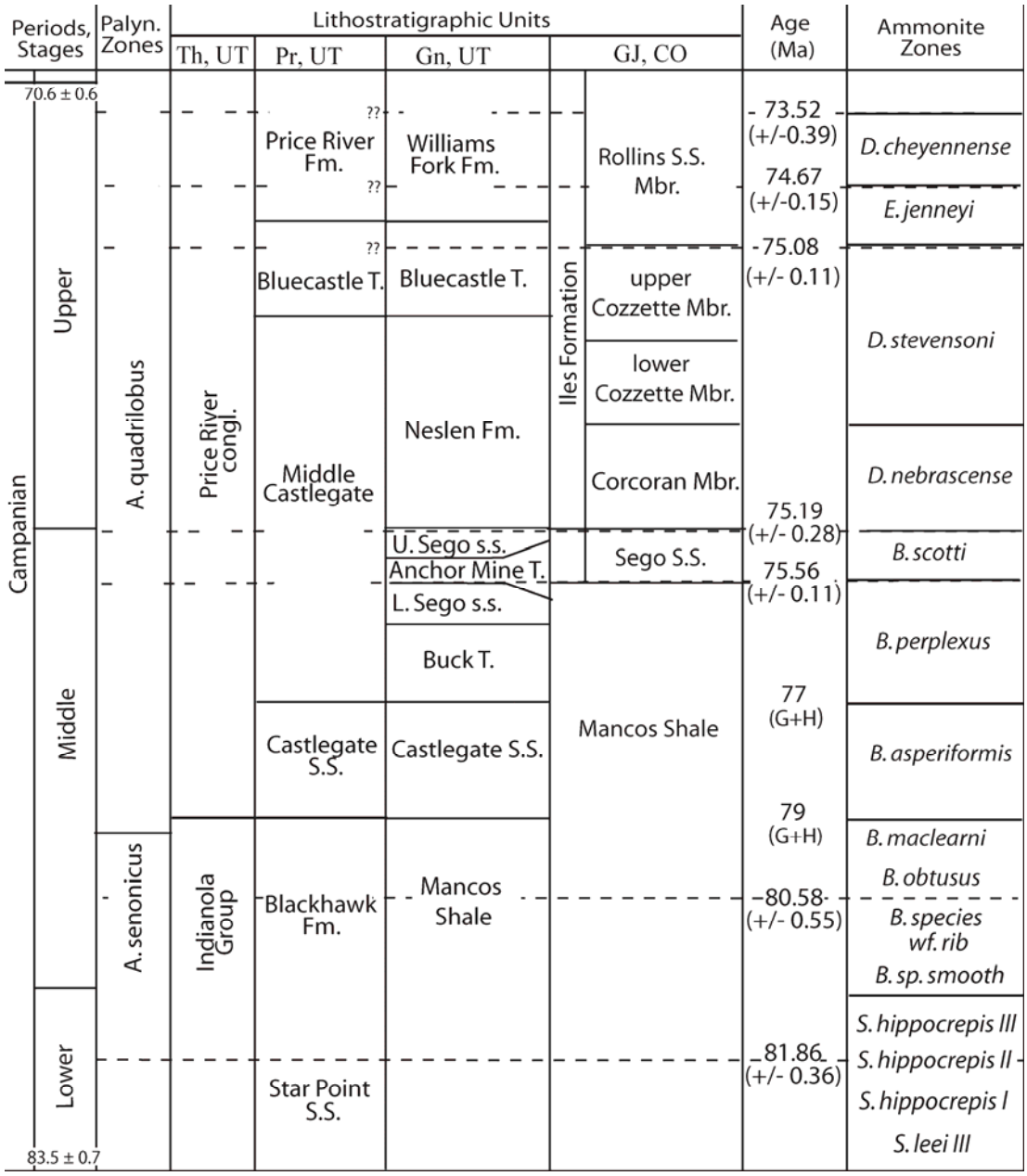

Figure 5.3 Correlation chart for middle and upper Campanian strata in the Utah-Colorado segment of the Cordilleran foreland basin.

stratigraphic surfaces were used to constrain the correlation. Sections were measured at an interval of 3-10 miles and between previously published sections whenever possible.

The stratigraphic correlation from marine to non-marine strata relies on correlation of marine flooding surfaces that correlate up-dip to transgressive intervals within coastal-plain and estuarine strata containing brackish-water and tidal-influence indicators, as well as strata with isolated fluvial sandstone bodies. Considerable progress toward accurate correlation of marine to non-marine strata has been made in the last 20 years, and is broadly accepted despite some key assumptions in general (Shanley et al., 1991; Shanley and McCabe, 1992), as well as in the study area (Olsen et al., 1995; McLaurin and Steel, 2000; but see also Yoshida et al., 2001). In proximal (0-100 km) areas, published palynologic data, field-estimated detrital modes and stratigraphic patterns in paleocurrent direction helped constrain the correlation. In distal areas, published ammonite biostratigraphy constrained the correlation (Lawton, 1986; Robinson and Slingerland, 1998; Horton et al., 2004).

Public well log data were integrated with outcrop data to construct isopach maps (Appendix B and C). These subsurface data were correlated to new, and published stratigraphic sections using flooding surfaces and correlation of extensive coal zones (Fisher, 1960). Because ammonites tend to concentrate in condensed sections at marine flooding surfaces I was able establish a link between well logs and high-resolution ammonite biostratigraphy.

DEPOSITIONAL FACIES: FUNDAMENTAL BUILDING BLOCKS OF CLASTIC WEDGES

A wide array of depositional environments are recorded in foreland basin strata exposed along the 400 km-long stratigraphic transect (Figures 5.2 and 5.4). Twenty-four facies are present within the regional transect, and group these into four lithofacies

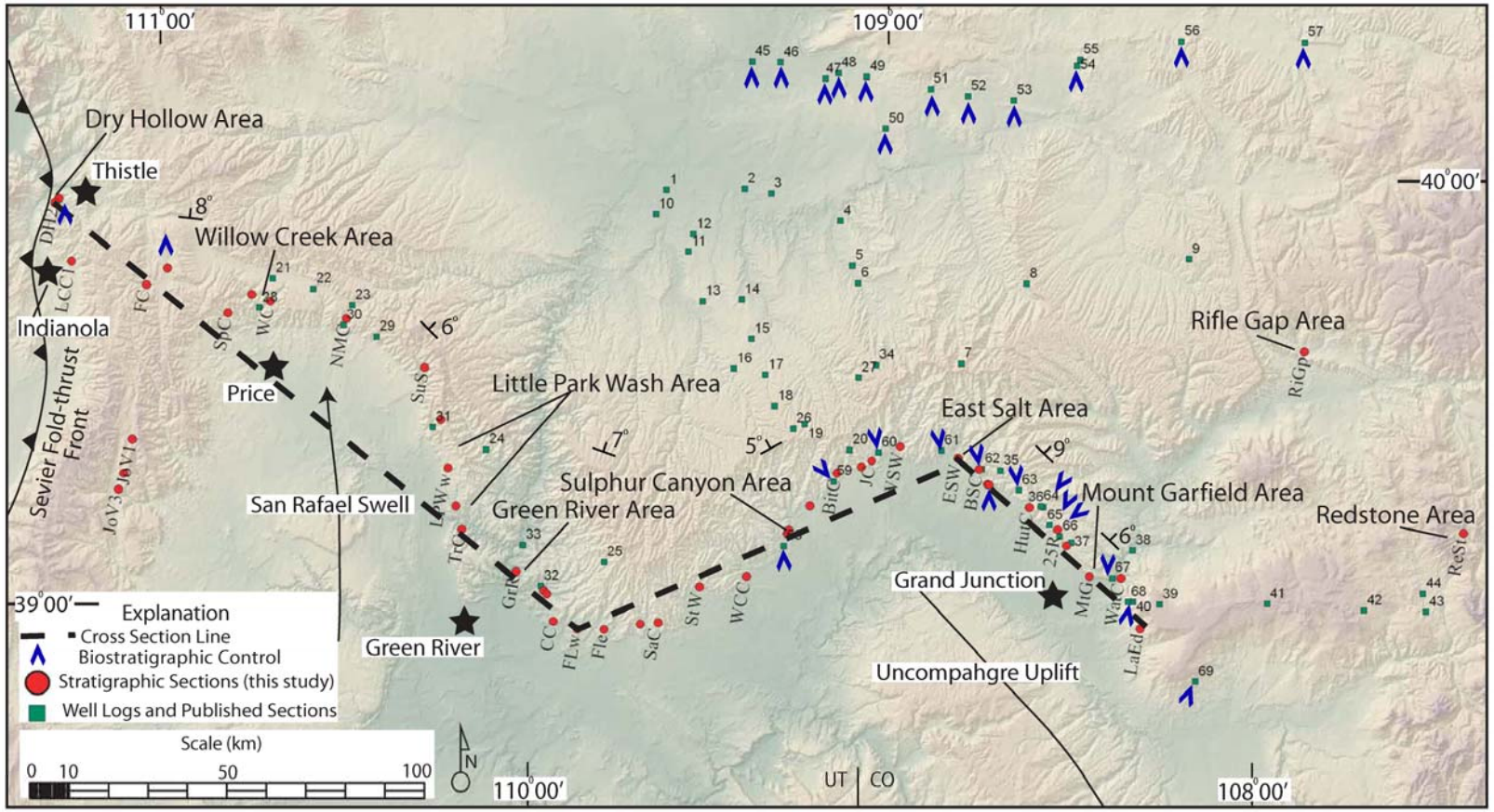

Figure 5.4 Digital elevation model of the Book Cliffs, Utah and Colorado, showing the data locations.

assemblages based on the relative proportion of conglomerate, sandstone and mudstone. Facies are distinguished based on characteristic bedding style, constituent sedimentary structures, fabric and grain-size. A broader definition of facies that contain suites of sedimentary structures was used to simplify the numerous and highly diverse depositional facies present in the regional transect.

Facies Assemblage A: Conglomeratic Facies

Description

Lithofacies Assemblage A consists of four conglomeratic facies (Figure 5.5). Facies comprising Assemblage A are restricted to the thrust-belt proximal (0-100 km from the Sevier fold-thrust belt) zones of the stratigraphic transect through the Cordilleran foreland basin. Facies A1 is a massive, ungraded cobble and pebble conglomerate with a disorganized fabric. Facies A2 consists of beds of massive, ungraded cobble and pebble monomict conglomerate with angular to subangular clasts, interbedded with lenses of trough cross-stratified, polymict pebble conglomerate with well rounded clasts. Facies A3 consists of imbricated, clast-supported cobble conglomerate interbedded with trough cross-stratified and low-angle stratified pebble conglomerate and pebbly sandstone (Figure 5.6). Facies A4 is a trough cross-stratified pebble and granule conglomerate with lenses of trough cross-stratified granules and sand (Figure 5.6).

Interpretation

Facies comprising Assemblage A are interpreted as alluvial fan, and gravel-dominated or mixed sand-gravel braided fluvial deposits (Table 1). Structureless beds, lack of scours, randomly oriented clasts, unsorted matrix and clast-rich character of Facies A1 suggest deposition by non-cohesive (clast-rich) debris flows (Nemec and Steel,

1984; Postma, 1986) (Figure 5.6); subordinate interbeds of low-angle stratified pebble conglomerate that fill interstices are consistent with winnowing of debris-flow material by overland flow (Blair and McPherson, 1994). Facies A1 is consistent with deposition and reworking of debris flows on a debris-flow dominated alluvial fan.

Facies A2 is interpreted as debris-flow dominated alluvial fan deposits with fluvial interaction (Doughety, 1995; Schmitt and Aschoff, 2003) (Figure 5.5). The massive, poorly organized, clast-supported character and poorly sorted matrix of thicker beds suggest that they were deposited by debris-flows. However, the numerous lenses of trough cross-stratified pebble conglomerate and scours into massive, disorganized conglomerate suggest excessive reworking of debris flow material by turbulent stream flow. The monomict character and abundance of more angular, labile clast lithologies suggests a proximal (~0-25 km) source with limited drainage basin for the disorganized cobble conglomerate component of Facies A2. By contrast, the polymict character and abundance of well rounded resistant lithologies in the cross-stratified pebble conglomerate lenses suggest a more distal, better-integrated drainage basin (Colombo, 1994; Dougherty, 1997). I interpret deposition of poorly organized, angular cobble conglomerates by debris flows deposited at the toe of a debris-flow dominated fan, followed by extensive reworking by fluvial processes by an adjacent (axial?) river, possibly during seasonally higher river discharge. Recognition of this subtle facies is important because, in a vertical section, it can be used to track the extent of progradation of alluvial fans into the adjacent basin.

Facies A3 and A4 are interpreted as braided fluvial deposits (Figure 5.5 and 5.6). Both facies have lenticular bedding geometries, numerous scours and fining-upward successions that suggest deposition within channels. Additionally, both facies have

trough, and planar-tabular cross-stratification suggesting angle-of-repose deposition on migrating 3D and 2D dunes. Broad, low-angle (2-5 degrees) bedding containing imbricated, clast-supported cobble conglomerates with a paleocurrent that is roughly parallel to the dip direction of the low-angle bedding suggests deposition by down-stream accreting bars. Down-stream accreting bars, imbrication, channel features, fining-upward successions and migrating bars are consistent with deposition within a braided fluvial environment (Miall, 1996). The more clast-rich character of Facies A3 suggests that the braided fluvial system was gravel-dominated. By contrast, the subequal proportions of sand and gravel in Facies A4 suggests deposition by mixed sand and gravel braided fluvial systems.

Facies Assemblage B: Sandstone-dominated Facies

Description

Lithofacies Assemblage B consists of eleven sandstone-dominated facies (Figure 5.7), that are present in various proportions throughout the stratigraphic transect with coarser-grained sandstones generally concentrated near the top of the succession and nearer to the Sevier fold-thrust belt. Facies B1, B2, B3 and B4 form broadly lenticular bed- sets that consist of ripple cross-laminated, trough cross-stratified, planar-tabular cross-stratified sandstone with numerous internal scours and subordinate mud drapes and/or pebble lenses. Facies B5 consists of basin-ward-inclined, offlapping bed-sets that contain trough cross-stratification, sigmoidal cross-bedding, climbing-ripple

Assemblage A

Facies	Bedding	Sedimentary Structures	Grain size/Grading	Other	Example	Depositional Process	Depositional Environment
1	3-6 m wide, 1-3 m thick	Low-angle stratification locally in small scours near base	Cobbles and pebbles ungraded	Massive, ungraded, polymict, clast-supported, subangular to subrounded clasts, sand and pebble matrix		Non-cohesive debris flow and "winnowing" by shallow, turbulent surface runoff (Postma, 1986; Blair and McPherson, 1994)	Debris-flow Alluvial Fan
2	3-6 m wide, 1-2 m thick	Massive conglomerate with lenses of trough cross-stratified pebble conglomerate, locally	Cobbles and pebbles ungraded with lenses of stratified fining-upward, pebble-granule conglomerate	Massive, ungraded, polymict, matrix-supported, rounded clasts, sand and pebble matrix with trough cross-stratified, fining-up, pebble-granule lenses		Debris flow and reworking by 3D dunes in turbulent flow conditions (Blair and McPherson, 1994; Dougherty, S.L., 1997; Schmitt and Aschoff, 2003)	Interaction of Debris-flow Alluvial Fan and Fluvial (Fan Toe)
3	2-4 m wide, 0.5-2 m thick	Clast imbrication, trough cross-stratification, low-angle stratification, accretion sets	Cobbles, pebbles and granules; fining-upward successions	Stratified, polymict, clast-supported, subrounded to rounded clasts, moderately sorted sand and granule matrix		Bed-load transport and deposition by down-stream accreting gravel bars and 2D dunes within channels under turbulent, upper flow regieme conditions (Williams and Rust, 1969; Miall, 1994)	Gravel-dominated Braided Fluvial
4	2-4 m wide, 0.5-2 m thick	Clast imbrication, trough cross-stratification, low angle stratification, accretion sets	Granules pebbles and sand; fining-upward successions	Stratified, polymict, clast-supported, subrounded to rounded clasts, moderately sorted sand and granule matrix		Angle-of-repose, bed-load transport by down-stream accreting sand-gravel bars and 2D dunes within channels under turbulent, upper flow regieme conditions (Williams and Rust, 1969; Miall, 1994)	Sand and Gravel Braided Fluvial

Figure 5.5 Summary of facies comprising facies Assemblage A- conglomeratic facies.

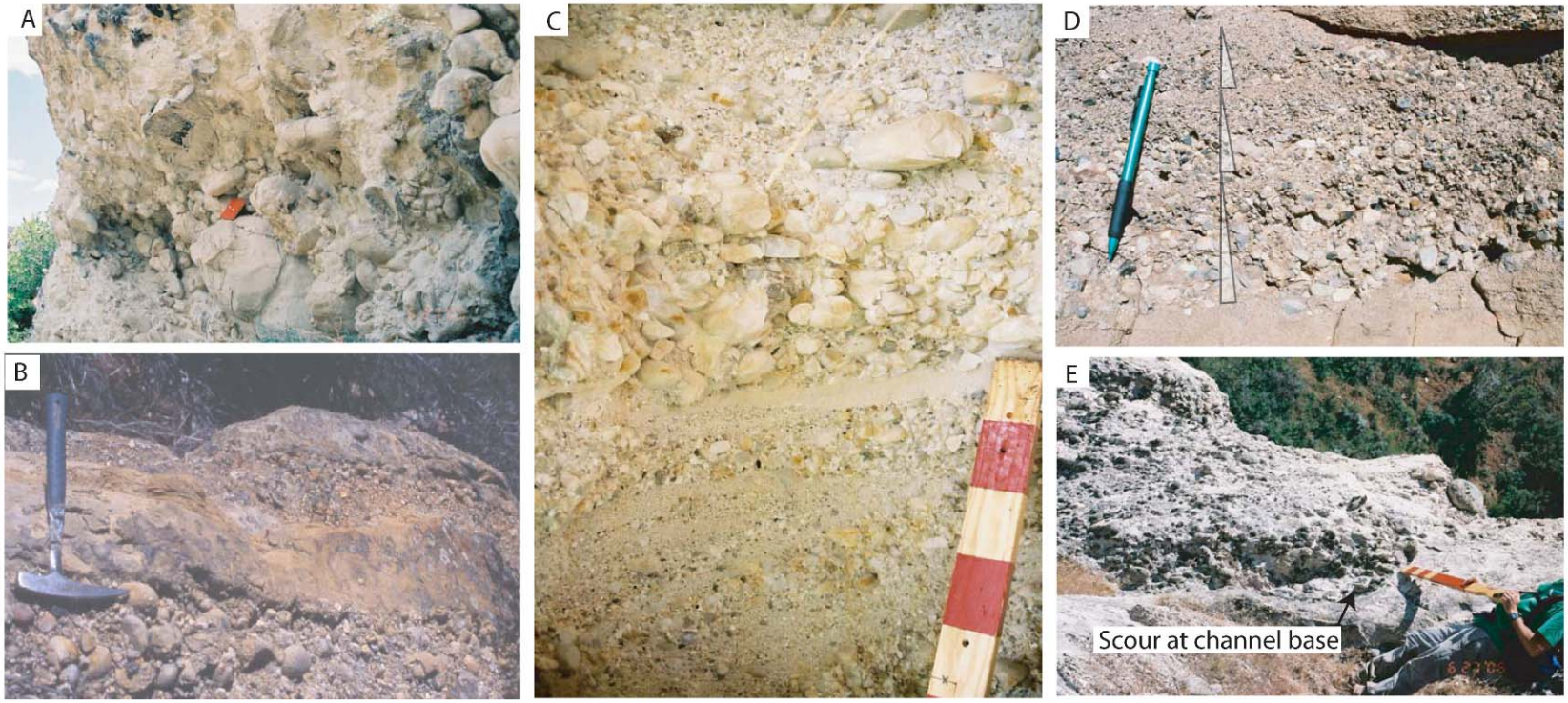

Figure 5.6 Examples of conglomeratic facies.

cross-lamination, bi-directional ripple cross-lamination, and subordinate mud drapes and flat-pebble conglomerates. Facies B6, B7, B8, B9, B10 and B11 are laterally continuous, flat-based sandstone units with various proportions of trough, planar-tabular and wedge-planar cross-stratification, hummocky cross-bedding, horizontal stratification, herringbone cross-stratification, wave-ripple lamination and subordinate mud drapes and trace fossils.

Interpretation

Facies B1, B2, B3 and B4 are interpreted as channel-fill deposits because of their sharp base, lenticular bed geometry, fining-upward grain-size trend and numerous internal scours (Figures 5.7 and 5.8). The markedly coarser-grained character, and waning-flow succession of sedimentary structures (trough cross-beds to ripple cross-laminations) of Facies B1 suggests deposition by a fluvial system with flashy, or seasonal discharge. Facies B2 is interpreted as braided fluvial deposits because it contains amalgamated, multi-lateral lenses (channel bodies) that contain moderate- to high-energy sedimentary structures such as trough, planar-tabular and wedge-planar cross-stratification that locally comprise low-angle, down-stream accreting bed-sets (Figure 5.8). However, Facies B2 lacks the "waning-flow" succession of sedimentary structures, and is therefore interpreted as a fluvial system with more consistent flow conditions such as those of a sandy braided fluvial system. Facies B3 is interpreted as meandering fluvial deposits because (1) it contains numerous low-angle, inclined bed-sets that have paleocurrents subnormal to the inclined beds, (2) have higher-energy sedimentary structures (trough cross-beds) concentrated at the toe of inclined beds and (3) have lower-energy sedimentary structures (ripple cross-laminations) near the top. These characteristics are the hallmark of laterally accreting bars (point-bars) within a sinuous,

meandering fluvial system (Miall, 1994). Unlike the other channelized facies, Facies B4 has clear evidence of tidal influence such as bi-directional ripple cross-lamination, bi-directional trough cross-stratification and subordinate double mud-drapes (Figure 5.8) (Dalrymple, 1992). Facies B4 is therefore interpreted as sandy, tidally influenced channels that may be part of an inner estuary or distributary channels on a tidally influenced delta.

The unique, offlapping, inclined bed-sets characteristic of Facies B5 are interpreted as bay–head delta clinoforms (Figure 5.8). The small scale (5-10 m thick, 20-30 m long) of the inclined beds and lack of marine trace fossils preclude a marine delta interpretation. Yet, the systematic down-clinoform decrease in energy, as recorded by sedimentary structures (i.e., trough cross-beds are concentrated near the top and ripple cross-laminations and mud drapes are concentrated near the base), precludes interpretation as a large fluvial point bar. Additionally, the inclined beds become muddier from top to toe suggesting that sand was transported into relatively quiet water, muddy environments such as a lagoon or central estuary basin (Figure 5.8). Steeply climbing ripple cross laminations and soft-sediment deformation near the toes of inclined beds suggest high rates of sediment fall-out from the feeding river channels. Additionally, mudstone rip-up clasts, subordinate sigmoidal cross-beds and double mud drapes suggest tidal influence. The bay-head delta facies (Facies B5) comprises deltas at the head of embayments or deltas at the head of an estuary (Dalrymple, 1992).

Assemblage B

Facies	Bedding	Sedimentary Structures	Grain-size/Grading	Other	Example	Interpretation
1	3-6 m wide, 1-2 m thick broad lenses	Trough cross-stratification, planar-tabular stratification and climbing ripple cross-lamination with numerous scours and cut/fill structures No bioturbation	Medium to coarse-grained sand with pebbles; fining-upward, couplets common	Sharp-based, isolated and amalgamated, lenticular beds with pebbles concentrated in scours and at base of beds and fine-grained ripple cross-laminated sandstone near top; mudstone interbeds and drapes are absent Multi-lateral channels and down-stream accretion sets present	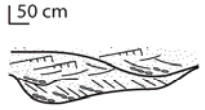	Sand and Gravel Braided Fluvial/ Fluvial Megafan
2	2-5 m wide, 0.5-3 m thick amalgamated lenses	Trough cross-stratification and planar-tabular stratification with numerous scours and cut/fill structures concentrated near base No bioturbation	Fine- to medium-grained sand; fining-upward couplets common	Sharp-based, amalgamated, lenticular beds with coarse sand and granules concentrated at base of beds; mudstone interbeds and drapes generally absent Multi-lateral channels, and down-stream accretion sets present		Sandy Braided Fluvial
3	3- 8 m wide, 0.5-2 m thick broad lenses	Trough cross-stratification and ripple cross-lamination No bioturbation	Fine- to medium-grained sand with ancillary silt and mud; fining-upward couplets common	Sharp-based, isolated and amalgamated lenticular beds with medium-grained sand concentrated at base of beds Multi-story and multi-lateral channels, and lateral accretion sets present Mudstone interbeds and organic material on upper part of accretion sets	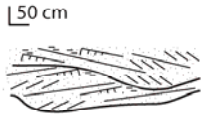	Sandy Meandering Fluvia
4	4- 15 m wide, 0.5-3 m thick offlapping inclinded beds	Trough cross-stratification, sigmoidal cross-bedding, and ripple cross-lamination Steeply-climbing ripple cross-lamination are common, and some bi-directional ripple cross-laminations are present No bioturbation	Fine-grained sand with ancillary silt and mud; coarsening-upward trend within inclined beds	Basinward-stepping, inclinded beds that thicken and coarsen-upwards Higher energy structures are at top of inclined beds (trough, sigmoidal), low-energy structures (climbing ripple cross-laminations) and mud-drapes are at the toes; soft sediment deformation and convoluted bedding found near clinoform break and toes	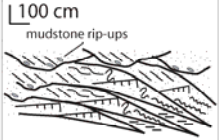	Bay-head Delta (Inner Estuary)
5	>15 m wide, 0.25-2 m thick amalgamated	Trough cross-stratification, planar-tabular and horizontal stratification No bioturbation	Fine- to medium grained sand	Flat-based, continuous (> 25 m long) beds Locally, beds comprise landward-directed, shingled lenses *Ophiomorpha* burrows rare	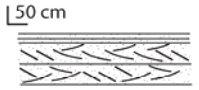	Upper Shoreface (Barrier, Strandplain and Wave-dominated Delta)
6	>15 m wide, 0.5-3 m thick amalgamated	Hummocky-swaley stratification Rare, low-diversity bioturbation	Fine-grained sand	Flat-based, amalgamated, continuous beds Hummocks are locally truncated by overlying hummocky beds Locally, beds are broad lenses with a landward-directed shingled pattern *Ophiomorpha* burrows abundant	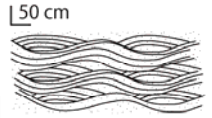	Middle to Lower Shoreface (Barrier, Strandplain and Wave-dominated Delta)

Figure 5.7 Summary of facies comprising facies Assemblage B- sandstone-dominated facies.

Assemblage B

Facies	Bedding	Sedimentary Structures	Grain-size/Grading	Other	Example	Interpretation
7	1-10 m wide 0.10-1 m thick	Hummocky-swaley stratification and wave-ripple cross lamination Moderate, low-diversity bioturbation	Fine- to very fine-grained sand	Flat-based, continuous (> 25 m long) bed sets Hummocks are locally truncated by overlying hummocky beds Locally, bed sets are broad lenses with a landward-directed shingled pattern *Ophiomorpha* burrows abundant	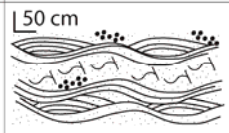	Lower Shoreface (Barrier, Strandplain and Wave-dominated Delta)
8	>15 m wide, 0.5-3 m thick amalgamated	Massive with relict hummocky-swaley stratification Abundant, low-diversity burrows	Fine- to very fine-grained sand	Flat-based, amalgamated, continuous beds Hummocks are locally truncated by overlying hummocky beds *Ophiomorpha* burrows are pervasive	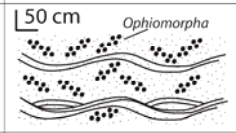	Lower Shoreface (Barrier, Strandplain and Wave-dominated Delta)
9	1-10 m wide 0.5-3 m thick	Planar-tabular and wedge-planar stratification with rhythmic beding and horizontal stratification Ancillary massive mudstone with mud cracks No bioturbation	Fine- to medium-grained sand	Flat-based, coaly beds with rhythmic, flat laminations that vary in thickness (1-8 cm) and organic content Current ripple forms are low amplitude (< 2 cm in height) Mud drapes common in rippled sections and locally have mud cracks Ancillary mud rip-up clasts on lower bounding surfaces	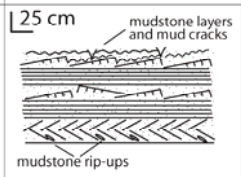	Sandy Tidal Flat
10	5-10 m wide 0.5-3 m thick	Bi-directional lanar-tabular and wedge-planar stratification (herringbone) with subordinate sigmoidal cross-bedding No bioturbation	Fine- to medium-grained sand	Flat-based, with Ancillary mud rip-up clasts on lower bounding surfaces	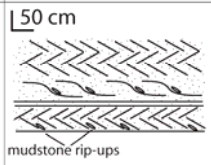	Sandy Tidal Bars
11	3- 8 m wide, 0.5-2 m thick broad lenses	Bi-directional ripple cross-lamination and climbing ripple cross-lamination with subordinate trough cross-stratification No bioturbation	Fine- to very fine-grained sand	Sharp-based, isolated lenticular beds Multi-story channels and lateral accretion sets present Thin mudstone interbeds (2-10 cm) and organic drapes	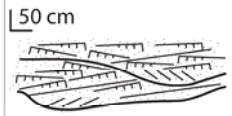	Sandy Tidal Channels

Figure 5.7 continued

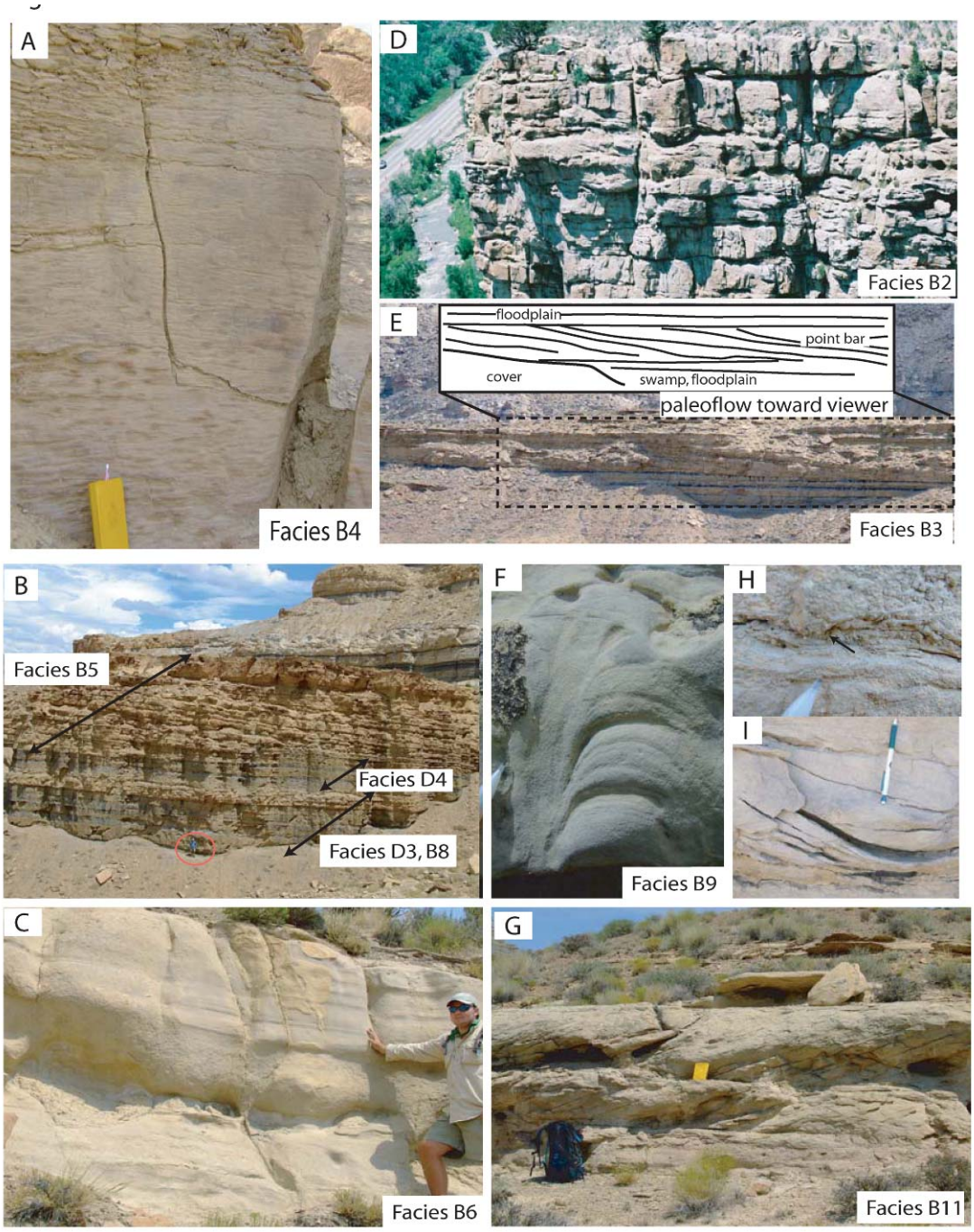

Figure 5.8 Examples of sandstone-dominated facies.

Facies B6, B7, B8, B9, B10 and B11 are laterally continuous, flat-based, sheet-like sandy units that record deposition in open marine to marginal marine environments. The flat-based sandstone units comprising Facies B6 are interpreted as upper shoreface and foreshore deposits (Figure 5.8). Continuous, sheet-like bed-sets are consistent with a shoreline setting. Trough cross-stratification and planar-tabular cross-stratification suggest angle-of-repose deposition of sand by migrating 2- and 3-D dunes in the upper part of the lower flow regime. Subordinate horizontal stratification with parting lineations suggest deposition under upper flow regime conditions; this, coupled with the sheet-like character, suggest deposition within the foreshore. Facies B7, B8 and B9 contain various proportions hummocky cross-stratification, wave-ripple cross-lamination and marine trace fossils that suggest deposition within a shoreface. Amalgamated hummocky cross-bedding present in Facies B7 suggests deposition well above storm wave base, but below fair-weather wave base such as the middle to lower shoreface.

Isolated hummocky cross-bedding with moderate to pervasive bioturbation found in Facies B8 and B9 suggests less frequent storm influence and that storm events alternated with periods of tranquil conditions; this is characteristic of the lower shoreface (Figure 5.8). Bi-directional current indicators and subordinate double mud-drapes present in Facies B10 and B11 suggest fluctuating current strengths and tidal influence. Rhythmic flat laminations, bi-directional ripple cross-lamination and mud cracks present in Facies B10 suggest deposition within the intertidal, zone of a tidal flat environment. Sigmoidal cross-stratified sets and herringbone cross-stratification is consistent with bedload deposition by reversing tidal currents in a subtidal bar complex.

Facies Assemblage C: Heterolithic Facies

Description

Facies Assemblage C consists of six heterolithic facies (Figure 5.9) that are most abundant east of Price, UT in the Middle Castlegate sandstone and west of the Colorado-Utah border in the Sego Sandstone and Neslen Formations. Facies C1, C2 and C3 form broadly lenticular bed-sets that consist of bi-directional ripple cross-laminated, flaser-bedded and sigmoidal cross-bedded sandstone sets with abundant mud drapes, and mudstone interbeds and lenses (Figure 5.10). Facies C1 forms thinner (<50 cm) sandstone units that are interbedded with structureless, organic-rich mudstone and siltstone that locally contain root traces. Facies C4 forms inclined (8-15˚) bedsets consisting of bi-directional ripple cross-laminated, flaser bedded and sigmoid cross-bedded sandstone with pervasive mud drapes and mudstone interbeds (Figure 5.10). Facies C5 and C6 are flat-based units that consist of lenses of sigmoidal cross-bedded sandstone interbedded with mudstone, or extensive layers of wave- and current-ripple cross-laminated sandstone.

Interpretation

The sharp-based nature and lenticular geometry of units of Facies C1, C2 and C3 suggest deposition within, or adjacent to channels (Figure 5.10). Facies C1 is interpreted as crevasse splay deposits in a fluvial overbank setting based on the thinner, more lobate geometry of the sandstone units and presence of root traces in the finer-grained components of the facies. Bi-directional current indicators, presence of double mud drapes, flaser bedding and sigmoidal cross-bedding suggest that Facies C2 and C3 were

Assemblage C

Facies	Bedding	Sedimentary Structures	Grain-size/Grading	Other	Example	Interpretation
1	2- 8 m wide, 0.1-1 m thick broad lenses	Ripple cross-lamination, root traces in mudstone Moderate bioturbation	Heterolithic with very fine- to fine-grained sand with mud; fining-upward sand couplets common	Thin, discontinuous lenticular beds of ripple cross-laminated sandstone interbedded with locally bioturbated mudstone Typically lateral to channel sandstone	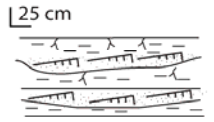	Crevase Splay (lateral to meandering fluvial and tidal channels)
2	0.25-2 m wide, 0.25- 2 m thick	Sigmoidal cross-bedding, bi-directional ripple cross-laminations, numerous double mud drapes and ancillary flaser and lenticular bedding	Heterolithic with fine- to medium-grained sand with lenses and thin layers of mudstone	Sharp-based, lenticular bed sets; lenticular mudstone interbeds and pervasive mud-drapes	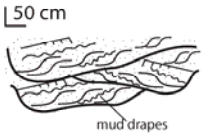	Tidal Channels (estuary or delta)
3	3-6 m wide, 2-4 m thick (inclined in multiple directions)	Bi-directional ripple cross-lamination, double mud drapes and ancillary, sigmoidal cross-bedding	Heterolithic with fine- to medium-grained sand with lenses and thin layers of mudstone	Sharp-based, lenticular bed sets with pebbles concentrated in scours and at the base; discontinuous mudstone interbeds and double mud-drapes are common Multi-story channels and lateral accretion sets present	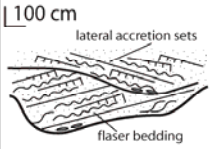	Estuarine Channel Fill (mid- outer estuary)
4	5-20 m wide, 0.1-2 m thick (inclined in similar direction)	Sigmoidal cross-bedding, bi-directional ripple cross-laminations, and flaser and lenticular bedding with numerous mud drapes	Heterolithic with very fine-to medium-grained sand with thin layers and lenses of mudstone and shale	Extensive, flat-based beds with a low angle inclination (1-2°) Numerous mud drapes, discontinuous lenses and interbeds of mudstone and shale	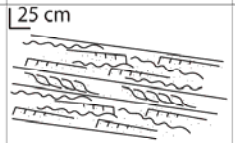	Muddy Tidal Bars (tidally influenced delta)
5	1- 4 m wide, 0.25-1 m thick	Sigmoidal cross-bedding	Heterolithic with fine- to medium-grained sand with lenses and thin layers of mudstone	Flat-based, thin, discontinuous, lenticular beds with sigmoidal cross-bedding interbedded with mudstone and shale	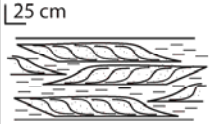	Tidal Bars (tidally influenced delta)
6	5-20 m wide, 0.1-2 m thick	Ripple cross-lamination (wave and current) Moderate bioturbation in massive mudstone units	Heterolithic with very fine-to medium-grained sand with thin layers of mudstone; bed sets coarsening-up	Flat-based, continuous beds; extensive mudstone interbeds are common and discontinuous mud-drapes are rare	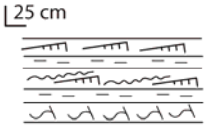	Offshore Marine

Figure 5.9 Summary of facies comprising facies Assemblage C- heterolithic facies.

tidally influenced. The small, locally amalgamated channels (up to 2 m wide and 2 m thick), higher proportion of sand and more abundant sigmoidal cross stratification suggests that Facies C2 was deposited in small tidal channels characterized by higher energy. Facies C3 fills broader channels, up to 10 m wide and 4 m thick, and contain more flaser bedding, higher proportion of mudstone and drapes compared to Facies C2 suggesting deposition within larger channels. The presence of inclined beds with paleocurrents oblique to inclined bed dip-direction within Facies C3 suggest deposition by point bars, and that these bars were infilling broader C3 channels, probably within an estuarine setting.

Like Facies C3, Facies C4 consists of bi-directional ripple cross-lamination, sigmoidal cross-stratified sets and a high proportion of mudstone and double mud-drapes that suggest tidal influence (Figure 5.10). The more extensive, flat-based character, and paucity of scours suggests that Facies C4 was not deposited within channels. The low angle (<5˚) and consistent dip direction of the inclined beds (toward the east and southeast) of Facies C4 strongly suggests deposition on deltaic clinoforms, as a tidally influenced marine delta. The presence of basinward-directed clinoforms allow us to distinguish prograding tidally influenced delta systems from retrograding estuarine systems, both of which are strongly influenced by tidal processes. Facies C4 is interpreted as deposits of muddy tidal bars as part of a tidally influenced marine delta.

Facies C5 is interpreted as tidal deposits of sandy tidal bars as part of a tidally influenced marine delta. Lenticular sandstone beds encased in mudstone, and presence of sigmoidal cross-bedding and bi-directional ripple cross-laminations suggests the influence of tidal currents. The flat-based character and lack of broad channel features suggests that this facies was deposited as part of a tidally influenced delta.

Facies C6 is interpreted as offshore marine deposits. The extensive nature of relatively fine-grained beds, trace fossil assemblage (namely, Ophiomorpha and Conicnus) and presence of wave-ripple cross lamination suggest deposition within a low-energy, offshore marine shelf environment. Alternation of thin sandstones and mudstone suggests episodic deposition of sand alternating with suspension deposition and bioturbation.

Facies Assemblage D: Mudstone-dominated Facies

Description

Facies Assemblage D consists of four mudstone-dominated facies (Figure 5.11). Facies comprising Assemblage D are most common east of Green River and are concentrated in the Buck Tongue and Sego Sandstone, with some facies prevalent in the Neslen Formation. Facies D1 and D2 are organic-rich facies with carbonaceous shale, coal, woody debris and root traces locally (Figure 5.12). Facies D1 and D2 generally occur lateral to Facies B1, B2, B3, B4, C1, C2 and C3 (i.e., channel deposits). Facies D3 and D4 are relatively extensive, mudstone and shale facies that generally intertongue with sandier facies toward the east, and generally lack woody debris and coal (Figure 5.12).

Interpretation

Facies D1 and D2 are interpreted as deposits of suspension deposition and paleosols on a fluvial floodplain and coastal plain, respectively. The fine-grained character and relict horizontal lamination of Facies D1 is consistent with suspension

Facies 5.10 Examples of facies comprising facies Assemblage C- heterolithic facies.

deposition. The general juxtaposition of Facies D1 with channel fill, high organic content and root traces are compatible with deposition and biogenic reworking (e.g., incipient paleosol formation) of floodplain deposits. Facies D2 contains a higher proportion of coal, which suggests water-logged, fresh-water environments such as those in coastal plain environments (McCabe, 1991). The extensive character and thick accumulation of coal, such as that of the Palisades Coal Zone, suggests aggradation of coal-producing environments in a series of raised coastal mires (McCabe, 1991; Kirschbaum, 2004). The regionally extensive nature and dearth of woody debris of Facies D3 is consistent with deposition in the offshore marine environment. The less exentsive character of Facies D4, higher abundance of woody debris, lack of distinct bedding and lower abundance, low diversity trace fossils (only pelecypodichnus) are consistent with deposition within the low-energy, brackish environment of the central basin region of an estuary (Dalrymple, 1992).

SEQUENCE-STRATIGRAPHIC FRAMEWORK

Disentangling the relative contribution of climate, eustasy, tectonics and sediment supply on stratigraphic development is challenging because these processes are typically overprinted in the stratigraphic record. Differences in the scale at which these processes operate are important for determining the relative contribution of these processes. Although some sequence-generating processes overlap in time-scale, or episodicity, comparison of cycle duration and episodicities of various sequence-generating processes are still a useful way of determining the relative roles of tectonics, eustasy and climate. A hierarchy of stratigraphic cycles helps to define cycle durations, although this is more

Assemblage D

Facies	Bedding	Sedimentary Stuctures	Grain-size/Grading	Other	Example	Interpretation
1	1- 10 m wide, 0.1-1 m thick	Massive, relict horizontal lamination, root traces in mudstone Moderate bioturbation	Clay and silt with ancillary v. fine sand	Typically lateral to Facies B2, B4, C1 and D2 Carbonaceous shale interbedded with massive mudstone and ancillary siltstone	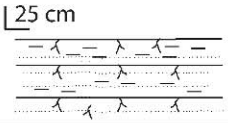	Fluvial Floodplain
2	10- 1000 m wide, 0.1-0.5 m thick	Massive, blocky texture, locally horizontal lamination	Clay and silt Coal	Coal interbedded with carbonaceous shale Typically lateral to Facies B2, B4 and D1 Some beds extend > 10 km Locally truncated by overlying units	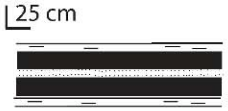	Coastal Plain
3	100- 1000 m wide, 0.1-0.5 m thick	Horizontal lamination, locally fissile	Clay and silt with ancillary v. fine sand	Some beds extend > 10 km Locally truncated by overlying units Typically lateral to Facies B8 and B9	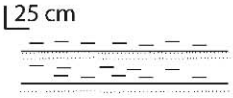	Offshore Marine
4	10- 50 m wide, 0.1-1 m thick	Horizontal lamination, locally fissile	Clay and silt with ancillary v. fine sand	Beds less extensive, and more organic-rich than Facies D3 Intertongue with Facies B5 up-dip	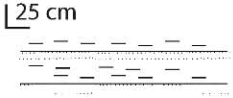	Central Basin

Figure 5.11 Summary of facies comprising facies Assemblage D- mudstone-dominated facies.

of a general guide (Van Wagoner et al., 1990; Duval et al., 1992). The four main scales of stratigraphic patterns are: (1) parasequence, (2) parasequence set, (3) sequence and (4) sequence set (Van Wagoner et al., 1990). Parasequences are generally less than ca. 10 ka in duration and parasequence sets are generally 10's of thousands of years in duration. Depositional sequences and sequence sets can range from ca. 100 Ky to 100 My in duration.

Parasequences

Depositional facies are highly varied within the extensive (400 km), internally complex low-aspect-ratio clastic wedge. To characterize the architecture of this wedge I define parasequence types (i.e., coarsening-upward, shoaling-upward successions) that comprise numerous depositional facies (Figure 5.13). Facies stack into six, general parasequence types (Figure 5.13). Proximal (0-100 km from the thrust-belt front) parasequence types are shoaling-upward successions that include braided fluvial, meandering fluvial, tidally influenced fluvial and alluvial fan deposits. Medial parasequence types (100-250 km from thrust-belt front) are shoaling-upward successions that include various proportions of estuarine, tidally influenced fluvial, meandering fluvial, offshore marine and marine shoreface deposits. Distal parasequence types (250-500 km from thrust-belt) are shoaling-upwards successions that consist almost entirely of offshore marine, marine shoreface and subordinate estuarine deposits. Medial (100-250 km) parasequences overwhelmingly contain the highest proportion of tidally influenced facies.

Two main parasequence types are found in proximal (0-100 km) zones of the study clastic wedge. Parasequence Type 1 (Figure 5.13) consists of braided

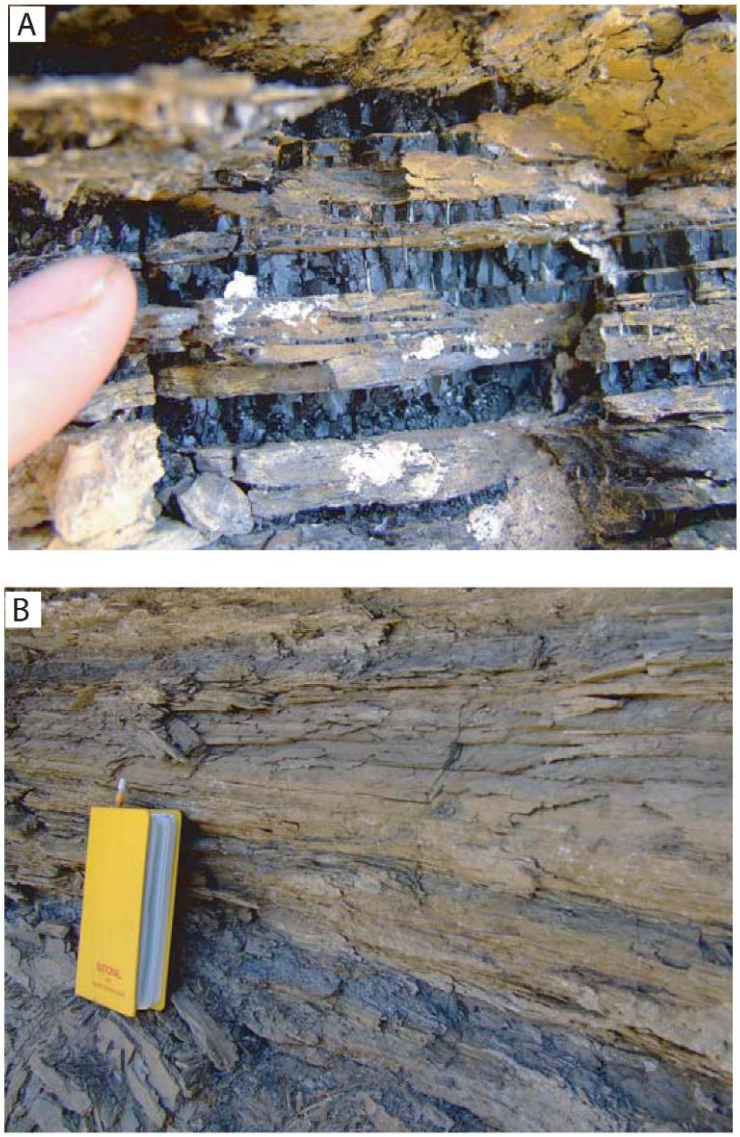

Figure 5.12 Examples of mudstone and coal facies comprising facies Assemblage D-mudstone facies.

fluvial deposits overlain by successions containing interbedded alluvial fan and fluvial deposits ("fan-fluvial interaction", sensu Dougherty, 1997), and alluvial fan deposits. In this region, some braided fluvial deposits have a transverse, distributary paleocurrent direction, and may be interpreted as fluvial megafan deposits. These parasequences are more difficult to distinguish than the medial and distal parasequence types because of the scarcity of marine-influenced deposits that clearly define flooding surfaces. Although parasequences are typically defined in marine settings, a coarsening-upward motif and up-section increase in proximal (0-100 km from highlands) alluvial deposits help define non-marine "parasequences". Parasequence Type 2 (Figure 5.13) consists of tidally influenced fluvial deposits overlain by meandering fluvial (isolated channels) and braided fluvial (amalgamated channels) deposits. These parasequences are easier to distinguish than the Type 1 parasequences because they contain tidal influenced zones that mark the base of the shoaling-upward succession. Proximal (0-100 km) parasequences are typically thicker than those occupying medial (100-250 km) and distal basin (250-500 km) locations, ranging from 10-20 m in thickness.

Two main parasequence types are found in medial (100-250 km from thrust-belt) zones of the anomalous clastic wedge. Parasequence Type 3 consists of estuarine and tidally influenced fluvial deposits overlain by meandering, and locally braided, fluvial deposits (Figure 5.13). Like Type 2 parasequnces, Type 3 parasequences are identified using the presence of tidally influenced units near the base of the shoaling-upward succession. Parasequence Type 4 consists of open marine barrier shoreface deposits overlain by estuarine, tidally influenced fluvial and meandering fluvial deposits. Parasequence Type 5 consists of offshore marine and lower shoreface deposits overlain

by tide- and wave-influenced middle and upper shoreface deposits. Paresequence Type 5 is also found in distal zones of the wedge. These parasequences are quite easily distinguished using the presence of open marine deposits near the base of the shoaling-upward succession. Medial (100-250 km from thrust-belt) parasequences range in thickness from 2 to 10 m, and are commonly truncated by younger unconformities.

Two parasequence types are found in distal (250-500 km from thrust-belt) zones of the clastic wedge. Parasequence Type 5 consists of offshore marine to middle and upper shoreface deposits, and is also found in medial zones (100-250 km) of the clastic wedge (Figure 5.13). Parasequence Type 6 is most common in distal zones, but is locally present within the medial zone of the clastic wedge. Parasequence Type 6 consists of open marine offshore to wave-dominated, middle- to upper-shoreface deposits. Distal zones are markedly dominated by more open marine, wave-dominated parasequence types. These parasequences are locally truncated by younger unconformities, and are 5-20 m thick.

Parasequence Stacking Patterns and Systems Tracts

Six parasequence types stack into parasequence sets that form three general patterns. Progradational parasequence sets consist of parasequences that get progressively shallower up-section. By contrast, retrogradational parasequence sets consist of parasequences that get progressively deeper (or, more distal) up-section. Aggradational parasequence sets maintain a relatively constant paleo-depth up-section. Parasequence stacking patterns provide information about high-frequency (<50,000 yr) cycles of base-level change and help to define the four main types of systems tracts.

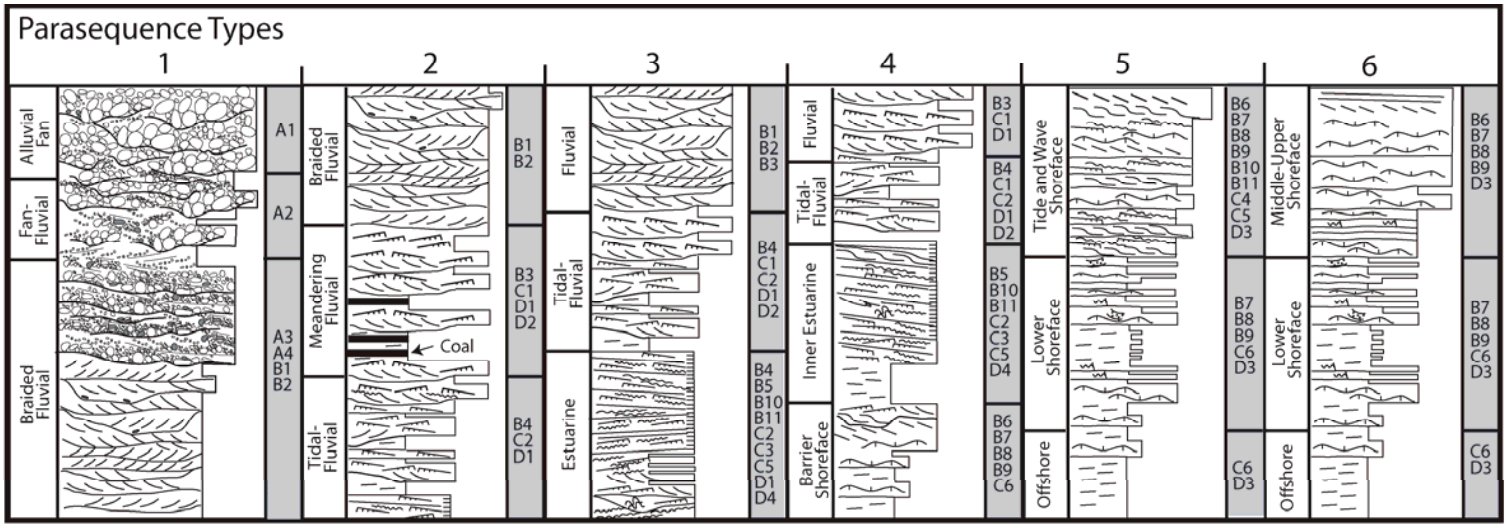

Figure 5.13 Generalized sections showing the six main parasequence types (including proximal coarsening upward successions) present in the study interval.

However, many parasequence sets, and parasequences in some instances, are incomplete due to truncation by younger unconformities.

Due to the incomplete nature of parasequence sets it is difficult to assign systems tracts within 4th and 3rd order sequences. Forced regressive systems tracts comprise the majority of the middle clastic wedge. These systems tracts consist of basinward-directed, offlapping tidally influenced shoreline deposits, such as those in the Sego Sandstone (Willis and Gabel, 2004). Lowstand systems tracts are locally preserved within incised valleys between Tuscher Canyon, Utah and East Salt Canyon, Colorado. Lowstand systems tracts typically consist of fluvial and tidally influenced fluvial deposits overlain by estuarine and open marine barrier deposits of the Transgressive systems tract.

The boundary between the lowstand and transgressive systems tract is the transgressive surface. There is some debate about whether to place the transgressive surface below the first strata with clear tidal influence (tidal ravinment surface), or below the first strata with clear evidence of open marine influence (Jackson et al., 2005; Yoshida et al., 2008). I place the transgressive surface at the base of strata with the first clear evidence of tidal influence (tidal ravinement) because this helps to correlate into largely non-marine successions. Transgressive systems tracts are typically thin (<10 m), but generally well preserved in the middle clastic wedge. Transgressive systems tracts chiefly consist of estuarine and tidally influenced fluvial deposits in proximal and medial zones of the transect (0-250 km). In distal zones, the transgressive systems tract consists of marine shale with shingled, landward-stepping, highly bioturbated marine sandstones, and estuarine deposits. The best example of shingled, landward-stepping barrier sandstones is found between Sagers Canyon, Utah and Jim Canyon, Colorado.

Sequences

The anomalous clastic wedge comprises a single 3rd-order (1-10 My cyclicity sensu Vail et al., 1977), composite, depositional sequence (Sequence S3-1) (Figures 5.14 and 5.3). This sequence is defined from the uppermost Castlegate Sequence Boundary to the base of the Price River Sequence Boundary. Sequence S3-1 is 100-250 m thick, and extends at least 400 km from the eastern edge of the Wasatch Plateau, UT. Sequence S3-1 is thickest adjacent to the former front of the Sevier fold-thrust belt and near the Colorado-Utah border. The thinnest part of the wedge is located between Willow Creek and Sunnyside, and corresponds with the location of the San Rafael Swell (Figure 5.15).

The 3rd order depositional sequence consists of six, 4th-order (1-0.5 My cyclicity), depositional sequences, termed S4-1, S4-2, S4-3, S4-4, S4-5 and S4-6 (Figure 5.16). The 4th-order sequences span ca. 250-500 Ky (Figures 5.15 and 5.3). These sequences have external geometries that are similar to the 3rd-order sequences, in the sense that they are generally thickest in the west and eastern parts of the study area. Sequence S4-1 is incomplete in the study succession, and is not described here. Sequences S4-2 and S4-3 are thickest adjacent to the former thrust-belt front and in the more distal regions of the basin, but thin considerably between Willow Creek and Sunnyside, across the San Rafael Swell. The upper-most 4th-order sequences (S4-4, S4-5 and S4-6) are thin in the west (< 50 m) and thicken considerably toward the east (100-150 m). Sequence S4-4 is the most laterally extensive unit in the Utah-Colorado segment of the Cordilleran foreland basin, extending more than 400 km east from the former front of the Sevier fold-thrust belt (Figures 5.15 and 5.16). Sequence S4-5 is completely removed by the overlying S4-6 sequence across the San Rafael Swell west of Horse

Canyon, UT. Both sequences have appreciable (up to 30 m) incision at their base across the San Rafael Swell.

Collectively, the 4th-order sequences form an up-section, eastward-stepping, offlapping pattern with a general up-section increase in the amount of incision across the San Rafael Swell. All of the sequences have a general eastward-stepping pattern, yet the uppermost sequences S4-5 and S4-6 (including the Rollins Sandstone and Williams Fork Fm.) become more northeast-directed. The increasing northerly component of progradation is consistent with the up-section northward shift in paleocurrents (Figure 5.15), and previous studies showing a more northerly progradation direction for the Rollins Sandstone (Cumella, 2006). The lower-most sequences have an east-directed, flat-trajectory offlapping pattern. By contrast, the upper sequences have a more rising-trajectory, east-stepping, offlapping pattern.

Each 4th-order sequence consists of 3-8, 5th-order (0.5-0.1 My cyclicity) depositional sequences (Figure 5.17). These high-order sequences are between 15-50 m thick, are generally less extensive (<100 km) and are highly amalgamated with numerous incisions, forming complex architectures. High-order sequences contain transgressive tracts with backstepping barrier sandstones that form discontinuous to semi-continuous beds of bioturbated sandstone with relict hummocky cross-stratification and trough cross-stratification (facies B8, B9) encased in mudstone and shale. Up-dip, bay-head delta, central basin and complex assemblages of transgressive tidal facies are present. Bay-head delta deposits form laterally discontinuous (< 50 m), 10-20 m thick, coarsening-upward successions. Bay-head delta deposits are typically cut by younger channel complexes on the up-dip end, and pinch out into mudstone successions on the down-dip end.

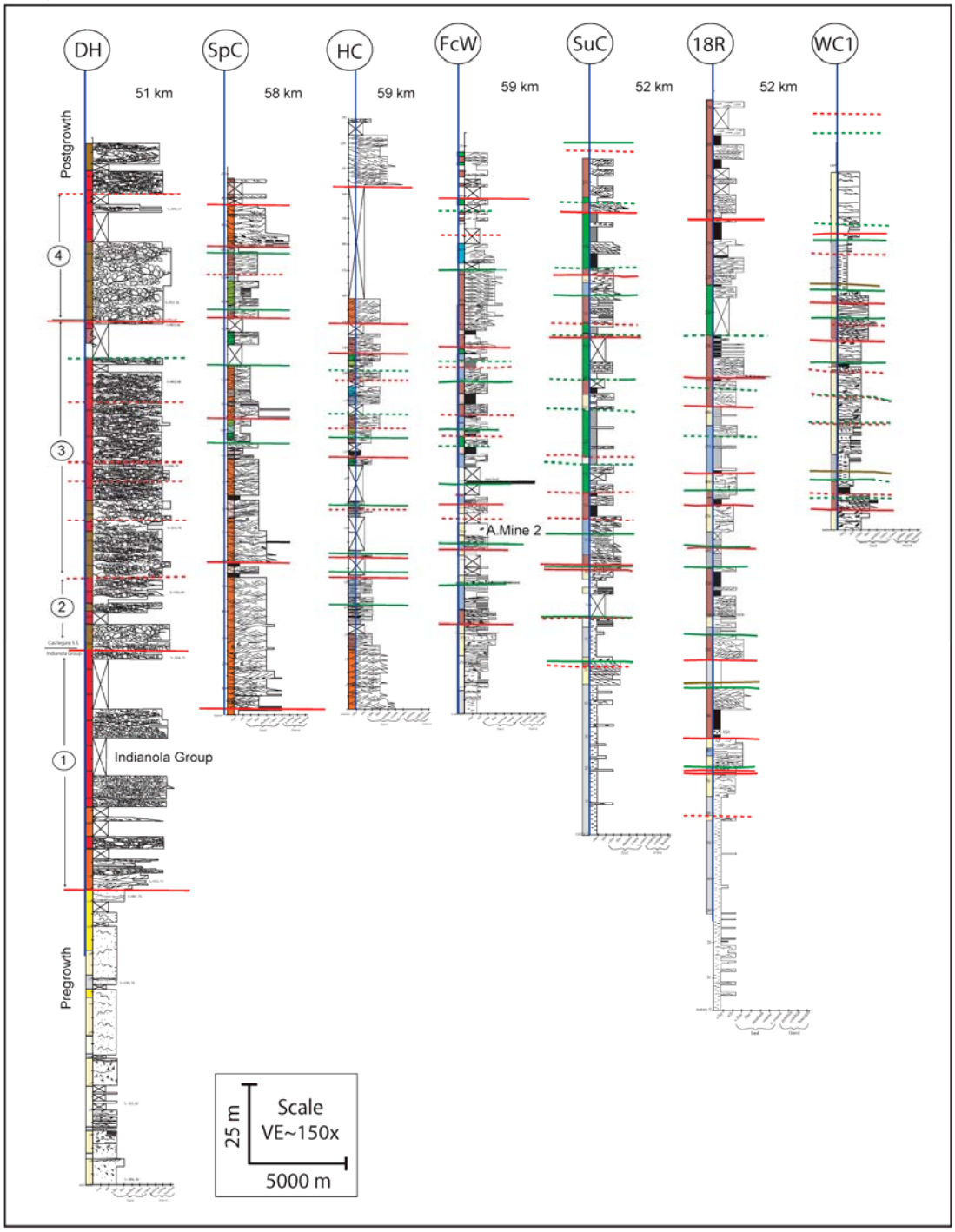

Figure 5.14 Examples of stratigraphic columns measured in the study interval.

Wedge Architecture

Externally, the low-accommodation clastic wedge has a characteristic low aspect-ratio (long and thin). The wedge extends more than 400 km from the eastern margin of the Wasatch Plateau (former front of the Sevier fold-thrust belt), and is between 50 and 250 m thick. The western part of the wedge onlaps Sevier fold-thrust belt structures in the vicinity of Thistle, UT. The eastern portion of the wedge is amalgamated, and downlaps onto the ramp of the Western Interior Seaway. The upper part of the wedge is locally truncated in the region of the San Rafael Swell, where incisions of up to 30 m are locally present.

Isopach maps (Figure 5.18) are consistent with the external, low aspect architecture of the low accommodation wedge. Isopach maps of the low accommodation wedge span *B. perplexus* through D. stevensoni ammonite zones. The maps show that the low accommodation wedge generally thickens toward the east-northeast. Additionally, the wedge thins toward the Sevier fold-thrust belt, and across the crest of the San Rafael Swell.

Internally, the low accommodation clastic wedge consists of 4th and 5th order sequences that generally stack with a flat-to-falling, offlapping pattern (Figures 5.15, 5.16, and 5.17). One exception to the offlapping pattern is in sequence S4-4 (4th-order sequence), which has a unique onlapping pattern. All sequences tend to preserve the forced regressive, lowstand and transgresive systems tracts. Depositional facies comprising the low accommodation clastic wedge are strongly tidal influenced. Tidal facies are concentrated on the inner portion of the wedge from Jim Canyon to Little Park Wash. Wave-dominated facies are present in relatively small proportions throughout the

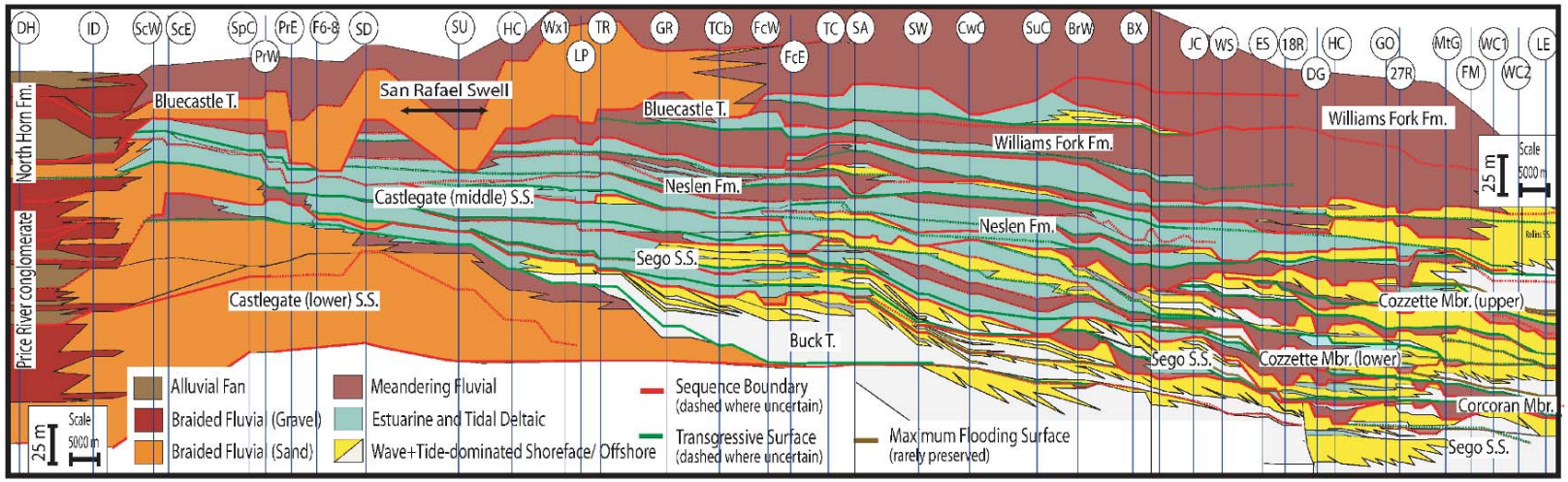

Figure 5.15 Stratigraphic correlation from the former Sevier Fold-thrust belt near Thistle, UT to Palisade, CO. See also Plate 1 for a larger version of this figure.

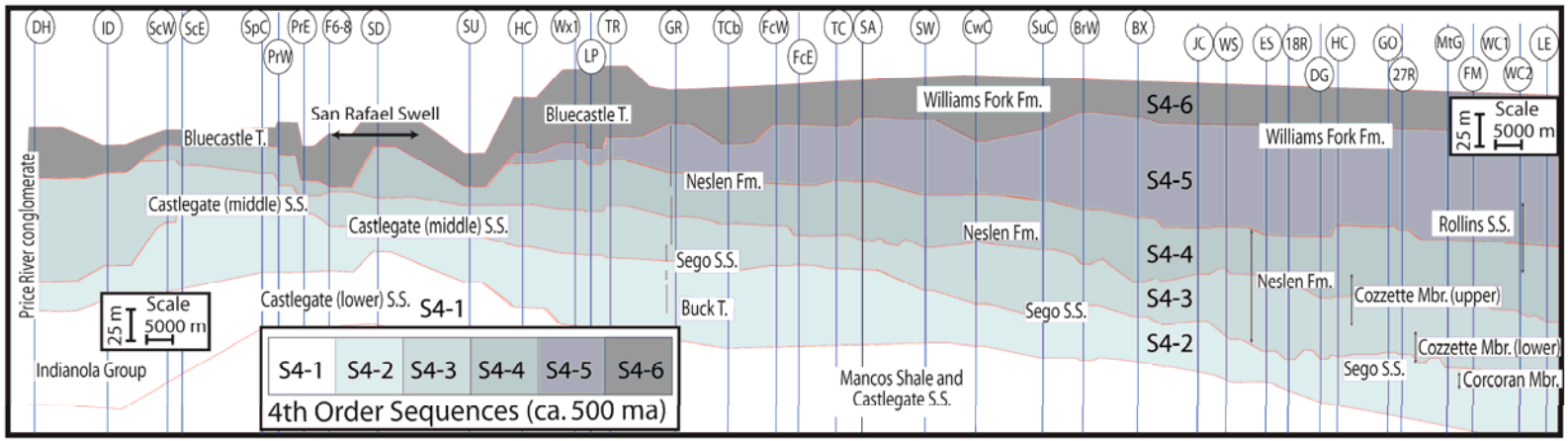

Figure 5.16 Outline of fourth-order sequences comprising Wedge B. See also Plates 1 and 2 for larger versions of this figure.

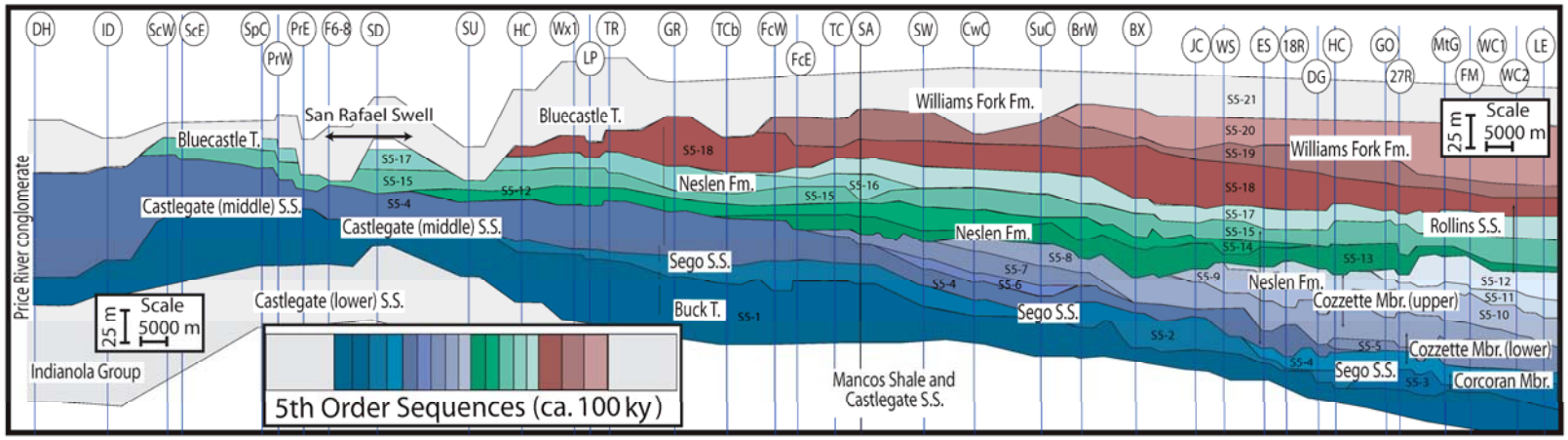

Figure 5.17 Outline of fifth-order sequences comprising Wedge B. See also Plates 1 and 2 for larger versions of this figure.

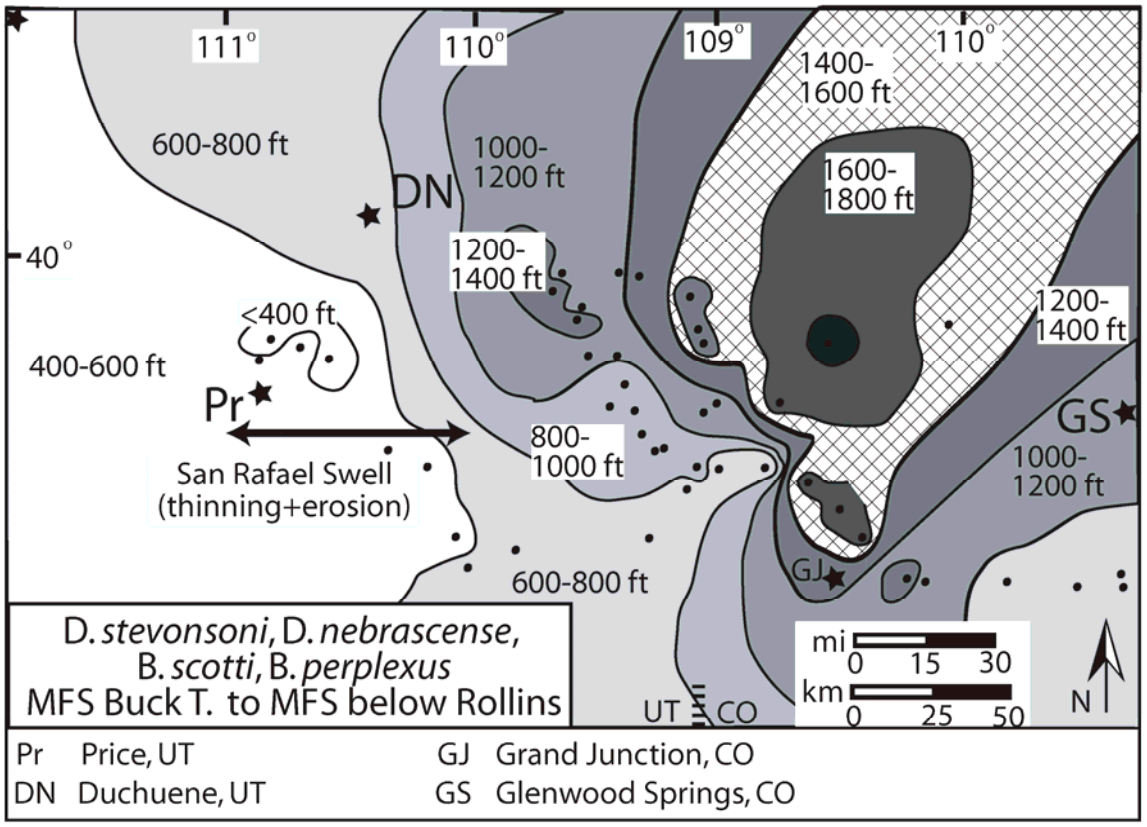

Figure 5.18 Isopach map of Wedge B showing thinning trend across the San Rafael Swell (Laramide-style structure).

low accommodation wedge, but are abundant east of Jim Canyon where they comprise the majority of the Corcoran and Cozette Members.

Numerous incisions and complex facies transitions are present within the central zone of the low accommodation clastic wedge, and introduce heterogeneities that are not typically present in the high accommodation types of wedge. Nested, high-frequency sequences and incisions are well documented by Willis and Gabel (2003), and are also documented in this study (Figure 5.15). Incisions occur at a number of scales, ranging from individual channel-cuts to regional sequence boundaries.

The low accommodation clastic wedge contains a high proportion of sandstone (70-85% sand), yet the sandstone facies typically alternate between heterolithic and sand-dominated and tend to be laterally discontinuous. Lateral facies transitions are very complex and difficult to map due to the abundance of local and regional unconformities.

DISCUSSION

External controls on clastic wedge development include tectonics, eustasy, climate and sediment supply. These processes tend to have characteristic episodicities, or time-scales over which they operate. For example, Milankovich cycles are cycles in the eccentricity, obliquity and precession of the earth's orbit. These cycles influence the earth's climate by varying the amount of incoming solar energy, and most of them operate at scales less than 100 ka (ca. 100, 41, 21 and 19 ka). In the stratigraphic record, parasequences and parasequence sets have episodicities less than 100 ka and possibly provide a record for shorter-term climatic signals. By contrast, global sea-level rise can occur at a wide range of scales, from 10 My to 20 Ky (Miall, 2000). Tectonics, is traditionally thought to influence stratigraphy at time-scales longer than 500 Ky. The stratigraphic record of tectonics therefore corresponds to cycles longer than 1 My, including 3rd, 4th and 5th-order depositional sequences.

However, the scale at which tectonics operates and its direct influence on stratigraphy is debated. Previous work in the Hornelen Basin (e.g., Steel et al., 1977; Anderson and Cross, 2001), and Ridge Basin (e.g., Crowell, 2003) suggest that alluvial fan cyclothems (< ca. 200 Ky) directly reflect fault motion in "fan skewness" and vertical stacking pattern. Recent work in glacial geology and neotectonics corroborate these short-term tectonic cycles. Research in neotectonic suggests that sedimentation can be influenced by structural development on time-scales less than 1 My (Burbank et al., 1996). Glacial geologists suggest that glacioisostatic readjustment occurs in less than 10 Ky, and at rates in excess of 40m/Ky; this suggests that subsidence and isostasy may also be recorded in short-duration time scales. Although epidocities of some processes overlap, and others are not fully understood, it is possible to compare the duration of specific stratigraphic cycles with episodicities for various processes to distinguish which processes were most influential.

Stratigraphic relations in the present study area suggest a direct link between development of the low accommodation wedge and both Sevier and Laramide deformation. Isopach maps show a distinct thinning trend across the crest of the San Rafael Swell beginning as early as *B. perplexus* (Buck Tongue of the Mancos Shale) (Figure 5.18). Furthermore, incisions of up to 30 m in the Bluecastle Tongue are present across the crest of the San Rafael Swell. Incision and thinning trends indicate that the San Rafael Swell influenced sedimentation patterns of stratigraphic units as early as ca. 77 ma (during deposition of the Buck Tongue), and developed relief by ca. 75 ma (during deposition of the Bluecastle Tongue). Coincidently, developments of thinning patterns coincide with the development of the low accommodation wedge. The regional correlation (Figure 5.15) highlights incisions across the San Rafael Swell, and indicates a correlation between thrust-belt-related growth strata at the basin margin and the entire

low accommodation wedge. These stratigraphic relations indicate that the low accommodation clastic wedge developed during a transition, or overlap in deformation styles from thin- to thick-skinned deformation.

I distinguish 3rd, 4th and 5th-order depositional sequences with durations of ca. 2 ma , 500 ka and 100 ka, respectively. This hierarchy, coupled with the regional correlation and isopach maps provide a link to thrust-belt and Laramide-style structures that constrain the timing of deformation provide clues about potential drivers of stratigraphic development.

Sequence S4-2 is interpreted as a lowstand sequence set (Figure 5.19). The great extent (>400 km) of 4th-order sequences (c1, c2) within the lower part of the S4-2 sequence (a 4th-order) suggests that initial regional accommodation was relatively great (Figure 5.19a). The upper part of the d2 sequence consists of local, nested or amalgamated higher-order (5th-order) sequences (c3, c4) that suggest decreasing accommodation space. Sequence S4-2 developed under long-term base-level fall, as evidenced by the up-section decrease in accommodation, overprinted by short-term base-level falls (Figure 5.19). Base-level fall was initially slow, as suggested by more extensive older sequences, but later quickened as indicated by the less extensive younger sequences with stronger offlapping pattern. Long-term base-level fall may have been caused by a combination of lowering global sea-level and decreased rates in subsidence (flexural and dynamic).

Sequence S4-3 is interpreted as a forced regressive to lowstand sequence set (Figure 5.19b). The lower part of this sequence consists of one relatively extensive high-order sequence (c4) (>250 km) that suggests that accommodation reduction was initially slow (Figure 5.19a). The upper part of sequence S4-3 consists of 8, localized (<50 km), high-frequency sequences (c5-c12) with a flat to falling offlapping character that suggests

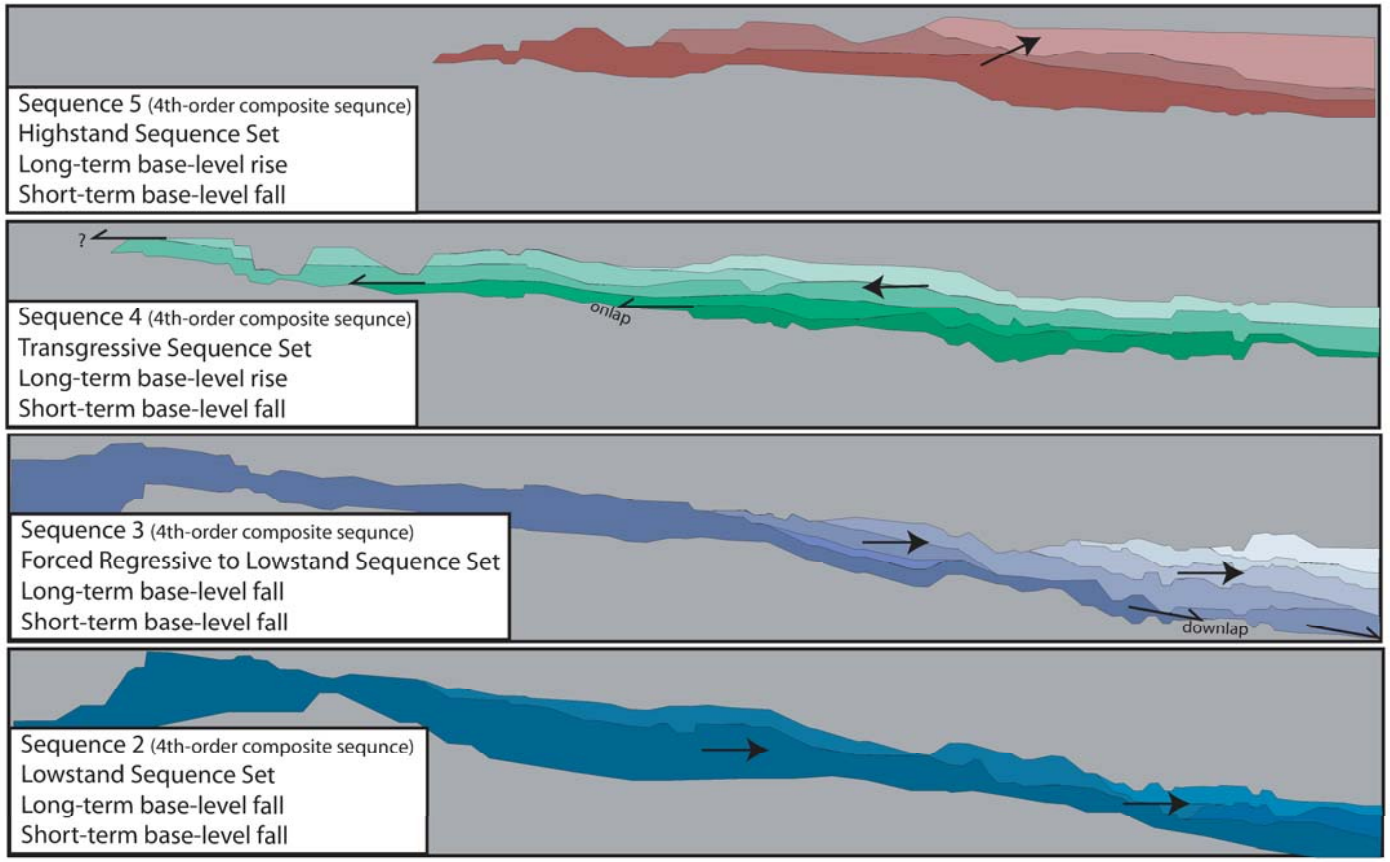

Figure 5.19 Summary of Wedge B stratigraphic architecture.

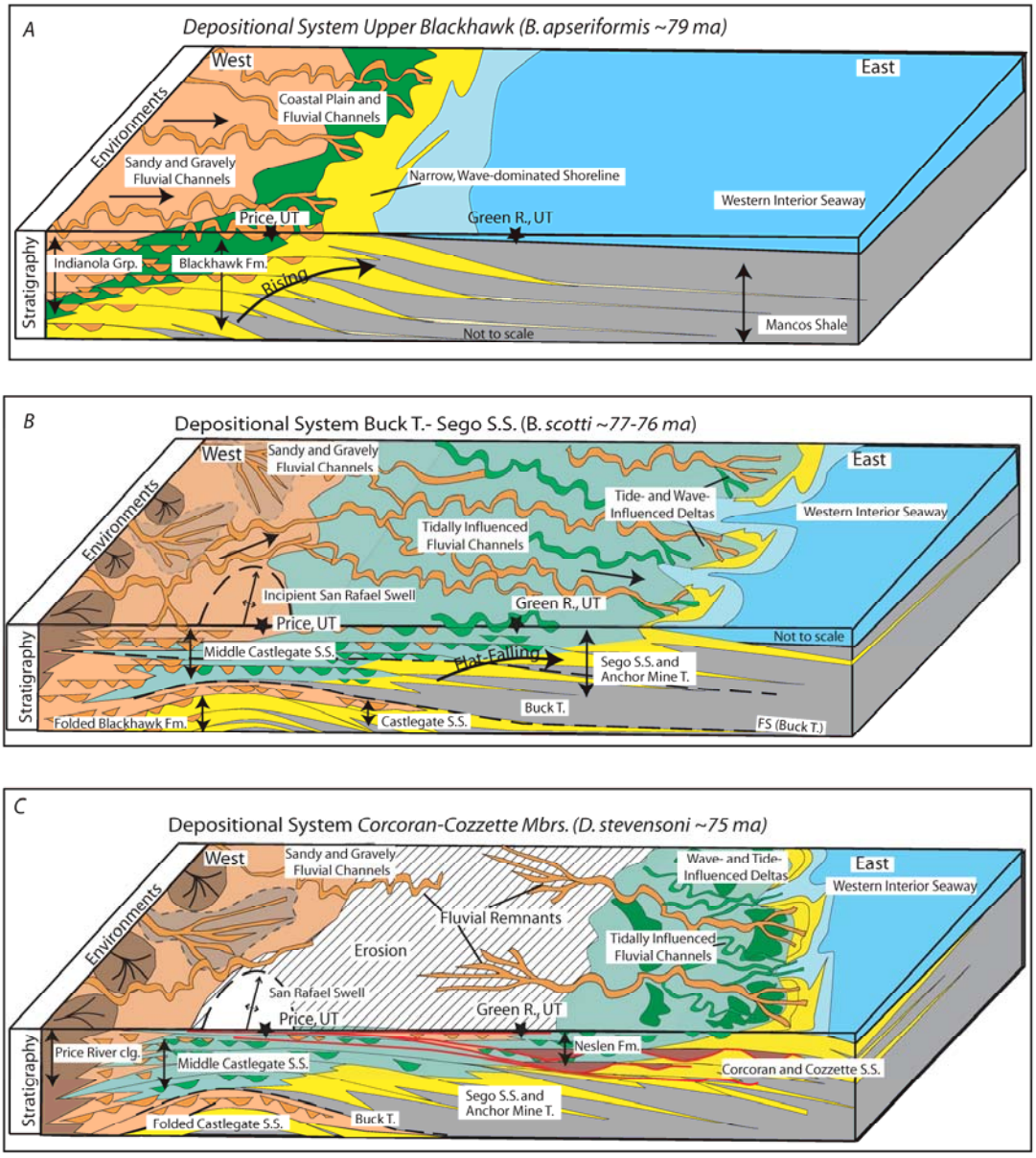

Figure 5.20 Summary of stratigraphic development of Wedge B with respect to the developing Laramide structure in the foredeep.

very low accommodation and rapid destruction of accommodation. The architecture of sequence S4-3 suggests long-term base-level fall overprinted by short-term base-level falls.

Sequence S4-4 is interpreted as a transgressive sequence set (Figure 5.19c). This sequence set has a distinctive, onlapping (west-stepping) pattern that suggests an overall rise in long-term base-level. The long-term rise in base-level was punctuated by short-term falls in base-level, as evidenced by the presence of high-frequency sequences.

Sequence S4-5 is interpreted as a partial highstand sequence set (Figure 5.19d). Unfortunately, additional work is needed to fully assess the development of the uppermost sequence. However, three high-frequency sequences are documented in sequence S4-5 and form a slight east-directed offlapping pattern with a rising trajectory. The rising trajectory character of the high-frequency sequences suggests a slow long-term base-level fall punctuated by short-term base-level falls.

CONCLUSIONS

Current models of foreland basin development are based on simplistic models of foreland basin fill, or detailed local stratigraphic studies. This study highlights important details within Cordilleran foreland basin fill that were previously overlooked. Two types of clastic wedges are identified in Cretaceous Cordilleran foreland basin fill of Utah and Colorado. These wedges are easily identified in regional stratigraphic data using their thickness, length and internal architecture. High-aspect clastic wedges are thick (>500 m), less extensive (< 300 km) successions that consist of numerous near-complete sequences and short-length shoreline tongues that form rising stratigraphic stacking patterns. Low-aspect wedges are thinner (<500 m), more extensive (>300 km) successions that consist of numerous, amalgamated, incomplete sequences and incisions that form flat- to falling-trajectory stacking patterns. The low-aspect wedge has an

external geometry and internal heterogeneity characteristic of low accommodation settings, and is anomalous in this segment of the Cordilleran foreland basin.

Detailed analysis of the architecture of the low accommodation clastic wedge, and high-resolution ammonite biostratigarphy help to disentangle the influence of tectonics, climate and eustatsy on wedge development. Internally, 25 lithofacies assemblages comprise 6 key parasequence types that stack into parasequence sets, and 3rd-, 4th- and 5th-order composite sequences. A single 3rd-order, depositional sequence comprises the low-accommodation wedge and spans ca. 2 ma.. The 3rd-order sequence consists of 6, 4th order depositional sequences that are composed of 3-8, 5th order sequences. 5th-order depositional sequences typically stack as basinward-stepping, offlapping sequences with a flat- to falling-trajectory, and are characteristic of forced regressive and lowstand sequence sets.

A regional sequence stratigraphic correlation and isopach maps were built from a robust stratigraphic database that includes 40 new stratigraphic sections, 31 published stratigraphic sections and 38 well logs. The regional correlation shows a physical connection between thrust-belt related growth strata, and is constrained by palynomorph and ammonite biostratigraphy. Isopach maps show distinct thinning trends across the crest of a Laramide structure (San Rafael Swell). These stratigraphic relations indicate that the unique low-aspect, low accommodation clastic wedge developed coeval with both Sevier and Laramide (thin- and thick-skinned) deformation. Development of the low-aspect wedge marks the onset of a key transition in deformation styles that was previously unrecognized. This study presents just one example of a low-aspect wedge within foreland basin fill. However, I postulate that recognition and analysis of these unique, low-aspect clastic wedges in other basins can be used as indicators of change in tectonics and basin dynamics.

Appendices

APPENDIX A: SECTION LOCATIONS AND ABBREVIATIONS.

Symbol	Location Name	Latitude (North)	Longitude (West)
18Ra	18-Road1 (Dry Gulch)	39.33797	-108.70030
18Rb	18-Road (ClinoDetail1,2,3)	39.33908	-108.70511
18Rc	18-Road2 (W.Dry Gulch-inc.)	39.33889	-108.70342
25R	Lane Wash (25-road)	39.23294	-108.49986
27.25R	27.25 Road	39.19633	-108.47337
BitC	Bitter Creek	39.36400	-109.14977
BryC	Bryson Creek	39.28957	-109.23058
BSC	Big Salt Creek	39.37300	-108.73008
BXC	W. Bar X Canyon	39.37819	-109.07781
CC	Coal Canyon	39.01964	-109.98417
DH1	Dry Hollow (Main Area)	39.97239	-111.47075
DH2	Dry Hollow2 (Wild Cat Cyn)	39.96208	-111.48253
ESW	East Salt Creek	39.39961	-108.79203
FC	Fish Creek (Scofield 1)	39.77856	-111.20319
Fle	Floy Canyon (east)	39.00161	-109.83363
FLw	Floy Canyon (west)	39.00237	-109.91214
GrR	Green River	39.13369	-110.09524
HoC	Horse Canyon	39.48124	-110.32330
HutC	East Hunter Canyon	39.28511	-108.58147
JC	Jim Canyon	39.39239	-109.04719
JoV1	Joes Valley 1	39.42168	-111.23467
JoV2	Joes Valley 2	39.34234	-111.25761
JoV3	Joes Valley 3	39.30627	-111.27140
LaEd	Lands End	39.00409	-108.25853
LCC1	East Little Clear Creek	39.82840	-111.42770
LPWe	Little Park Wash	39.28271	-110.27419
LPWw	Little Park Wash (West)	39.36875	-110.30058
MtG	Mt. Garfield	39.12639	-108.40647
NMC	Nine Mile Canyon	39.70967	-110.60794
PrC	Price Canyon	39.76067	-110.89027
ReSt	Redstone	39.21339	-107.30322
RiGp	Rifle Gap	39.63811	-107.76481
SaC	Sagers Canyon	39.01796	-109.67627
SC2	Scofield Reservoir (Scofiled 2)	39.81829	-111.14254
SpC	Spring Canyon	39.71746	-110.96033
StW	E. Strychnine Wash	39.10186	-109.55472
SuC1	Sulphur Canyon	39.22569	-109.29705
SuC2	Sulphur Canyon (I.Valley)	39.23283	-109.29224
SuS	Sunnyside	39.60046	-110.37338

APPENDIX A: SECTION LOCATIONS AND ABBREVIATIONS (CONTINUED).

Symbol	Location Name	Latitude (North)	Longitude (West)
ThC	Thompson Canyon	39.01492	-109.72715
TrC	Trail Canyon	39.22854	-110.25622
TuC1	Tuscher Canyon 1	39.08977	-110.01255
TuC2	Tuscher Canyon 2	39.08248	-110.00340
WatC	Watson Creek	39.12070	-108.31416
WC	Willow Creek	39.74619	-110.83426
WCC	W. Cottonwood Canyon	39.12617	-109.41567
WSW	West Salt Wash	39.42575	-108.96322

APPENDIX B: ISOPACH DATA LOCATIONS AND REFERENCES.

Symbol	Name	Lat. (N)	Long. (W)	Type	API	Biostr.	Reference
1	Cont Federal 22-1	40.01577	-109.65941	Well-log	A43047301110000	no	Dubiel/Johnson 02
2	Belco 5 Chapita Wells	40.01956	-109.42639	Well-log	A43047150510000	no	Dubiel/Johnson 02
3	Cont 2Chap	40.00846	-109.34805	Well-log	na	no	Dubiel/Johnson 02
4	Moab 2Gem	39.94609	-109.14088	Well-log	A43047107350000	no	Dubiel/Johnson 02
5	Continental 22-1 Evacuation Cr.	39.84308	-109.10579	Well-log	A43047102610000	no	Dubiel/Johnson 02
6	Pacific 23-2-1 Evacuation Cr.	39.80277	-109.08857	Well-log	A43047156750000	no	Dubiel/Johnson 02
7	ElPaso5TwinButtes	39.61662	-108.7824	Well-log	A05045051090000	no	Dubiel/Johnson 02
8	TwinArrow3-11	39.80054	-108.58685	Well-log	na	no	Dubiel/Johnson 02
9	Mobil T52-19	39.85434	-108.10344	Well-log	na	no	Dubiel/Johnson 02
10	Mnt Fuels 3 Island	39.95987	-109.69136	Well-log	A43047156430000	no	Johnson 02
11	CIG 2-29-10-21 NatB.	39.87376	-109.59324	Well-log	A43047302430000	no	Johnson 02
12	Mapco 2-8 Hope	39.91459	-109.57929	Well-log	A43047301890000	no	Johnson 02
13	Gulf1GrayknollsFed	39.75994	-109.55045	Well-log	A43047302260000	no	Johnson 02
14	Amoco 1 Buck Camp	39.76443	-109.43471	Well-log	A43047303570000	no	Johnson 02
15	Texaco 4 Seep Ridge	39.67391	-109.40513	Well-log	A43047301680000	no	Johnson 02
16	PineSprgs15-16-14-22	39.60485	-109.45687	Well-log	A 43047309600000	no	Johnson 02
17	Exxon 1 CrookedCan	39.59094	-109.36341	Well-log	A43047302710000	no	Johnson 02
18	Coseka13-15MainCan	39.51863	-109.3354	Well-log	A43047306180000	no	Johnson 02
19	GreatBasin2Blkhorse Can.	39.47805	-109.24655	Well-log	A43047302480000	no	Johnson 02
20	Benson Montin Norton 1	39.41824	-109.11289	Well-log	A43019101070000	no	Johnson 02
21	Pacific Federal 6-8	39.79937	-110.82917	Well-log	A43007301400000	no	HettingerKirschb.02
22	Mtn. Fuel Whitmore 1	39.77752	-110.70827	Well-log	A43007300670000	no	HettingerKirschb.02
23	Walton Iriart Fee # 1	39.74103	-110.59152	Well-log	A43007202530000	no	HettingerKirschb.02
24	Bow Valley 1-24 Wilcox	39.41345	-110.18844	Well-log	A43015300800000	no	HettingerKirschb.02
25	Tenneco 16-4 Rattlesnake Can	39.15746	-109.83599	Well-log	A43019308040000	no	HettingerKirschb.02

APPENDIX B: ISOPACH DATA LOCATIONS AND REFERENCES (CONTINUED).

Symbol	Name	Lat. (N)	Long. (W)	Type	API	Biostr.	Reference
26	BlackhorseCynFed31-1	39.46736	-109.28001	Well-log	A43047307650000	no	HettingerKirschb.02
27	Rat Hole Can	39.58482	-109.08661	Well-log	A43047327050000	no	HettingerKirschb.02
28	Price River	39.73182	-110.86697	Outcrop	na	no	HettingerKirschb.02
29	Pace Canyon	39.66962	-110.51733	Outcrop	na	no	HettingerKirschb.02
30	Soldier Canyon	39.69522	-110.61512	Outcrop	na	no	HettingerKirschb.02
31	Horse Canyon	39.46336	-110.34672	Outcrop	na	no	HettingerKirschb.02
32	Tusher Canyn	39.10065	-110.02165	Outcrop	na	no	HettingerKirschb.02
33	Green River	39.19481	-110.07593	Outcrop	na	no	Lawton, 1983
34	Taiga 1-5-23	39.61403	-109.0349	Well-log	A05045061570000	no	HettingerKirschb.02
35	Coal Gulch	39.37013	-108.6672	Well-log	A05045060170000	no	HettingerKirschb.02
36	Winter Flat	39.28565	-108.54178	Well-log	A05077085180000	no	HettingerKirschb.02
37	US1-8-MR	39.20426	-108.45847	Well-log	A05077084150000	no	HettingerKirschb.02
38	USGS CA77-2	39.18475	-108.2793	Well-log	na	no	HettingerKirschb.02
39	Sommerville #1	39.06019	-108.20102	Well-log	A05077082710000	no	HettingerKirschb.02
40	Smith 1-C	39.06583	-108.27926	Well-log	A05077050110000	no	HettingerKirschb.02
41	Michelson-2	39.05847	-107.88465	Well-log	A05029050310000	no	HettingerKirschb.02
42	ColoradoFed# C-1	39.04001	-107.6	Well-log	A05029050010000	no	HettingerKirschb.02
43	Hotchkiss3-11	39.03426	-107.41751	Well-log	A05051060030000	no	HettingerKirschb.02
44	Pasco-Spadafore1	39.07682	-107.42563	Well-log	A05051050060000	no	HettingerKirschb.02
45	Green River	40.31199	-109.4065	Outcrop	na	yes	Gill and Hail, 1975
46	Kane Hollow-west/Bitter	40.31079	-109.32188	Outcrop	na	yes	Gill and Hail, 1975
47	First Gap	40.27271	-109.18639	Outcrop	na	yes	Gill and Hail, 1975
48	Bonanza	40.28652	-109.14838	Outcrop	na	yes	Gill and Hail, 1975
49	Snake J	40.27794	-109.06393	Outcrop	na	yes	Gill and Hail, 1975
50	Drip Rock	40.15804	-109.00629	Outcrop	na	yes	Gill and Hail, 1975

APPENDIX B: ISOPACH DATA LOCATIONS AND REFERENCES (CONTINUED).

Symbol	Name	Lat. (N)	Long. (W)	Type	API	Biostr.	Reference
51	BlueMtn	40.24934	-108.87194	Outcrop	na	yes	Gill and Hail, 1975
52	Red Wash-West	40.23281	-108.75963	Outcrop	na	yes	Gill and Hail, 1975
53	Coal Ridge	40.22289	-108.62363	Outcrop	na	yes	Gill and Hail, 1975
54	Piryon Ridge	40.30169	-108.43263	Outcrop	na	yes	Gill and Hail, 1975
55	Winter Valley	40.31588	-108.42268	Outcrop	na	yes	Gill and Hail, 1975
56	Dickman Draw	40.35557	-108.11976	Outcrop	na	yes	Gill and Hail, 1975
57	Duffy Mtn	40.35	-107.75	Outcrop	na	yes	Gill and Hail, 1975
58	Sulphur Canyon	39.19701	-109.307	Outcrop	na	yes	Gill and Hail, 1975
59	Bitter Creek	39.34613	-109.1595	Outcrop	na	yes	Gill and Hail, 1975
60	Prairie Canyon	39.41245	-109.0277	Outcrop	na	yes	Gill and Hail, 1975
61	Demaree Canyon	39.41641	-108.8418	Outcrop	na	yes	Gill and Hail, 1975
62	Big Salt Wash	39.37441	-108.7223	Outcrop	na	yes	Gill and Hail, 1975
63	Dry Gulch	39.32543	-108.6126	Outcrop	na	yes	Gill and Hail, 1975
64	Adobe Creek	39.28842	-108.5489	Outcrop	na	yes	Gill and Hail, 1975
65	Corcoran Mine	39.24421	-108.5226	Outcrop	na	yes	Gill and Hail, 1975
66	Grasso Mine	39.21842	-108.4935	Outcrop	na	yes	Gill and Hail, 1975
67	Farmers Mine	39.12131	-108.3396	Outcrop	na	yes	Gill and Hail, 1975
68	Watson Creek	39.06621	-108.2931	Outcrop	na	yes	Gill and Hail, 1975
69	Rollins Mine	38.88126	-108.09729	Outcrop	na	yes	Gill and Hail, 1975

APPENDIX C: ISOPACH DATA.

Symbol	Zone Thickness (ft)							
	B. asperiformis	B. perplexus	B. scotti	D. nebrascense	D. steve	Ds+Dn	Bs+Bperp	Ds+Dn+Bs+Bperp
1	210	380	230	Combined	Combined	580	610	1190
2	180	370	370	Combined	Combined	290	740	1030
3	240	420	290	Combined	Combined	540	710	1250
4	300	240	110	Combined	Combined	1340	350	1690
5	300		250	Combined	Combined	1110	250	1360
6	270		335	Combined	Combined	1360	335	1695
7	150		320	Combined	Combined	1370	320	1690
8	250		390	Combined	Combined	2720	390	3110
9	140		480	Combined	Combined	900	480	1380
10	250		560	Combined	Combined	725	560	1285
11	200	250	450	Combined	Combined	710	700	1410
12	265		520	Combined	Combined	510	520	1030
13	260		380	Combined	Combined	625	380	1005
14	375							
15	270		375	Combined	Combined	515	375	890
16	255		375	Combined	Combined	510	375	885
17	190		390	Combined	Combined	520	390	910
18	210		425	Combined	Combined	435	425	860
19	225		500	Combined	Combined	625	500	1125
20	185		490	Combined	Combined	440	490	930
21	260			210	170	380		380
22	280			250	200	450		450
23	285			280	110	390		390
24	210	70	140	Combined	Combined	340	210	550
25	210	290	70	Combined	Combined	330	360	690

APPENDIX C: ISOPACH DATA (CONTINUED).

Symbol	Zone Thickness (ft)							
	B. asperiformis	B. perplexus	B. scotti	D. nebrascense	D. steve	Ds+Dn	Bs+Bperp	Ds+Dn+Bs+Bperp
26	200	360	130	Combined	Combined	320	490	810
27	125	450	150	Combined	Combined	550	600	1150
28	290			240	100			
29								
30								
31	200			400	95	495		
32	180	260	50	Combined	Combined	300	310	610
33	220	90	70	Combined	Combined	400	160	560
34	300	420	300	180	310	490	720	1210
35	300	810	320	220	320	540	1130	1670
36	300	720	380	180	510	690	1100	1790
37	240	610	280	170	600	770	890	1660
38					280			0
39	210	440	180	250	200	450	620	1070
40				200	220	420		420
41			250	230	240	470		720
42			240	170	230	400		640
43			250	180	240	420	250	670
44			250	200	225	425	250	675
45	200							
46	210							
47	230						350	
48	150						340	
49	170						300	
50	180						330	

APPENDIX C (CONTINUED).

Symbol	Zone Thickness (ft)							
	B. asperiformis	B. perplexus	B. scotti	D. nebrascense	D. steve	Ds+Dn	Bs+Bperp	Ds+Dn+Bs+Bperp
51	150						400	
52	120						460	
53	60						530	
54	80						570	
55	50						650	
56	80						440	
57	50						480	
58	30	380	160				540	540
59	40	500	140				640	640
60	10	480	110				590	590
61		500	205				705	705
62			250					
63			260					
64			380					
65			410	240	150			
66		560	300	200			860	
67			250	210				
68			200	100				
69					100			

References

Anadón, P., Cabrera, L., Colombo, F., Marzo, M., and Riba, O., 1986, Syntectonic intraformational unconformities in alluvial fan deposits, eastern Ebro Basin margins (NE Spain), in Allen, P.A. and Homewood, P. eds, Foreland basins: International Association of Sedimentologists Special Publication no. 8, p. 259-271.

Aschoff, J.L., and Giles, K.A., 2005, Salt diapir-influenced, shallow-marine sediment dispersal patterns: Insights from outcrop analogs: American Association of Petroleum Geologists Bulletin, v. 89, no. 4, p. 447-469.

Axen, G.J., Wernicke, B.P., Skelly, M.F., and Taylor, W.J., 1990, Mesozoic and Cenozoic tectonics of the Sevier thrust belt in the Virgin River Valley area, southern Nevada, in Wernicke, B.P. ed., Basin and Range extensional tectonics near the latitude of Las Vegas, Nevada: Geological Society of America Memoir 176 p. 123-153.

Barbeau, D.L., and Geslin, J.K., 2002, Kinematic sequences and systems tracts; a perspective from growth strata: American Association of Petroleum Geologists, 2002 Annual Meeting Abstracts with Programs, p. 12.

Barron, E.J., and Washington, W.M., 1982, Cretaceous climate: A comparison of atmospheric simulations with the geological record: Palaeogeography, Palaeoclimatology, Palaeoecology, v. 40, p. 103-133.

Beaumont, C., 1981, Foreland basins: Geophysical Journal of the Royal Astronomical Society, v. 65, p. 291-329.

Benvenuti, M., and Martini, I.P., 2002, Analysis of terrestrial hyperconcentrated flows and their deposits, in Martini, I.P., Baker, V.R., and Garzon, G., eds., Flood and megaflood processes and deposits; recent and ancient examples: Special Publication of the International Association of Sedimentologists, v. 32, p. 167-193.

Bernal, A., Hardy, S., Gawthorpe, R. and Finch, E., 2004, Stratigraphic expression of the lateral propagation and growth of isolated fault-related uplifts, Basin Research, v.16, p.219-233.

Belt, E. S., 1993, Tectonically induced clastic sediment diversion and the origin of thick, widespread coal beds (Appalachian and Williston basins, USA), in Frostick L. E. and Steel R. J. ,eds, Tectonic controls and signatures in sedimentary successions: International Association of Sedimentologists Special Publication no. 20, p. 337-397.

Bes de Berc, S., Soula, J.C., Baby, P., Souris, M. Christophoul, F., and Rosero, J., 2005, Geomorphic evidence of active deformation and uplift in a modern continental wedge-top-foredeep transition: example of the eastern Ecuadorian Andes: Tectonophysics, v. 399, p. 351-380.

Blair, T.C., and McPherson, J.G., 1994, Alluvial fans and their natural distinction from rivers based on morphology, hydraulic processes, sedimentary processes, and facies: Journal of Sedimentary Research, v. 64, p. 451-490.

Blair, T.C., 2000, Sedimentology and progressive tectonic unconformities of the sheetflood-dominated Hell's Gate alluvial fan, Death Valley, California: Sedimentary Geology, v. 132, p. 233-262.

Blair, T.C., 2003, Features and origin of the giant Cucomungo Canyon alluvial fan, Eureka Valley, California in Chan, M.A and Archer, A.W., eds., Extreme depositional environments; mega end members in geologic time: Geological Society of America Special Paper no. 370, p. 105-126.

Bluck, B.J., 1967, Deposition of some upper Old Red Sandstone conglomerates in the Clyde area; a study in the significance of bedding: Scottish Journal of Geology v. 3, no. 2, p. 139-167.

Blum, M.D. and Tornqvist, T.E., 2000, Fluvial responses to climate and sea-level change:a review and look forward: Sedimentology, v. 47 (Supplemental), p. 2-48.

Bohannon, R.G., 1983, Mesozoic and Cenozoic tectonic development of the Muddy, North Muddy and northern Black Mountains, Clark County, Nevada, in Miller, D.M., Todd, V.R., and Howard, K.A., eds, Tectonic and stratigraphic studies in the eastern Great Basin: Geological Society of America Memoir 157, p. 125-148.

Braithwaite, C.J.R., 1992, Perspective: Cement sequence stratigraphy in carbonates: Journal of Sedimentary Research, v. 63, no. 2, p.295-303.

Breyer, J.A. and McCabe, P.J., 1986, Coals associated with tidal sediments in the Wilcox Group (Paleocene), South Texas: Journal of Sedimentary Petrology, v. 56, no. 4, p. 510-519.

Bridge, J. S., and Best, J. L. 1988, Flow, sediment transport and bedform dynamics over the transition from dunes to upper-stage plane beds: implications for the formation of planar lamination: Sedimentology, v. 35, p. 753–764.

Bump, A.P. and Davis, G.H., 2003, Late Cretaceous-early Tertiary Laramide deformation of the northern Colorado Plateau, Utah and Colorado: Journal of Structural Geology, v. 25, p. 421-440.

Burbank, D.W., Beck, R. A., Robert G. H., Raynolds, R. ,Hobbs, and R. A. K. Tahirkheli, 1988, Thrusting and gravel progradation in foreland basins; a test of post-thrusting gravel dispersal: Geology, v. 16, p. 1143 - 1146.

Burbank, D.W., and Vergés, J., 1994, Reconstruction of topography and related depositional systems during active thrusting: Journal of Geophysical Research, v. 99, no. 20, p. 281-297.

Burbank, D.W., Meigs, A. and Brozovic, N., 1996, Interactions of growing folds and coeval depositional systems: Basin Research v. 8, no. 3, p. 199-224.

Cant, D.J., 1991, Geometric modeling of facies migration: theoretical development of facies successions and local unconformities: Basin Research, v. 3, p. 51-62.

Camerlo, R.H., and Benson E.F., 2006, Geometric and seismic interpretation of the Perdido fold belt: Northwestern deep-water Gulf of Mexico: American Association of Petroleum Geologists Bulletin, v. 90, p. 363 – 386.

Carpenter, D. G., 1989, Geology of the North Muddy Mountains, Clark County, Nevada, and regional structural synthesis; fold-thrust and Basin-Range structure in southern Nevada, Southwest Utah and Northwest Arizona [unpublished M.S. thesis]: Oregon State University, Corvallis 145 p.

Catuneanu, O., Beaumont, C. and Waschbusch P.J., 1997, Interplay of static loads and subduction dynamics in foreland basins; reciprocal stratigraphies and the "missing" peripheral bulge: Geology, v. 25, p. 1087 - 1090.

Catuneanu, O., 2004, Basement control on flexural profiles and the distribution of foreland facies: The Dwyka Group of the Karoo Basin, South Africa: Geology, v. 32, no. 6, p. 517–520.

Cobban, W.A., Obradovich, J.D., Walaszcyk, I. and McKinney, K.C., 2006, A USGS zonal table for the Upper Cretaceous middle Cenomanian-Maastrichtian of the Western Interior of the United States based on ammonites, Inoceramids, and radiometric ages: USGS Open-File Report 2006-1250, 46 pp.

a. Clevis, Q., De Jager, G., Nijman, W., De Boer, P., 2004, Stratigraphic signatures of translation of thrust-sheet top basins over low-angle detachment faults: Basin Research, v. 16, p. 145-163.

b. Clevis, Q., De Boer, P.L. and Nijman, W., 2004, Differentiating the effect of episodic tectonism and eustatic sea-level fluctuations in foreland basins filled by alluvial fans and axial deltaic systems: insights from a three-dimensional stratigraphic forward model: Sedimentology, v. 51, p. 809-835.

Cobban, W.A., Obradovich, J.D., Walaszcyk, I. and McKinney, K.C., 2006, A USGS zonal table for the Upper Cretaceous middle Cenomanian-Maastrichtian of the Western Interior of the United States based on ammonites, Inoceramids, and radiometric ages: USGS Open-File Report 2006-1250, 46 pp.

Costa, J.E., 1988, Rheologic, geomorphic, and sedimentologic differentiation of water floods, hyperconcentrated flows and debris flows, in Baker, V.R., Kochel, R.C., Patton, P.C., eds., Flood Geomorphology, p. 113-122.

Crowell, J. C., 2003, Evolution of Ridge Basin, Southern California; an interplay of sedimentation and tectonics: Geological Society of America Special Paper no. 367, 247 p.

Cumella, S.P., 2006, Overview of giant basin-centered gas accumulation, Mesaverde Group, Piceance Basin, Colorado: The Mountain Geologist, v. 43, no. 3, p. 219-224.

Dalrymple, R.W., Zaitlin, B.A., and Boyd, R., 1992, Estuarine facies models; conceptual basis and stratigraphic implications: Journal of Sedimentary Research, v. 62, p. 1130-1146.

Damanti, J.F., 1993, Geomorphic and structural controls on facies patterns and sedimentation: Association of Sedimentologists no. 17, p. 221-233.

DeCelles, P.G., 1988, Lithologic provenance modeling applied to the Late Cretaceous synorogenic Echo Canyon Conglomerate, Utah: A case of multiple source areas: Geology, v. 16, p. 1039-1043.

DeCelles, P.G., Lawton, T.F., and Mitra, G., 1995, Thrust timing, growth of structural culminations, and synorogenic sedimentation in the Sevier Orogenic belt, western United States: Geology, v.23, p. 699-702.

DeCelles, P.G. and Giles, K.A., 1996, Foreland basin systems: Basin Research, v. 8, p. 105-123.

DeCelles, P.G., 2004, Late Jurassic to Eocene evolution of the Cordilleran Thrust Belt and foreland basin system, western U.S.A: American Journal of Science, v. 304, p. 105-168.

Dickinson, W.R., 1970, Interpreting detrital modes of greywhacke and arkose: Journal of Sedimentary Petrology, v. 40, p. 695 -707.

Dickinson, W.R., 1974, Plate tectonics and sedimentation, in Dickinson, W.R., ed., Tectonics and Sedimentation: Society of Economic Paleontologists and Mineralogists Special Publication, no. 22, p. 1-27.

Dickinson, W.R., and Snyder, W.S., 1978, Plate tectonics of the Laramide orogeny, in Matthews, V., III, ed., Laramide folding associated with basement block faulting in the western United States: Geological Society of America Memoir 151, p. 355–366.

Dickinson, W.R. and Suczek, 1979; Plate tectonics and sandstone composition: AAPG Bulletin v. 63, p. 2164 - 2182.

Dickinson, W.R., Lawton, T.F. and Inman, K.I., 1986, Sandstone detrital modes, central Utah foreland region: stratigraphic record of Cretaceous-Paleogene tectonic evolution: Journal of Sedimentary Petrology, v. 56, p. 276-293.

Dott, R.H., 1978, Tectonics and sedimentation a century later: Earth Science Reviews v. 14, p. 1-34.

Dougherty, S.L., 1997, Alluvial fan and fluvial interaction in a foreland basin wedge-top depozone; Upper Cretaceous Beaverhead Group, SW Montana [M.S. thesis]: Bozeman, Montana State University, 111 pp.

Erslev, E.A., 1991, Trishear fault-propagation folding: Geology, v. 19, p. 617-620.

Fernàndez, O., Munoz, J.A., Arbues, P., Falivene, O., and Marzo, M., 2004, Three-dimensional reconstruction of geological surfaces: An example of growth strata and turbidite systems from the Ainsa basin (Pyrenees, Spain): American Association of Petroleum Geologists Bulletin, v. 88, no. 8, p. 1049-1068.

Fielding, C. R., 2006, Upper flow regime sheets, lenses and scour fills; extending the range of architectural elements for fluvial sediment bodies: Sedimentary Geology v. 190, no. 1-4, p. 227-240.

Flemings, P.B., and Jordan, T.E., 1989, A Synthetic Stratigraphic Model of Foreland Basin Development, Journal of Geophysical Research, vol. 94, p. 3851-3866.

Flemings, P.B. and Jordan, T.E., 1990, Stratigraphic modeling of foreland basins: interpreting thrust deformation and lithosphere rheology: Geology, v. 18, no. 5, p. 430-434.

Ford, M., Williams, E.A., Artoni, A., Vergés, J., and Hardy, S., 1997, Progressive evolution of a fault-related fold pair from growth strata geometries, Sant Llorenç de Morunys, SE Pyrenees: Journal of Structural Geology, v. 19, no. 3-4, p. 413-441.

Frakes, L. A., 1979. Climates Throughout Geologic Time, Elsevier, Amsterdam, 310 pp.

Frostick, L.E. and Steel, R.J., 1993, Tectonic signatures in sedimentary basin fills: an overview: International Association of Sedimentology Special Publication no. 20, p. 1-9.

Gallaway, W.E., 2001, Cenozoic Evolution of Sediment Accumulation in Deltaic and Shore-zone Depositional Systems, Northern Gulf of Mexico: Marine and Petroleum Geology, v. 18, p. 1031-1040.

Gawthorpe, R. and Hardy, S., 2002, Extensional fault-propagation folding and base-level change as controls on growth-strata geometries (in Growth strata): Sedimentary Geology, v. 146, no. 1-2, p. 47-56.

Giles, K.A., and Lawton, T.F., 2002, Halokinetic sequence stratigraphy adjacent to the El Papalote diapir northeastern Mexico: American Association of Petroleum Geologists Bulletin v. 86, no. 5, p. 823-841.

Giles, K.A., Lawton, T.F. and Rowan, M.G., 2003, Halokinetic sequences: American Association of Petroleum Geologists Annual Meeting, Abstracts with Program, v. 35, no. 6, p. 642.

Gloppen, T. G., and Steel R., 1981, The deposits, internal structure and geometry in six alluvial fan-fan delta bodies (Devonian, Norway)- a study in the significance of bedding sequence in conglomerates, in Ethridge, F. and Flores, R.M., eds., Recent and ancient nonmarine depositional environments: Models for exploration: Society of Economic Paleontologists and Mineralogists Special Publication no. 31, p. 46-69.

Grabeau, A.W., 1913, Principles of Stratigraphy, New York A.G. Seiler and Company, 1185 p.

Graham, S.A., Tolson, R.B., DeCelles, P.G., Ingersoll, R.V., Bargar, E., Caldwell, M., Cavazza, W., Edwards, D.P., Follo, M.F., Handschy, J.R., Lemke, L., Moxon, I., Rice, R., Smith, G.A. and White, J., 1986, Provenance modeling as a technique for analyzing source terrane evolution and controls on foreland sedimentation, in Homewood, P., and Allen, P.A., eds., Foreland Basins: International Association of Sedimentologists Special Publication 8, p. 141-152.

Gurnis, M., 1992, Rapid continental subsidence following the initiation and evolution of subduction: Science, v. 255, p. 29-32.

Haley, C.J., 1985, Upper Cretaceous (Beaverhead) synorogenic sediments of the Montana-Idaho thrust belt and adjacent foreland; relationships between sedimentation and tectonism: Dissertation, Johns Hopkins University, Baltimore, MD, United States, 542 p.

Helland-Hansen, W. and Martinsen, O.J., 1996, Shoreline trajectories and sequences: description of variable depositional dip scenarios: Journal of Sedimentary Research, v. 66, p. 670-688.

Heller, P.L., Angevine, C.L., Winslow, N.S. and Paola C., 1988, Two-phase stratigraphic model of foreland-basin sequences: Geology, v. 16, p. 501 - 504.

Hardy, S., and Poblet, J., 1994, Geometric and numerical model of progressive limb rotation in detachment folds: Geology, v. 22, no. 4, p. 371-374.

Hettinger, R. D. and Kirschbaum, M. A., 2002, Stratigraphy of the Upper Cretaceous Mancos Shale (upper part) and Mesaverde Group in the southern part of the Uinta and Piceance basins, Utah and Colorado: USGS Geologic Investigations Series I-2764, 21 pp.

Holl, J.E., and Anastasio, D.J., 1993, Paleomagnetically derived folding rates, southern Pyrenees, Spain: Geology, v. 21, no. 3, p. 271-274.

Horton, B.K., B.A. Hampton, and G.L. Waanders, 2001, Paleogene synorogenic sedimentation in the Altiplano plateau and implications for initial mountain building in the central Andes: GSA Bulletin, v. 113, p. 1387 - 1400.

Horton, B. K. and DeCelles, P. G., 2001, Modern and ancient fluvial megafans in the foreland basin system of the Central Andes, southern Bolivia; implications for drainage network evolution in fold-thrust belts: Basin Research, v. 13, p. 43-63.

Horton, B.K., Constenius, K.N., and DeCelles, P.G., 2004, Tectonic control on coarse-grained foreland-basin sequences: An example from the Cordilleran foreland basin, Utah: Geology, v. 32, no. 7, p. 637-640.

Houston, W. S., Huntoon, J. E. and Kamola D.L., 2000, Modeling of Cretaceous foreland-basin parasequences, Utah, with implications for timing of Sevier thrusting: Geology, v. 28, p. 267 - 270.

Hoy, R.G., and Ridgway, K.D., 2002, Syndepositional thrust-related deformation and sedimentation in an Ancestral Rocky Mountain basin, Central Colorado trough, Colorado, USA: Geological Society of America Bulletin, v. 114, no. 7, p. 804-828.

Izett, G.A., Cobban, W.A., Dalrymple, G.B., and Obradovich, J.D., 1998, 40Ar/39Ar age of the Manson impact structure, Iowa, and correlative impact ejecta in the Crow Creek Member of the Pierre Shale (Upper Cretaceous), South Dakota and Nebraska. Geological Society of America Bulletin, 110: 361-76.

Jackson, M.D., Yoshida, M., Muggeridge, A.H. and Johnson, H.D., 2005, Three-dimensional reservoir characterization and flow simulation of heterolithic tidal sandstones: AAPG Bulletin, v. 89, p. 507 - 528.

Jervey, M. T., 1988, Quantitative geological modeling of siliciclastic rock sequences and their seismic expression, *in* Wilgus, C.K., Hastings, B.S., Ross, C.A., Posamentier, H., Van Wagoner, J.C. and Kendall, C.G.S.C., eds., Sea-level changes; an integrated approach: Society of Economic Paleontologists and Mineralogists Special Publication 42, p. 47-69.

Jordan, T.E., 1981, Thrust loads and foreland basin evolution, Cretaceous, western United States: AAPG Bulletin, v. 65, p. 2506 - 2520.

Jordan, T. E., and Allmendinger, R. W., 1986, The Sierras Pampeanas of Argentina: A modern analogue of Laramide deformation: American Journal of Science, v. 286, p. 737–764.

Kamola, D.L. and Huntoon, J.E., 1995, Repetitive stratal patterns in a foreland basin sandstone and their possible tectonic significance: Geology, v. 23, p. 177 - 180.

Kaufmann, E.G., Sageman, B.B., Kirkland, J.I., Elder, W.P., Harries, P.J., and Villamil, T., 1993, Molluscan biostratigraphy of the Cretaceous Western Interior basin, North America, *in* Caldwell, W.G.E. and Kauffman, E.G., eds., Evolution of the Western Interior basin: Geological Association of Canada Special Paper 39, p. 397-434.

Kay, M., 1951, North American geosynclines: Geological Society of America Memoir 48, 143p.

Kay, M., 1974, Geosynclines, flysch and mélange, *in* Dott, R.H., Shaver, R.H., eds., Modern and ancient geosyclinal sedimentation: SEPM Special Publication 19, p. 377-380.

Ketzer, M.J., Holz, M., Morad, S. and Al-Aasm, I.S., 2003, Sequence stratigraphic distribution of diagenetic alterations in coal-bearing, paralic sandstones: evidence from the Rio bonito Formation (early Permian), southern Brazil: Sedimentology, v. 50, p.855-877.

Kirschbaum, M.A. and Hettinger, R.D., 2004, Facies analysis and sequence stratigraphic framework of Upper Campanian Strata (Neslen and Mount Garfield Formations, Bluecastle Tounge of the Castlegate Sandstone, and Mancos Shale), Eastern Book Cliffs, Colorado and Utah: US Geological Survey Digital Data Series Report DDS-69-G.

Knopf, A., 1948, The geosynclinal theory: Geological Society of America Bulletin, v. 57, p. 649-670.

Kraus, M.J., 2002, Basin-scale changes in floodplain paleosols: implications for interpreting alluvial architecture: Journal of Sedimentary Research, v. 72, p. 500-509.

Krumbein, W.C., and Sloss, L.L., 1963, Stratigraphy and sedimentation, W.H. Freeman and Co., San Francisco.

Krynine, P.D., 1948, The megascopic study and field classification of sedimentary rocks: Journal of Geology, v. 56, p. 130-165.

Krystinik, L.F. and DeJarnett, B.B., 1995, Lateral variability of sequence stratigraphic framework in the Campanian and Lower Maastrichtian of the Western Interior Seaway, in Van Wagoner, J.C., and Bertram, G.T., eds., Sequence Stratigraphy of Foreland Basin Deposits: AAPG Memoir 64, p. 11-25.

Lawton, T.F., 1986, Fluvial systems of the Upper Cretaceous Mesaverde Group and Paleocene North Horn Formation, central Utah; a record of transition from thin-skinned to thick-skinned deformation in the foreland region, *in* Peterson, J.A., eds., Paleotectonics and sedimentation in the Rocky Mountain region, United States: AAPG Memoir 41, p. 423-442.

Lawton, T.F., Boyer, S.E. and Schmitt, J.G., 1994, Influence of inherited taper on structural variability and conglomerate distribution, Cordilleran fold and thrust belt, Western United States: Geology, v. 22, p. 339 - 342.

Lawton, T.F., Roca, E., and Guimera, J., 1999, Kinematic-stratigraphic evolution of a growth syncline and its implications for tectonic development of the proximal foreland basin, southeastern Ebro basin, Catalunya, Spain: Geological Society of America Bulletin, v. 111, no. 3, p. 412-431.

Lawton, T.F., Pollock, S.L. and Robinson, R.A.J., 2003, Integrating sandstone petrology and nonmarine sequence stratigraphy: Application to the Late Cretaceous fluvial systems of southwestern Utah, U.S.A: Journal of Sedimentary Research, v.73, p.389-406.

Liu, S.F., Nummedal, D., Yin, P.G., and Luo, H.J., 2005, Linkage of Sevier thrusting episodes and Late Cretaceous foreland basin megasequences across southern Wyoming (USA): Basin Research, v. 17, p. 487-506.

Lopez, J.A., 1990, Structural styles of growth faults in the U.S. Gulf Coast basin, in Brooks, J., ed., Classic Petroleum Provinces, Geological Society Special Publication no. 50, p. 203-219.

Martinson, O.J., Ryseth, A., Helland-Hansen, W., Flesche, H., Torkildsen, H., Torkildsen, G. and Idil, S., 1999, Stratigraphic base level and fluvial architecture: Ericson Sandstone (Campanian), Rock Springs Uplift, SW Wyoming, USA: Sedimentology, v. 46, p. 235-259.

McBride, E.F., 1963, A classification of common sandstones: Journal of Sedimentary Petrology, v. 33, no. 3, p.661-669.

McBride, E.F., Milliken, K.L., Cavazza, W., Cibin, W., Fontana, D., Picard, M.D. and Zuffa, G.G., 1995, Heterogeneous distribution of calcite cement at the outcrop scale in Tertiary sandstones, Northern Apennines, Italy: AAPG Bulletin, v. 79, p. 1044-1063.

McCarthy, P.J. and Plint, A.G., 2003, Spatial variability of palaeosols across Cretaceous interfluves in the Dunvegan Formation, NE British Columbia, Canada: palaeohydrological, palaeogeomorphological and stratigraphic implications. Sedimentology v. 50: 1187-1220.

McLaurin, B.T. and Steel, R.J., 2000, Fourth-order non-marine to marine sequences, middle Castlegate Formation, Book Cliffs, Utah: Geology, v. 28, p. 359 - 362.

Miall, A,D., 1985, Architectural element analysis: a new method of facies analysis applied to fluvial deposits: Earth Science Reviews v. 22, p. 261-308

Miall, A,D., 1994, Reconstructing fluvial macroform architecture from two-dimensional outcrops: examples from the Castlegate Sandstone, Book Cliffs, Utah: Journal of Sedimentary Research, v. 64, p. 146-158.

Miall, A,D., 1996, Fluvial styles and facies models, in Miall, A.D., ed., The geology of fluvial deposits: Berlin, Springer-Verlag, p. 198-244.

Miall, A.D. and Arush, M., 2001, The Castlegate Sandstone of the Book Cliffs, Utah: Sequence stratigraphy, paleogeography, and tectonic controls: Journal of Sedimentary Research, v. 71, p.537-548.

Moretti, M., Pieri, P., and Tropeano, M., 2002, Late Pleistocene soft-sediment deformation structures interpreted as seismites in paralic deposits in the city of Bari (Apulian foreland, southern Italy) in Ettensohn, F.R., Rast, N., and Brett, C.E. eds., Ancient Seismites: Geological Society of America Special Paper no. 359, p. 75-85.

Nemec, W. and Steel, R.J., 1984, Alluvial and coastal conglomerates; their significant features and some comments on gravelly mass-flow deposits, in Koster, E.H. and Steel, R.J., Sedimentology of gravels and conglomerates Canadian Society of Petroleum Geologists Memoir no.10, p. 1-31.

Nigro, F., and Renda, P., 2004, Growth pattern of underlithified strata during thrust-related folding: Journal of Structural Geology, v. 26, p. 1913-1930.

Obradovich, J. D., 1994, A Cretaceous time scale. In Caldwell, W.G.E., and Kauffman, E. G., eds., Evolution of the Western Interior Basin: Geological Association of Canada Special Paper no. 39, p. 379-396.

Olsen, T., Steel, R.J., Høgseth, K Skar, T., and Røe, S.L., 1995, Sequential architecture in a fluvial succession- Sequence stratigraphy in the Upper Cretaceous Mesaverde Group, Price Canyon, Utah: Journal of Sedimentary Research, v. B65, no. 2, p. 265-280.

Paola, C., 1988, Subsidence and gravel transport in alluvial basins, in Kleinspehn, K.L. and Paola, C., eds., New Perspectives in Basin Analysis, p. 231-243. Springer-Verlag, New York.

Paola, C., 2000, Quantitative models of sedimentary basin filling: Sedimentology, v. 47, p. 121-178.

Patton, T., 2004, Numerical models of growth-sediment development above an active monocline: Basin Research, v. 16, p. 25-39.

Pettijohn, F.J. and Potter, P.E., 1964, Atlas and Glossary of Primary Sedimentary Structures. Springer-Verlag, New York.

Pierson, T.C., and Costa, J.E., 1987, A rheologic classification of subaerial sediment-water flows: Geological Society of America, Reviews in Engineering Geology, v. 7, p. 1-12.

Postma, G., 1986, Classification for sediment gravity-flow deposits based on flow conditions during sedimentation: Geology, v. 14, no. 4, p. 291 – 294.

Prossser, D.J., Daws, J.A., Fallick, A.E. and Williams, B.P.J., 1993, Geochemistry and diagenesis of stratabound calcite cement layers within the Rannoch Formation of the Brent Group, Murchison Field, North Viking Graben (Northern North Sea): Sedimentary Geology, v. 87, p. 139-164.

Prosser, S., 1993, Rift-related linked depositional systems and their seismic expression, in Williams, G.D. and Dobb, A., Tectonics and Seismic Sequence Stratigraphy: Geological Society Special Publication no 71, p. 31-66.

Reese, J.A., 1989, Initial deposition in the Sevier foreland basin of southern Nevada; conglomerates of the Cretaceous Willow Tank Formation, Clark County, Nevada [unpublished M.S. thesis]: University of Nevada, Las Vegas, 143 p.

Riba, O., 1976, Syntectonic unconformities of the Alto Cardener, Spanish Pyrenees: a genetic interpretation: Sedimentary Geology v. 15, p. 213-233.

Robinson, R.A. and Slingerland, R.L., 1997, Grain-size trends and basin-subsidence in the Campanian Castlegate Sandstone and equivalent conglomerates of central Utah foreland basin: Basin Research, v. 10, p. 109-128.

Schmitt, J.G. and Steidtmann, J. 1990, Interior ramp-supported uplifts; Implications for sediment provenance in foreland basins: Geological Society of America Bulletin, v. 102, p. 494-501.

Schmitt, J., G., and Aschoff, J.L., 2004 Distinguishing alluvial fan and fluvial systems interactions at foreland basin margins: criteria and significance: Geological Society of America, Annual Meeting, Abstracts with Program, v. 37, no. 7, p. 482.

Shanley, K.W., McCabe, P.J. and Hettinger, R.D., 1992, Tidal influence in Cretaceous fluvial strata from Utah, USA: A key to sequence stratigraphic interpretation: Sedimentology, v. 39, no. 5, p. 905-930.

Shanley, K.W. and McCabe, P.J., 1994, Perspectives on the sequence stratigraphy of continental strata: AAPG Bulletin, v. 78, no. 4, p. 544-568.

Shelley, D.C., and Lawton, T.F., 2006, Sequence stratigraphy of tidally influenced deposits in a salt-withdrawal minibasin: Upper sandstone member of the Potrerillos Formation (Paleocene), La Popa basin, Mexico: American Association of Petroleum Geologists Bulletin, v. 89, p. 1157-1179.

Stille, H., 1936, The present tectonic state of the earth: AAPG Bulletin, v. 20, p. 849-880.

Sohn, Y.K., Rhee, C.W., and Kim, B.C., 1999, Debris flow and hyperconcentrated flood-flow deposits in an alluvial fan, northwestern part of the Cretaceous Yongdong Basin, Central Korea: Journal of Geology, v. 107, p. 111-132.

Spieker, E.M., 1946, Late Mesozoic and early Cenozoic history of central Utah: U. S. Geological Survey Professional Paper 205-D, p. 117-161.

Suppe, J., Chou, G.T., and Hook, S.C., 1992, Rates of folding and faulting determined from growth strata, in McClay, K.R. ed., Thrust tectonics: Chapman and Hall, Suffolk, p. 105-121.

Sloss, L.L., 1972, Synchroneity of Phanerozoic sedimentary-tectonic events of the North American Craton and the Russian Platform: XXIV International Geological Congress Proceedings, Montreal, Section 6, p. 24-32.

Sloss, L.L., 1979, Global sea-level change, a view from the Craton: AAPG Memoir, v. 29, p. 461-467.

Steel, R. J., Maehle, S. , Nilsen, H., Roee, S. L. and Spinnangr, A., 1977, Coarsening-upward cycles in the alluvium of Hornelen Basin (Devonian) Norway; sedimentary response to tectonic events: GSA Bulletin, v. 88, p. 1124 - 1134.

Steel, R.J., 1988, Coarsening upward and skewed fan-bodies: symptoms of strike-slip and transfer fault movement in Nemec, W. and Steel, R.J. eds., Fan Deltas: Sedimentology and Tectonic Settings, Blackie, Glasgow, p. 75-83.

Suppe, J., Chou, G.T. and Hook, S.C., 1992, Rates of folding and faulting determined from growth strata, in Thrust Tectonics, McClay, K.R., ed., p. 105-121.

Taylor, K.G., Gawthorpe, R.L., Curtis, C.D., Marshall, J.D. and Anwiller, D.N., 2000, Carbonate cementation in a sequence-stratigraphic framework: Upper Cretaceous sandstones, Book Cliffs, Utah-Colorado: Journal of Sedimentary Research, v. 70, no.2 p. 360-372.

Taylor, W.J., Bartley, J.M., Fryxell, J.E., Schmitt, J.G., and Vandervoort, D.S., 1993, Tectonic style and regional relations of the Central Nevada thrust belt, in Lahren, M.M., Trexler, J.H., Jr., and Spinosa, C. eds., Crustal Evolution of the Great Basin and Sierra Nevada: Cordilleran and Rocky Mountain Section, Geological Society of America Guidebook, Department of Geological Sciences, University of Nevada, Reno p. 57-96.

Vail, P.R. and Todd, R.G., 1981, Northern Sea Jurassic unconformities, chronostratigraphy and sea-level changes from seismic stratigraphy In: Illing, L.V., Hobston, G.D., eds., Petroleum geology of the continental shelf of northwest Europe. Institute of Petroleum, London, p. 216-235.

Vail, P. R., Audemanrd, F., Bowmann, S.A., Eisner, P.M, Perez-Crus, C., 1991, The stratigraphic signatures of tectonics, eustasy and Sedimentology- an overview In Einsele, G., Ricken, W., Seilacher, A., eds., Cycles and events in stratigraphy. Springer-Verlag, Berlin Heidelberg New York, p. 617-659.

Van Wagoner, J.C., 1991, Sequence stratigraphy and facies architecture of the Desert Member of the Blackhawk Formation and the Castlegate Formation in the Book Cliffs of eastern Utah and western Colorado, in Van Wagoner, J.C., Jones, C.R., Taylor, D.R., Nummedal, D., Jennette, D.C., and Riley, G.W., eds., Sequence Stratigraphy Applications to Shelf Sandstone Reservoirs: Outcrop to Subsurface Examples. American Association of Petroleum Geologists Field Conference, September 1991, 12 p.

Vergés, J., Burbank, D.W., and Meigs, A., 1996, Unfolding: an inverse approach to fold kinematics: Geology, v. 24, no. 2, p. 175-178.

Vergés, J., Marzo, M., and Munoz, J.A., 2002, Growth strata in foreland settings: Sedimentary Geology v. 146, p. 1-9.

Williams, E.A., Ford, M., Verges, J., and Artoni, A., 1998, Alluvial gravel sedimentation in a contractional growth fold setting, Sant Llorenç de Morunys, southeastern Pyrenees, in Mascle, A., Puigdefàbregas, C. Luterbacher, H.P. and Fernàndez, M., eds., Cenozoic Foreland Basins of Western Europe: Geological Society of London Special Publication, no. 134, p. 69-106.

Wood, L.J. 2004, Predicting tidal sand reservoir architecture using data from modern and ancient depositional systems, *in* Grammer, G.M., Harris, P.M., and Eberli, G.P., eds., Integration of outcrop and modern analogs in reservoir modeling: AAPG Memoir (2004), 80 45-66.

Willis, B.J., and Gabel, S.L., 2003, Formation of deep incisions into tide-dominated river deltas: Implications for the stratigraphy of the Sego Sandstone, Book Cliffs, Utah, U.S.A: Journal of Sedimentary Geology, v. 73, p. 246-263.

Yoshida, S., Willis, A., and Miall, A., 1996, Tectonic Control of Nested Sequence Architecture in the Castlegate Sandstone (Upper Cretaceous), Book Cliffs, Utah: Geology, v. 66, p. 737-748.

Yoshida, S., Steel, R.J. and Dalrymple, R.W., 2008, Changes in Depositional Processes-An Ingredient in a New Generation of Sequence-Stratigraphic Models: Journal of Sedimentary Research, v. 77, p. 447 - 460.

Zapata, T. R. and Allmendinger, R. W., 1996, Growth strata record of instantaneous and progressive limb rotation, Precordillera thrust belt and Bermejo Basin, Argentina: Tectonics, v. 15, no. 5, p. 1065-1083.

Vita

Jennifer Aschoff was born in southern Maine on February 28, 1978 to Alan and Diane Aschoff. She graduated from Exeter Area High School, NH in 1996. Later, she received a Bachelor of Science degree in Earth Sciences at Montana State University-Bozeman in 2000, and a Master of Science degree in Geology at New Mexico State University- Las Cruces in 2003. Under the supervision of Drs. K. Giles, J. Schmitt and T. Lawton she authored/co-authored three papers at the onset of her Ph.D. program at The University of Texas at Austin in 2004. Under the supervision of Dr. Ron Steel she published an "audacious" paper during her Ph.D. program that made a lasting impression on her. Jennifer worked as a geoscience intern for BP-America and ConocoPhillips, a research associate at Montana State University-Bozeman, and volunteered for the U.S. Geological Survey in Denver, CO while completing her M.S. and Ph.D. degrees. She joined the faculty in the Department of Geology and Geologic Engineering at Colorado School of Mines, Golden, CO in 2008.

Permanent address: 32 Prescott St. Brentwood, NH 03833

This dissertation was typed by the author.